

Preparation and evaluation of nanoporous
aerogel particles based on biopolymers for
pharmaceutical applications

Dissertation

with the aim of achieving a doctoral degree

at the Faculty of Mathematics, Informatics and Natural Sciences

Department of Chemistry

Universität Hamburg

submitted by

Tamara Athamneh

Hamburg 2020

Reviewer of the thesis: Professor Dr. Claudia S. Leopold

Professor Dr. Hans-Ulrich Moritz

Thesis defense committee: Professor Dr. Claudia S. Leopold

Professor Dr.-Ing. Irina Smirnova

Professor Dr. Michael Steiger

Professor Dr. Ralph Holl

Professor Dr. Markus Fischer

Date of thesis defense: 24.07.2020

The experimental studies and the preparation of this thesis were carried out between May 2016 and May 2020 in the Department of Chemistry at the University of Hamburg, in the division of Pharmaceutical Technology, under supervision of Professor Dr. Claudia S. Leopold and in the Institute of Thermal Separation Processes at Hamburg university of technology under the supervision of Professor Dr.-Ing. Irina Smirnova.

Zusammenfassung

Aerogel-Partikel sind hochporöse und leichte Feststoffe, welche durch den Austausch vorhandener Flüssigkeit in einer Gelmatrix durch Luft hergestellt werden, ohne dass die poröse Struktur des Gels kollabiert. Diese Flüssigkeitsextraktion erfolgt normalerweise mit Hilfe der überkritischen Extraktion. Die große Oberfläche und die offene Porenstruktur dieser Trägermaterialien machen eine effektive Beladung und eine verbesserte Bioverfügbarkeit möglich, weshalb sich Aerogele als vielversprechende Strukturen für die Verabreichung von Medikamenten und andere biomedizinische Anwendungen eignen. Eines der Hauptziele der vorliegenden Arbeit ist die Untersuchung des Einsatzpotentials von Alginat und Alginat-Hyaluronsäure-Aerogelen als Medikamententräger, wobei hier die Anwendung für den pulmonalen Arzneimitteltransport von besonderem Interesse ist. Zu diesem Zweck sollten die Aerogel-Partikel einen aerodynamischen Durchmesser zwischen 0,5 - 5 μm aufweisen.

Für die pulmonale Medikamentenverabreichung wurden Aerogel-Partikel mit Hilfe der Emulsions-Gelbildungstechnik und überkritischer CO_2 -Trocknung hergestellt. Um die Partikelgröße und -dichte der hergestellten Partikel (die sich direkt auf die aerodynamischen Eigenschaften auswirken) zu kontrollieren, wurden die Rührgeschwindigkeit und die Viskosität der inneren Phase während des Emulgierschritts optimiert. Außerdem konnten die aerodynamischen Durchmesser der hergestellten Partikel mathematisch durch die resultierenden Werte der Dichte und Partikelgröße vorhergesagt werden. Daraufhin erfolgte ein Vergleich der mathematisch vorhergesagten aerodynamischen Durchmesser mit den Ergebnissen der in vitro hergestellten aerodynamischen Durchmesser, die mit dem Kaskaden-Schlagkörper analysiert wurden. Die resultierenden Aerogel-Partikel wurden durch das Zeta-Potential, die Fourier-Transformations-Infrarotanalyse und die Rasterelektronenmikroskopie charakterisiert. Darüber

hinaus wurde eine Analyse der Partikeldichte, Porosität und Brunauer-Emmett-Teller-Oberfläche durchgeführt. Im Anschluss an die Partikelherstellung sowie deren Charakterisierung, wurden die Aerogel-Partikel mit dem Medikament Naproxen beladen und das Freisetzungsverhalten untersucht.

Die Vorhersage, Kontrolle und Herstellung von Alg- und Alg-HA-Aerogel-Partikel, die für die pulmonale Medikamentenverabreichung geeignet sind, wurden erfolgreich mit der Emulsionsgelationstechnik und der überkritischen CO₂-Trocknung erreicht. Die hergestellten Alg-HA-Aerogel-Partikel erfüllten die Anforderungen des pulmonalen Wirkstoffträgers hinsichtlich aerodynamischer Durchmesserwerte im Bereich von 0,5-5 µm. Neben der Möglichkeit zur Einstellung der Partikeldurchmesser durch Steuerung der Emulgierungsrate und der Viskosität der inneren Phase war es zudem möglich, die Mikrokugeldurchmesser mit Hilfe der Kapillaranzahlberechnungen vorherzusagen. Die Studie zur Wirkstofffreisetzung zeigte keine signifikanten Veränderungen in den Freisetzungsprofilen und des Gehaltes von Naproxen aus Alginat und Alginat-Hyaluronsäure.

Obwohl Alginat als Nahrungsmittelzusatz, als Arzneimittel sowie in biomedizinischen Anwendungen weit verbreitet ist, wurde die Wirkung von Calciumalginat in Form von Aerogel-Partikeln auf Leber und Niere in keiner früheren in-vivo-Studie untersucht. Auch über die Wirkung von Alginat-Aerogelen auf die Darmmikroorganismen, welche für deren Abbau verantwortlich sind, ist wenig bekannt. Daher war ein weiteres Ziel dieser Arbeit, die Wirkung von Calciumalginat-Aerogel auf Niere und Leber zu untersuchen und seine Wirkung auf die Darmflora zu bewerten. In vivo-Tests wurden durchgeführt, um die Wirkung des Calciumalginat-Aerogels als potentiellen Wirkstoffträger im Hinblick auf Leber- und Nierentoxizität sowie auf die Darmmikroorganismen von Wistar-Ratten zu bewerten. Das untersuchte Alginat-Aerogel wurde

mit Hilfe der Strahlschneidtechnik in Partikelform gebracht. Die In-vivo-Bewertung der Leber- und Nierentoxizität wurde durch zwei Arten von Experimenten durchgeführt: eine einwöchige Kurzzeitstudie zur subakuten Toxizität und eine zweiwöchige Langzeitstudie zur subakuten Toxizität. Hierbei konnte eine Veränderung der Darmflora durch die Analyse der 16S rRNA-Gensequenzierung festgestellt werden.

Die Ergebnisse der aktuellen Arbeit ergaben, dass weder eine sofortige noch eine verzögerte Nieren- oder Lebertoxizität nach 14 tägiger Verabreichung von 250 mg Tagesdosis eines kalziumvernetzten Alginats im Tierversuch nachgewiesen werden konnte. Dagegen zeigten die Mikroorganismen im Darm unterschiedliche Aktivitäten, welche von irreversibler oder reversibler Abnahme bis zu irreversibler oder reversibler Zunahme der Häufigkeit reichten.

Abstract

Aerogel particles are highly porous and light-weight powders that can be prepared by replacing the liquid inside a gel matrix with air without collapsing the porous structure of the gel. Usually this liquid extraction is done by using the supercritical fluid technology. The large surface area and the open pore structure, which allow an effective loading and enhanced bioavailability proved aerogels as very promising candidates for drug delivery and other biomedical applications. One of the main goals of the present thesis was to investigate the potential of using alginate and alginate-hyaluronic acid aerogel as a drug carrier, of particular interest as carriers for the pulmonary route. For this purpose, the aerogel particles should have an aerodynamic diameter between 0.5-5 μm .

For the purpose of pulmonary drug delivery, aerogel particles were prepared using the emulsion gelation technique and supercritical CO_2 drying. To control the particle size and density of produced particles (that are directly affecting the aerodynamic properties), the stirring speed and the inner phase viscosity were optimized during the emulsification step. Also, the aerodynamic diameters of the prepared particles were mathematically predicted through the resulted values of the density and particle size. Eventually the mathematically predicted aerodynamic diameters were compared with the in vitro aerodynamic diameter results, which were analyzed by the cascade impactor. The final aerogel particles were characterized by Zeta potential, Fourier transform infrared analysis and scanning electron microscopy. Furthermore, the particle density, porosity and Brunauer–Emmett–Teller surface area were analyzed. The prepared aerogel particles were loaded with naproxen drug, and the release behavior was studied.

Predicting, controlling and preparing of Alg and Alg-HA aerogel particles that is suitable for pulmonary drug delivery were successfully achieved using the emulsion gelation technique and supercritical CO₂ drying. The prepared Alg-HA aerogel particles met the requirement of the pulmonary drug carrier in term of aerodynamic diameter values in the range of 0.5 - 5 µm. In addition to the possibility for adjusting the microsphere diameters by controlling the emulsification rate and the inner phase viscosity, it was also possible to predict the microsphere diameters using the capillary number calculations. The drug release study revealed no significant changes in the release profiles and in the extent of naproxen from alginate and alginate-hyaluronic acid.

Although Alginate has been widely used in food products and as pharmaceutical as well as in biomedical applications, no previous *in vivo* studies have examined the effect of calcium alginate in the form of aerogel on the liver and kidney. Also, little is known about its effect on gut microbiota that is responsible for its degradation. Thus, another aim of this thesis was to explore the effect of calcium alginate aerogel on the kidney and liver, and to assess its effect on the intestinal microbial community. The *in vivo* tests were conducted to evaluate the effect of the calcium alginate aerogel as a potential drug carrier, on the liver and kidney toxicity as well as on the gut microbiota of Wistar rats. The studied alginate aerogel was prepared as particles using the jet cutting technique. The *in vivo* liver and kidney toxicity evaluation was performed by two types of experiments; short term subacute toxicity study, which lasted for one week and long-term subacute toxicity study, which lasted for two weeks. While the shift in gut microbiota was obtained by analyzing the 16S rRNA gene sequencing.

The results of the current thesis revealed that neither immediate nor delayed renal or liver toxicity were identified when calcium-crosslinked alginate aerogel is given to the Wistar rats for 14 days

with a daily dose of 250 mg. While the gut microbiota showed different behaviors ranging from irreversible or reversible decrease to irreversible or reversible increase in the abundance.

List of Abbreviations

| | |
|--------------------|---|
| ACI | Andersen Cascade Impactor |
| Alg | Alginate |
| ALP | Alkaline Phosphatase |
| ATR | Attenuated total reflectance |
| BET | Brunauer–Emmett–Teller specific surface area |
| Ca | Capillary number |
| Ca-Alg | Calcium alginate |
| CaCl ₂ | Calcium chloride |
| CaCO ₃ | Calcium carbonate |
| Ca _{crit} | Critical capillary number |
| CO ₂ | Carbon dioxide |
| d _A | Aerodynamic diameter |
| DPI | Dry powder inhalers |
| DV _{90%} | Diameter below which 90 % of the total volume of material in the sample is included |
| FTIR | Fourier transform infrared |
| GDL | Gluconic acid δ -lacton |
| gDNA | Genomic DNA |
| HA | Hyaluronic acid |
| HLB | hydrophile-lipophile balance |
| IFT | Interfacial tension |
| LC % | Loading capacity |
| MDIs | Metered dose inhalers |

List of Abbreviations

| | |
|----------------------|--------------------------------------|
| MiSeq | Microbiome sequencing |
| MMI | MarpleMiller Impactor |
| MSLI | Multi-Stage Liquid Impinger |
| Na-Alg | Sodium alginate |
| NGI | Next Generation Impactor |
| O/W | oil-in-water |
| O/W/O | oil-in-water-in-oil |
| OECD | Economic Cooperation and Development |
| PBS | Phosphate buffer saline |
| P_{cr} | Critical pressure |
| PCR | Polymerase Chain Reaction |
| Ph.Eur | European Pharmacopoeia |
| pMDI | pressurized metered-dose inhalers |
| Re | Reynold numbers |
| SEM | Scanning electron microscope |
| Span [®] 80 | Sorbitan Monooleate |
| T_c | Critical temperature |
| USP | United States Pharmacopeia |
| UV | Ultraviolet |
| W/O | Water-in-oil |
| W/O/W | water-in-oil-in-water |

Table of Content

| | |
|---|----|
| Zusammenfassung..... | I |
| Abstract..... | IV |
| List of abbreviations | VI |
| 1. Introduction | 1 |
| 2. Fundamental and state of the art..... | 4 |
| 2.1. Aerogel particles production techniques | 4 |
| 2.1.1. Droplets formation in a gaseous phase | 5 |
| 2.1.1.1. Conventional dropping method | 5 |
| 2.1.1.2. Vibrating nozzle method | 6 |
| 2.1.1.3. Electrostatic Method | 6 |
| 2.1.1.4. Jet cutting method..... | 6 |
| 2.1.1.5. Atomization/ Spraying | 7 |
| 2.1.1.6. Inkjet printing | 7 |
| 2.1.2. Droplets formation in a liquid phase (emulsification) | 8 |
| 2.1.3. Solvent exchange | 9 |
| 2.1.4. Supercritical drying..... | 10 |
| 2.2. Current aerogel uses and potential applications in life sciences | 12 |
| 2.2.1. Cosmetics applications of aerogels..... | 14 |
| 2.2.2. Biomedical applications of aerogels | 14 |
| 2.2.2.1. Wound dressing applications of aerogels..... | 14 |
| 2.2.2.2. Tissue engineering applications of aerogels..... | 15 |
| 2.2.3. Pharmaceutical applications of aerogels | 16 |
| 2.2.3.1. Aerogel for oral drug delivery application..... | 17 |
| 2.2.3.2. Aerogel for transdermal drug delivery application..... | 19 |
| 2.2.3.3. Aerogel for pulmonary drug delivery application | 19 |
| 2.3. Challenges associated to pulmonary drug carrier | 20 |
| 2.4. Future of pulmonary drug delivery by DPI | 22 |
| 2.5. Polysaccharides as potential drug carrier | 23 |
| 2.5.1. Chemistry of alginate | 23 |
| 2.5.2. Chemistry of hyaluronic Acid | 25 |

| | | |
|------------|---|----|
| 2.6. | Conventional methods for the production of pulmonary drug carrier | 26 |
| 2.7. | Spray drying | 26 |
| 2.7.1. | Spray freeze drying | 27 |
| 2.7.2. | Jet milling | 27 |
| 2.8. | Emulsion gelation and supercritical drying as novel technology for drug carrier production | 27 |
| 2.8.1. | Emulsion formation | 28 |
| 2.8.2. | Forces between emulsion droplets | 29 |
| 2.8.2.1. | Van der Waals attraction | 29 |
| 2.8.2.2. | Electrostatic repulsion | 30 |
| 2.8.2.3. | Steric repulsion | 32 |
| 2.8.3. | Thermodynamics aspects of stable emulsions and destabilization mechanisms | 32 |
| 2.8.3.1. | Creaming and sedimentation | 34 |
| 2.8.3.2. | Flocculation | 35 |
| 2.8.3.3. | Coalescence | 36 |
| 2.8.3.4. | Ostwald Ripening | 36 |
| 2.8.3.5. | Phase inversion | 36 |
| 2.8.4. | Emulsion stabilization | 37 |
| 2.8.4.1. | Role of surfactants in emulsion stability | 37 |
| 2.8.4.2. | Selection of the surfactant | 38 |
| 2.8.5. | Predicting droplet size of emulsion | 40 |
| 2.9. | Derivation of the objectives of the thesis based on the state of the art | 42 |
| 3. | Materials and methods | 44 |
| 3.1. | Materials | 44 |
| 3.2. | Methods | 45 |
| 3.2.1. | Aerogel particles for pulmonary drug delivery applications | 45 |
| 3.2.1.1. | Rheological characterization for the emulsion components | 45 |
| 3.2.1.1.1. | Rheological analysis for the oil and polymers stock solutions | 45 |
| 3.2.1.1.2. | Rheological study to assess polymers interaction | 45 |
| 3.2.1.1.3. | Rheological characterization to assess HA interaction with calcium | 46 |
| 3.2.1.2. | Gelation assessment | 46 |
| 3.2.1.2.1. | Gel visual assessment | 46 |
| 3.2.1.2.2. | Gel rheological assessment | 48 |

| | | |
|------------|---|----|
| 3.2.1.3. | Preparation of Alg and hybrid Alg-HA aerogel particles and monoliths | 49 |
| 3.2.1.3.1. | Preparation of polymers stock solutions | 49 |
| 3.2.1.3.2. | Preparation of aerogel particles by emulsion gelation and supercritical drying 49 | |
| 3.2.1.3.3. | Preparation of aerogel monoliths | 51 |
| 3.2.1.3.4. | Solvent exchange and HA content uniformity in the final particles | 52 |
| 3.2.1.4. | Emulsion characterization and droplet size estimation..... | 53 |
| 3.2.1.4.1. | Interfacial tension measurements..... | 54 |
| 3.2.1.4.2. | Viscosity of the dispersed and the continuous phase | 54 |
| 3.2.1.4.3. | Estimation of the emulsification of shear rate at 1200 rpm..... | 55 |
| 3.2.1.4.4. | The actual droplet sizes analysis in the emulsion | 55 |
| 3.2.1.5. | Aerogel particles characterization | 56 |
| 3.2.1.5.1. | Zeta potential measurements | 56 |
| 3.2.1.5.2. | Fourier transform infrared | 56 |
| 3.2.1.5.3. | Scanning electron microscopy | 56 |
| 3.2.1.5.4. | Particle size and distribution..... | 57 |
| 3.2.1.5.5. | Particle density and porosity and BET surface area | 57 |
| 3.2.1.6. | Analysis of aerodynamic diameter | 58 |
| 3.2.1.7. | Supercritical drug impregnation and in-vitro release from the particles | 59 |
| 3.2.2. | The liver and kidney <i>in vivo</i> toxicity study of calcium alginate aerogel and it effect on the gut microbiota | 61 |
| 3.2.2.1. | Preparation of aerogel particles for the in vivo toxicity and microbiota shift studies | 62 |
| 3.2.2.2. | The in vivo toxicity of Alg aerogel as a potential oral drug carrier | 63 |
| 3.2.2.2.1. | Animals | 63 |
| 3.2.2.2.2. | Short-term toxicity (Sighting study) | 63 |
| 3.2.2.2.3. | Long-term toxicity study (15 days repeated dose study) | 64 |
| 3.2.2.2.4. | Clinical and behavioral observation..... | 65 |
| 3.2.2.2.5. | Serum biochemistry and feces analyses | 65 |
| 3.2.2.3. | Intestinal microbial community analysis | 66 |
| 4. | Result and discussion | 68 |
| 4.1. | Rheological characterization for the emulsion components..... | 68 |
| 4.1.1. | Rheological analysis for the oil and polymers stock solutions..... | 68 |

| | | |
|----------|--|-----|
| 4.1.2. | Rheological study to assess the polymers interactions | 74 |
| 4.1.3. | Rheological characterization to assess HA interaction with calcium | 76 |
| 4.2. | Gelation assessment | 77 |
| 4.2.1. | Gel visual assessment..... | 77 |
| 4.2.2. | Gel rheological assessment | 78 |
| 4.3. | Determining the conditions of solvent exchange under consideration of HA leaching .. | 80 |
| 4.4. | Emulsion characterization and droplet size estimation..... | 83 |
| 4.4.1. | Surface tension measurements..... | 83 |
| 4.4.2. | Estimation of the emulsification shear rate | 86 |
| 4.4.3. | Viscosity of the dispersed and the continuous phase..... | 87 |
| 4.4.4. | Capillary number calculation and droplet size estimation | 88 |
| 4.5. | Aerogel particles characterization | 90 |
| 4.5.1. | Zeta potential analysis..... | 90 |
| 4.5.2. | Fourier transform infrared analysis for the aerogel particles | 91 |
| 4.5.3. | Scanning electron microscopy..... | 93 |
| 4.5.4. | Particle size analysis | 95 |
| 4.5.5. | Particle density, porosity and BET surface area..... | 97 |
| 4.5.6. | Analysis of aerodynamic diameter | 104 |
| 4.6. | Supercritical drug impregnation and <i>in-vitro</i> release from the particles..... | 108 |
| 4.7. | <i>In vivo</i> toxicity study of calcium alginate aerogel | 116 |
| 4.7.1. | Short-term toxicity (Sighting study) | 117 |
| 4.7.1.1. | ALP level analysis | 118 |
| 4.7.1.2. | Creatinine level analysis | 120 |
| 4.7.2. | Long-term toxicity study..... | 122 |
| 4.7.2.1. | ALP level analysis | 122 |
| 4.7.2.2. | Creatinine level analysis | 123 |
| 4.7.3. | Shift in gut microbiota | 125 |
| 5. | Conclusion..... | 130 |
| 6. | References | 133 |
| 7. | Appendix | 160 |

List of figures

| | |
|--|----|
| Figure 1. Scheme of different dropping techniques for bead or particles production: (a) conventional dropping method, (b) vibrating nozzle method, (c) electrostatic forces, (d) jet cutting method, (e) atomization and (f) inkjet printing..... | 5 |
| Figure 2. Schematic representation of emulsification gelation process..... | 8 |
| Figure 3. The binary phase diagram of supercritical drying for ethanol/ CO ₂ mixture. | 11 |
| Figure 4 metered dose inhaler and dry powder inhaler [100]. | 20 |
| Figure 5. Alginate chemical structure..... | 25 |
| Figure 6. Chemical structure of hyaluronic acid. | 26 |
| Figure 7. Schematic picture of the structure of the double layer according to Gouy–Chapman and Stern..... | 31 |
| Figure 8. Schematic representation of the various destabilization mechanisms in emulsion [141]. | 34 |
| Figure 9. Graphical representation of O/W surfactant (left) and W/O surfactant (right)..... | 38 |
| Figure 10. The preparation method of aerogel particles using the emulsion gelation and supercritical the CO ₂ drying. | 51 |
| Figure 11. Concentration dependence of the intrinsic viscosity of Alg in water at 25 °C..... | 69 |
| Figure 12. Concentration dependence of the intrinsic viscosity of HA in water at 25 °C. | 69 |
| Figure 13. Effect of shear rate and temperature on the viscosity of rapeseed oil. | 70 |
| Figure 14. Effect of shear rate on the viscosity of different Alg solutions at room temperature. | 71 |
| Figure 15. Effect of shear rate on the viscosity of different Alg-HA solutions at room temperature. | 71 |
| Figure 16. Results of the viscosity of the Alg-HA solutions with different mass ratios and total polymer concentrations of 0.25 and 1.00 % w/w at a shear rate of 5 s ⁻¹ . Means ± SD, n = 3..... | 75 |
| Figure 17. Change of the HA solution (1 % w/w) viscosity upon addition of calcium chloride. Means ± SD, n = 3..... | 76 |
| Figure 18. Dot plot of the different prepared hydrogels and their ultimate gelation status after the CO ₂ induced gelation. | 78 |
| Figure 19. Gelation over time for a 1 % w/w polymer blend made of HA 0.8 fraction and Q = 0.5 CaCO ₃ (corresponding to 0.01825 g of CaCO ₃ to each 1g of Alg)..... | 79 |
| Figure 20. Gelation over time for a 1 % w/w of Alg-HA polymer solution made 0.8 fraction of HA, 0.2 fraction of Alg and Q = 0.75 CaCO ₃ (corresponding to 0.02737 g of CaCO ₃ to each 1 g of Alg)..... | 80 |
| Figure 21. Residual HA content in the gel after the solvent exchange if using a starting ethanol concentration of 46% w/w. | 82 |
| Figure 22. The dynamic interfacial tensions between Alg polymer solutions and rapeseed oil in the absence of surfactant. | 84 |
| Figure 23. The dynamic interfacial tensions between Alg-HA polymer solutions and rapeseed oil in the absence of surfactant. | 84 |
| Figure 24. Equilibrium interfacial tensions between Alg and Alg-HA polymer solutions and rapeseed oil in the presence of 1 % w/w surfactant (Span [®] 80); means ± SD, n = 3..... | 85 |
| Figure 25. The dynamic interfacial tensions between both Alg and Alg-HA (0.75 % w/w) polymer solutions and rapeseed oil in the presence of 1 % w/w surfactant (Span [®] 80)..... | 86 |
| Figure 26. The calculated critical capillary number values using Equation 12 for Alg in rapeseed oil emulsions, at different viscosity ratio and at emulsification speed of 1200 rpm corresponding to a shear rate of 655.86 s ⁻¹ | 89 |
| Figure 27. FTIR spectra of plain Alg, plain HA, Alg-HA powder and Alg-HA aerogel..... | 92 |

Figure 28. Scanning electron micrographs of different Alg and Alg-HA particles which were prepared by an emulsion gelation process with a subsequent drying step by supercritical CO₂ (the right side of each picture is a magnified part taken from the left side). 94

Figure 29. True density of Alg particles (prepared at 1200 rpm) compared to the true density of monoliths prepared at various concentrations of Alg; means \pm SD, n = 3. 102

Figure 30. True density of Alg-HA particles (prepared at 1200 rpm) compared to the true density of monoliths prepared at various concentrations of Alg-HA, means \pm SD, n = 3. 104

Figure 31. Aerodynamic diameter (d_A) of selected samples of the Alg-HA particles which..... 107

Figure 32. In vitro release profile of sodium naproxen from 0.75 % Alg and Alg-HA microspheres. Study was conducted in phosphate buffer solution (pH 7.4 ± 0.05) at 100 rpm in a shaking water bath at 37 °C, means \pm SD, n = 3. 112

Figure 33. Two examples on the swelling of the gastro-intestinal tract of the rats belonging to the group of 500 mg aerogels. 118

Figure 34. Short term analysis for the effect of different doses of calcium alginate aerogels and sodium alginate on ALP serum levels (aerogel corresponding to Ca-Alg aerogel and alginate corresponding to Na-Alg). 119

Figure 35. Box-plot for the in vivo serum creatinine level analysis that was done for the different doses of the aerogels and the alginate. The dotted lines in all the panels represent the creatinine values for all the control groups. 121

Figure 36. Box-plot for ALP test that was done for the 250 mg Ca-Alg aerogels (A) and Na-Alg (B) during a long-term experiment. The dotted lines in all the panels represent the ALP values for all the control groups. 123

Figure 37. In vivo serum creatinine analysis, for the 250 mg calcium alginate aerogels (A) and sodium alginate (B) during a long-term experiment..... 124

Figure 38. Microbial community structure of the gut at the class level at the class level in rats treated with Ca-Alg aerogel. 126

Figure 39. Temporal shift in gut microbiota in response to the Ca-Alg aerogel exposure, representing the species that increased, decreased, or totally disappeared due to the treatment. 129

List of Tables

| | |
|--|-----|
| Table 1. Examples for the most common applications of the respective aerogels. | 13 |
| Table 2. Future challenges and objectives for DPIs [106]. | 22 |
| Table 3. Summary of HLB ranges and their application [136]. | 39 |
| Table 4. Required HLB numbers to emulsify various oils [136]. | 40 |
| Table 5. Preparation conditions of different Alg- HA in the gelation assessment study. | 47 |
| Table 6. Microsphere mass (g) and corresponding drug mass (g) used during the supercritical CO ₂ impregnation method. | 60 |
| Table 7. Power law parameters of Alg and Alg-HA (of a weight ratio 1:1) solutions and their corresponding emulsions. | 73 |
| Table 8. The effect of the ethanol concentration on the residual HA during the solvent exchange steps as performed with Alg-HA monoliths (2 % w/w of 1:1 Alg:HA). | 81 |
| Table 9. Estimated maximum shear rate using correlation from Bowen [160]. | 87 |
| Table 10. The apparent viscosities of the investigated Alg in rapeseed oil emulsions, their inner phases and the corresponding viscosity ratio and at emulsification speed of 1200 rpm corresponding to a shear rate of 655.86 s ⁻¹ | 88 |
| Table 11. The estimated largest stable droplet sizes in the emulsions using Equation 11 compared to the actual droplet sizes (dv90%) obtained by the microscope for the emulsion prepared at a stirring rate of 1200 rpm corresponding to a shear rate of 655.86 s ⁻¹ | 90 |
| Table 12. d _v values of Alg and Alg-HA (1:1) aerogel particles (means ± SD, n = 3). | 96 |
| Table 13. BET surface areas of the investigated aerogel particles; means ± SD, n = 3. | 98 |
| Table 14. Densities (g/cm ³) of the prepared plain Alg aerogel particles (g/cm ³); means ± SD, n = 3. | 100 |
| Table 15. Densities (g/cm ³) of the prepared Alg-HA aerogel particles; means ± SD, n = 3. | 101 |
| Table 16. The estimated dA values of Alg and Alg-HA (of a wt. ratio 1:1) particles aerogel particles prepared by the emulsion gelation technique at different conditions (means ± SD, n = 3). | 106 |
| Table 17. Loading efficiency and pore properties of the loaded aerogel particles of Alg and Alg-HA prepared at 1200 rpm of polymer concentration 0.75 % w/w. | 109 |
| Table 18. Values of the exponent n in Equation 23 and the corresponding release mechanisms from a delivery system of various geometries [196]. | 113 |

1. Introduction

Aerogels are unique solid material which has puzzled the scientists since 1932 due to their outstanding properties, such as high porosity (up to 99%), high surface area (up to 2000 m²/g), very low density, adjustable framework, low thermal conductivity, low dielectric constant and low index of refraction [1], [2]. The first time an ‘aerogel’ terminology has been introduced to the scientific community was in 1932 by Samuel Kistler, who replaced the liquid inside a gelatin matrix with air without collapsing the porous structure of the gel using the supercritical fluid technology [3]. Few years after that, Kistler prepared silica aerogels out of water glass jelly and laid the first stone for aerogel application as thermal insulator [4]. Later on, and due to its outstanding features, aerogels were proposed into many other fields, like aerospace sector [5], [6], catalysis [7], chemical sensors [8], energy storage devices [9], optical fiber cladding [10], gas cleaning [11] and biomedical and drug delivery [12].

Aerogels can be tailored in the form of beads, microparticles, sheets, blankets, tubes, membranes, or coatings, by using different precursors, such as silica, polymers [13], cellulose [14], alginate [15], alginate–hyaluronic acid [16] and protein [17]. Even though aerogels can be produced from a large variety of organic and inorganic materials, only in the last decade organic aerogels have been intensively investigated. It was shown that a number of different organic precursors, especially biopolymers can be utilized to produce biocompatible aerogels with specific functions, which can be successfully used in the biomedical and pharmaceutical field. However, it was found, that each biopolymeric aerogel matrix has its limitation, such as weak mechanical properties, too strong water absorption or limited pore size. At the same time, it is well known that mixtures of different biopolymers can form more sophisticated multicomponent networks, which resulting in

forming synergetic effects of both polymers. Unfortunately, very limited amount of bio-based aerogel or bio-based hybrid aerogels exist so far.

Among all proposed applications, aerogels have recently attracted researchers in the area of drug delivery, and specifically pulmonary drug delivery using aerogel microparticles, because of their low density, high porosity, open porous structure and consequently outperforming air flowability. For pulmonary drug delivery purposes, the inhaled particles need to have low particle densities and optimum particle geometrical size, in order to have aerodynamic diameter in the range between 0.5 - 5 μm to achieve a deep lung deposition [18].

Recently, López-Iglesias et al. prepared calcium alginate microspheres for pulmonary drug delivery using thermal inkjet printing combined with supercritical CO_2 drying. However, this method shows limitations to use broader range of polymer concentration and higher viscosities as well as to produce larger amount of particles in a short time [19]. Therefore, the emulsion gelation technique combined with supercritical CO_2 drying was suggested as a better and more flexible choice, especially because of its ability to be scaled up into a continuous production mode [20].

Although many studies have described novel formulations with suitable aerodynamic properties to be used as pulmonary drug carrier, far too little attention has been paid to particles which are produced by the aerogel technology. Whereas some researchers investigated the emulsion gelation technique and supercritical CO_2 drying to prepare particles, the characterization of such particles as potential pulmonary drug carrier were not of their interest. Even as an oral drug carrier, aerogels were not evaluated for the in vivo toxicity. Thus, in this work there are following primary objectives:

1. To investigate the possibility of producing aerogel microspheres consisting of either alginate or alginate–hyaluronic acid using the emulsion gelation technique and supercritical CO₂ drying.
2. To optimize the aerogel particles of both alginate and alginate–hyaluronic acid, to get suitable aerodynamic diameters (d_A 0.5 – 5 μ m) for pulmonary drug delivery purposes.
3. To control the aerogel microsphere sizes and consequently the aerodynamic properties by controlling the droplet sizes during the emulsification process.
4. To investigate the ability of predicting the emulsion droplet sizes using Alg as a model polymer.
5. To test the *in vivo* suitability of alginate aerogel for the potential use as an oral drug delivery system

2. Fundamental and state of the art

2.1. Aerogel particles production techniques

Aerogels can be prepared from unlimited number of gel forming materials, by exchanging the solvent filling the pores into gas using supercritical fluid, which is subsequently vented out without inducing capillary pressure and collapsing the pores [3]. Nevertheless, saving the nanostructure of a gel can be achieved by freeze drying or even conventional evaporative drying, if the gel structure is robust that can withstand the growth of ice crystal or capillary forces [21].

The production technique of aerogel depends mainly on the intended application, taking into consideration the precursor characteristics. Generally, aerogel production involves three main steps; gelation, solvent exchange and supercritical drying, in case of aerogel particles a further step namely droplet formation is added at the beginning of the process before the gelation step. Such droplets formation can be achieved by two main approaches [22]:

- i. Droplets formation in a gaseous phase with subsequent fall in a bath that induces gelation.
- ii. Droplets formation in a liquid phase which is immiscible with the biopolymer solution (emulsion).

In both approaches, size and shape of the liquid droplet is influenced by: the interfacial tension between the polymer solution and the surrounding medium (gas or liquid), the viscosity of each phase, and the dynamic interactions of the droplets with the matrix fluid [22]. Accordingly, aerogel droplet productions techniques will be described below.

2.1.1. Droplets formation in a gaseous phase

2.1.1.1. Conventional dropping method

The conventional dropping method is so far the easiest method, in which a droplet flows out of a sharp nozzle (e.g. pipettes or syringes), Figure 1a, when the gravity force of the droplet exceeds the adhesion force at the nozzle, the droplet falls freely under the effect of gravity till it hits the gelation bath. Although this method is simple and able to produce monodispersed droplets, the production capacity is very low and the droplet size can only be in the millimeters ranges. However, those disadvantages can be overcome by multiplying the number of nozzles and using a co-axial gas flow around the nozzle, but not spraying, to improve the speed of particles detachment from the nozzle [23].

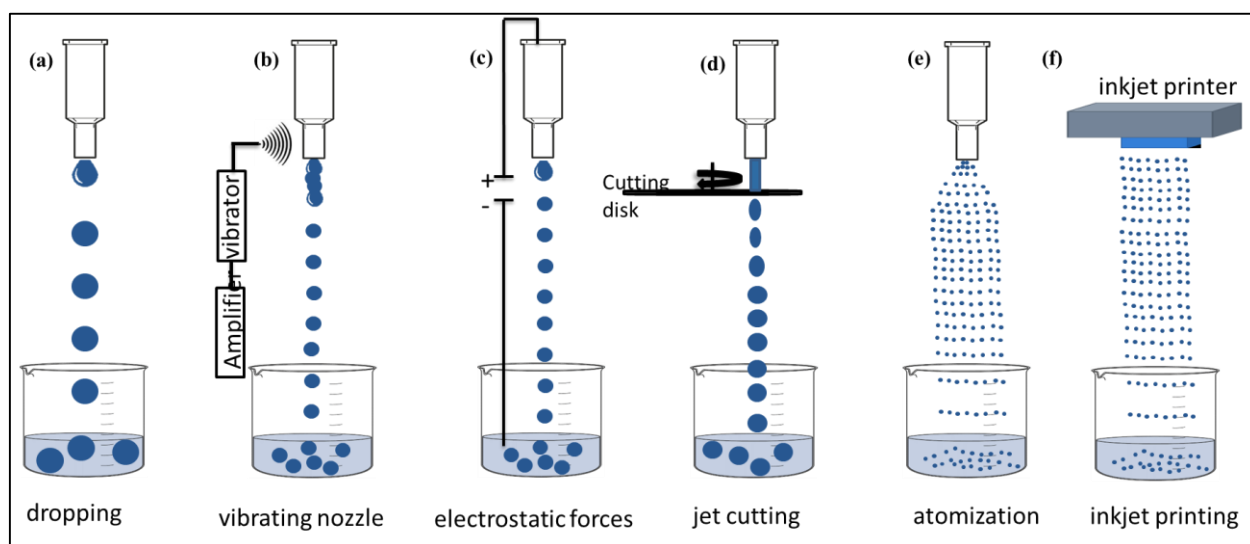


Figure 1. Scheme of different dropping techniques for bead or particles production: (a) conventional dropping method, (b) vibrating nozzle method, (c) electrostatic forces, (d) jet cutting method, (e) atomization and (f) inkjet printing.

2.1.1.2. **Vibrating nozzle method**

In the vibration technique (Figure 1b), monodispersed droplets are produced by applying an oscillation on a pressurized liquid coming out of a nozzle. This vibration leads to destabilization of the jet which eventually disintegrates into separated beads that can be collected afterwards. Similar to the conventional dropping method, vibration technique enables the production of monodispersed beads in millimeters ranges. The major limitation of this technique is that it can only be applied on low viscous liquids in the range of few hundreds mPa.s. Fortunately, the scale-up of this technique is possible by multi-nozzle systems [24].

2.1.1.3. **Electrostatic Method**

The electrostatic dropping (Figure 1c) is somehow similar to the previous two methods, however, the formation of a droplet is generated by an electric field, which pulls the solution out from the nozzle, and the droplet is detached when the gravity force and the electrostatic force exceeds the adhesion at the nozzle. This technique allows the production of particles in the range of 0.3 - 5 mm with a very narrow particle size distribution. Nevertheless, this method is not applicable for the highly viscous solution [25].

2.1.1.4. **Jet cutting method**

In 1996 geniaLab[®] developed a new technique to prepare particles with the size range 0.2 - 0.8 mm with a high productivity and an economic efficiency [26]. In this technique (Figure 1d) the solution is pressurized and ejected through a nozzle with a high velocity to obtain a stable liquid jet, a rotating disk with wires cuts the liquid jet into small cylinders which became almost spherical droplets during falling into the gelation bath. The main advantages for this technique is the high

productivity and the ability to work with high viscous solutions. One disadvantage of the Jet cutter technology is the liquid loss through cutting and spraying [27]. In a study of Preibisch et al. (2018), aerogel beads based on amidated pectin, sodium alginate and chitosan were prepared for the first time using jet cutting technique. Spherical aerogel particles in the size range of 400 to 1500 μm with narrow particle size distributions were prepared. In this study it was found that the sphericity of the particles was not perfect in some cases. Nevertheless, the it might be enhanced by adjusting the process parameters.

2.1.1.5. **Atomization/ Spraying**

In the atomization process (Figure 1e), a stream of an incompressible liquid in a gas phase passes through atomizer nozzles, which leads to the disintegration of this stream and the formation of poly- or monodispersed droplets, which then fall down into the gelation bath. Different types of atomizers and nozzles have got their own advantages and disadvantages. Currently, there are several atomizing devices available in the market to be used in a pilot scale, such as fan spray atomization, pressure jet atomization, twin-fluid atomization, effervescent atomization, rotary atomization, electrostatic atomization, vibration atomization and whistle atomization [28], [29]. Different types of atomizers have got their own advantages and drawbacks, and they also produce different droplets sizes and size distribution.

2.1.1.6. **Inkjet printing**

Inkjet printing has recently emerged as a relevant technique for several applications like electronic devices, photoelectrochemical cells or drug products. Using this technique, polymer solution droplets are ejected from small nozzles due to the expansion of a vapor bubble produced by electrical heating of the liquid itself. The produced ejected droplet has a diameter close

to that of the nozzle itself (10 - 50 μm) [30], [31]. Several inkjet-printed pharmaceutical formulations in the form of particles, hydrogels and films were reported for different administration routes (e.g. oral, respiratory or parenteral) [32]. The advantages of inkjet printing are the ease of mass fabrication, its flexibility, narrow particle size distribution and the ability of depositing very small amounts of material. A drawback is the restriction to low viscosities, and therefore low polymer concentrations [31].

2.1.2. Droplets formation in a liquid phase (emulsification)

Emulsification is a process in which one liquid is dispersed in a second immiscible liquid by applying energy as stirring or agitation, such dispersion is stabilized by an emulsifier (surfactant). For particles production, when a stable emulsion is formed, chemical or physical impact is added to trigger the gelation (Figure 2. Schematic representation of emulsification gelation).

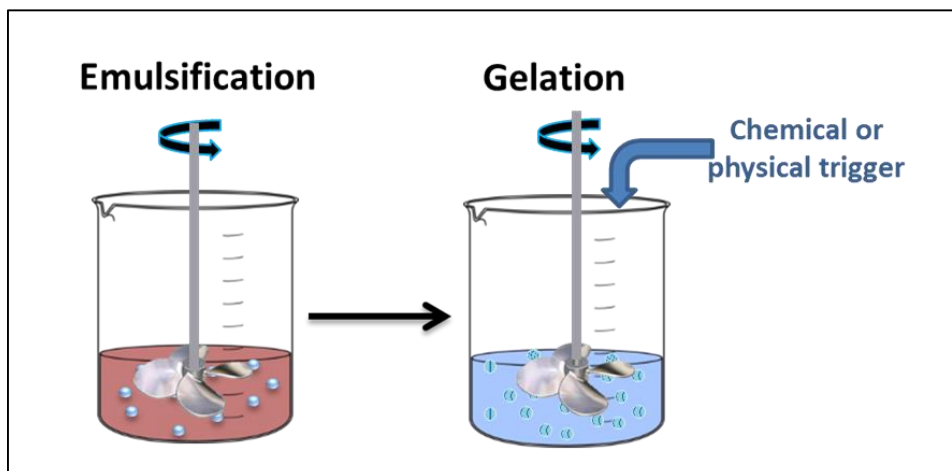


Figure 2. Schematic representation of emulsification gelation process

There are many parameters influencing the droplet size in an emulsion, such emulsification rate and time, viscosity of both phases, surfactant type and concentration, the rotor/stator design and the volume ratio of the two phases [33], [34]. This approach for particles production together with

the supercritical drying is often employed for the production of aerogel particles from water soluble polysaccharides, such as alginate, pectin, starch, chitosan and cellulose [35].

2.1.3. Solvent exchange

The preparation of an aerogel starts first with the formation of gel particles in an appropriate solvent (which is usually aqueous media for biopolymers) using the previously mentioned approaches, in this case the gel is called hydrogel. It was found by Kistler that to convert water into a supercritical fluid, high temperature and pressure are required (22 MPa and 373 °C) [3]. To avoid this harsh conditions, it is needed to replace water with another solvent which has a lower critical point in order to perform supercritical drying. The common approach for solvent exchange is displacing the water with an organic solvent which has high solubility in supercritical CO₂, usually alcohol or acetone [36], in this case the gel is called lyogel, if the replaced solvent is alcohol it is called alcogel. However, such solvent has to be completely miscible with water, at the same time not dissolving the gel structure. Special attention should be paid if the aerogel is used in the pharmaceuticals or food applications [37], [38].

Solvent exchange can be done by two different approaches; a single step, in which the hydrogel is soaked directly in a 100 % of the new solvent, or in a sequence soaking steps in different water/new solvent mixtures, in which the concentration of the new solvent is increased stepwise till it reaches the 100 % [39].

Usually, during the transformation of the hydrogel into lyogel there might be a certain degree of shrinkage, which can be defined as the difference in the volume of the original hydrogel and the lyogel. Such phenomenon is influenced by the biopolymer concentration; biopolymer hydrogels prepared from a concentrated solutions are generally more robust against shrinkage [40]. On the

molecular basis, the solvent-polymer interaction is also related to the hydrogel shrinkage; with increasing the concentration of the organic solvent the solvent polarity and the ability to form hydrogen bonds are reduced, therefore, the polymer swollen fibrils become closer and denser, and it was found that even ethanol, which is considered one of the best solvent for solvent exchange, is responsible for high shrinkage degree when used in a single-step solvent exchange [40], [41]. In case of beads below a few millimeters in diameter, lower shrinkage was observed even when immersed in water-free ethanol [42]. Gurikov et al. (2019) refer this to the reduced concentration gradients between the particle outer surface and the center, which leads to less so mechanical stress. Another explanation was proposed; that the gel shrinkage in the outer layer drags the inner fibers in the gel bead toward the bulk phase, rupturing the gel [40].

2.1.4. Supercritical drying

The most important and the last step in making an aerogel is the supercritical drying. If using the ambient pressure drying, the liquid inside a porous material is evaporated, and the produced gas is continuously removed from the system. Thus, during such drying technique there are two phases (liquid and gas), consequently, there are interfacial tension forces (γ) builds on the gel structure, which leads to a capillary pressure difference (ΔP) sustained at the liquid and gas interface. For a given capillary radius r the capillary pressure is given by the Young-Laplace equation (Equation 1).

$$\Delta P = \frac{2\gamma \cos \theta}{r} \quad \text{Equation (1)}$$

Such capillary pressure difference at the liquid gas interface can vary from 40 - 100 MPa (400 - 1000 bar) for a pore size in the range of 10 - 100 nm, which may lead to pore collapse [43], [44].

The two-phase boundary could be avoided by removing the solvent from the gel above the critical

temperature and pressure of the liquid entrapped in the gel matrix (Figure 3.). If the liquid and gaseous phases are compressed and heated to the critical point, they are driven to be in a single-phase, thus, the two phases boundary is diminished, and then by depressurization to the atmospheric pressure and cooling down to the room temperature, the liquid inside the pores is extracted in a gaseous phase without crossing the vapor liquid saturation curve.

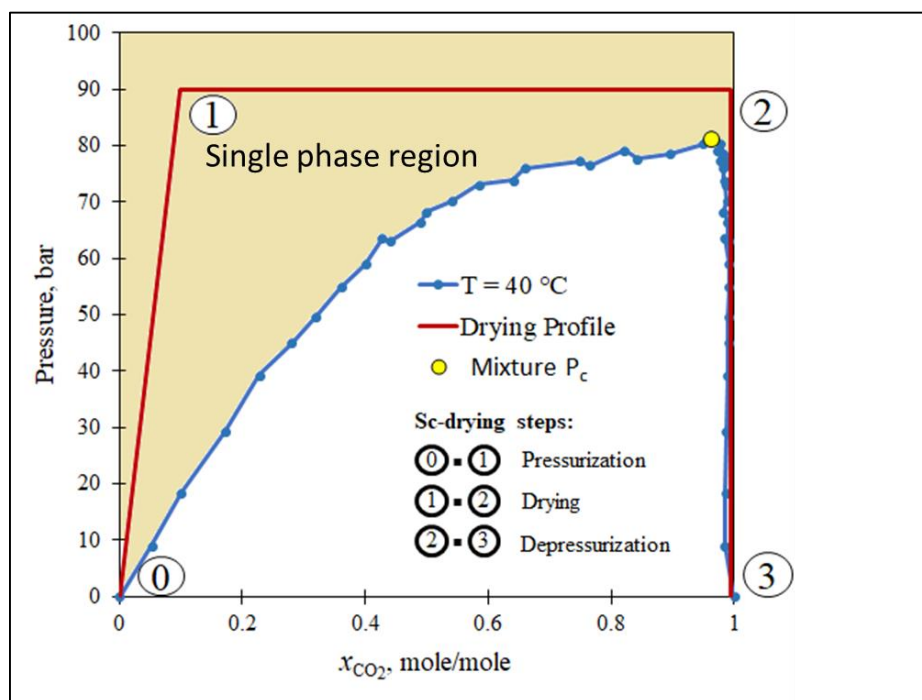


Figure 3. The binary phase diagram of supercritical drying for ethanol/ CO₂ mixture.

The old fashion approach of supercritical drying followed by Kistler was to exchange water first with ethanol and then extract the ethanol with supercritical ethyl ether, because of its lower critical temperature (T_c) and critical pressure (P_c) and reactivity [3]. In 1985 Tewari et al. proposed using of supercritical carbon dioxide (CO₂) instead of ethyl ether, which has lower supercritical pressure and temperature ($T_{cr} = 31\text{ }^\circ\text{C}$ and $P_{cr} = 7.4\text{ MPa}$) [45]. Many solvents were later suggested to be used in supercritical drying. However, the most popular solvent is still CO₂, because of being environment friendly, recoverable, low energy demanding, non-flammable and nontoxic.

It was found that both the drying time and the overall drying kinetics are strongly dependent on the gel thickness. Thus, for gel monoliths the drying time is limited by the diffusion length within the gel network. Therefore, an increase in the pressure and/ or decrease in the temperature are expected to lower the diffusion rate within the gel network, and consequently slow down the drying process. Besides, increasing the flowrate of the CO₂ accelerates the outer mass transport and the drying [46]–[52]. Accordingly, the supercritical drying process of particles is expected to be faster compared to the monolith of an equivalent volume, this refer to the shorter diffusion path within the gel. Selmer et al. (2019) showed in their theoretical model that the drying time for microparticles (~ 100 μm) is very short being even in the range of seconds [52].

2.2. Current aerogel uses and potential applications in life sciences

Because of their outstanding properties and tunable shape and size, aerogels found applications in many fields. Table 1 highlights examples for the most common applications of the respective aerogel.

Table 1. Examples for the most common applications of the respective aerogels.

| Aerogel precursor | Application | Reference |
|--------------------------|---|------------------|
| Silica | Thermal insulators, electrodes, batteries capacitors, microelectronics, microwave electronics, high voltage insulators, cherenkov detectors, acoustic devices, aerospace applications, green technology, biosensors and diagnostics, cosmetics and drug delivery applications | [6], [53]–[67] |
| Carbon | Super-capacitors, solar-energy collectors, catalysis | [68]–[70] |
| NCF/collagen | Tissue engineering and wound dressing | [71] |
| Alginate | Drug delivery applications | [12], [32], [72] |
| Cellulose | Thermal insulation and oil absorption | [73]–[75] |
| Alginate/ starch | Tissue engineering and wound dressing | [76] |
| Alginate/pectin | Drug delivery | [77] |

Although the current aerogel application in the market is mainly as thermal insulator, further applications are developed in the life sciences such as in the cosmetics, the pharmaceuticals and the biomedical fields.

2.2.1. Cosmetics applications of aerogels

Because of their benefits, several cosmetics and personal care companies are using aerogels within their formulations for the skin and beauty care applications, such as fragrance retention and controlled release, anti-caking and free-flow, superior oil and sebum absorption, low-gloss, matting optical effects and highly efficient viscosity enhancement of oil phase [67].

Silicasilylate aerogel particles in the size range of 5 - 15 μm are currently produced in the market by DOW chemicals under the name of DOWSIL™ VM-2270 Aerogel. These particles are completely hydrophobic and can be used in hair care, skincare, fragrance delivery, and antiperspirants / deodorants. L'Oréal reported in a study that the silicasilylate aerogel-based formula appears can be considered a high promising material for concealing the facial skin shine [78]. L'Oréal has also discovered that a combination of UV filter with TiO_2 and hydrophobic silica aerogel particles, creates effective and aesthetically pleasing sunscreen formulas [79]. In another patent for L'Oréal, they described using of a mixture of silica silylate aerogel particles and silicone oils in make-up products that can provide a matte and soft-focus deposit [80].

2.2.2. Biomedical applications of aerogels

2.2.2.1. Wound dressing applications of aerogels

The optimal wound dressing material should be able to absorb wound exudates while keeping the wound moist, insulate the wound to keep it at an appropriate biological temperature, allow gases to permeate through the dressing to allow for oxygen exchange and exhibit desirable mechanical characteristics so they are easy to handle but remain stable for extended periods of time [81]. In the case of medicated wound dressings, the dressing material preferred to have a high inner surface

area to allow for loading and sustained release of the drug[81]. Thus, aerogels present a suitable option for wound dressing, specifically, bio-based aerogels, because of their high stability, low toxicity, non-allergenic characteristics and good biological performance [82].

Several aerogels have been investigated as a wound dressing material. For example, aerogel microcapsules consisted of a core made from amidated pectin and loaded with antibacterial drug, and a shell consisting of high mannuronic content alginate was prepared by De Cicco, Felicetta, et al. (2016), and it was found that the drug release was prolonged till 48 h [83]. Another study was done on vancomycin-loaded chitosan aerogel particles. It was found in the cell studies with fibroblasts and antimicrobial tests against *S. aureus* that the vancomycin-loaded aerogel particles were cytocompatible and effective in preventing high bacterial loads at the wound site [84]. Another study on alginate aerogel carrying zinc cations indicated a potential anti-inflammatory activity of prepared aerogel [85].

2.2.2.2. Tissue engineering applications of aerogels

The high porosity and the interconnectivity of mesopores in the aerogels give them the features to be used as scaffolds for promoting cell attachment and vascularization, to allow the transport of nutrient and waste for tissue regeneration [86]. In the recent years, aerogel scaffolds have been made of several biomaterials such as cellulose, chitosan, alginate and silk.

The sulfated cross-linked cellulose nanocrystal aerogel was investigated for bone tissue scaffolding applications, and it showed increased bone volume fraction up to 50 %, compared to controls. It indicated the ability of this aerogel to facilitate bone growth after implantation in bone defects [87]. Silk fibroin aerogel was *in vitro* examined as a scaffold for skin regeneration, and it demonstrate the cytocompatibility and the potential for such application [88]. Another study was

done on the alginate–lignin aerogels revealed the presence of the suitable textural and morphological properties for tissue engineering applications [89]. A recent study was performed on the chitosan aerogel proved that the proposed aerogels were biocompatible and have a positive effect on fibroblasts proliferation, thus, it can be applied in tissue engineering for skin regeneration [90].

Yin et al. (2010) prepared polyurea nanoencapsulated surfactant-templated aerogel. It was found that the produced aerogel has a suitable biocompatibility toward platelets, plasma, and vascular endothelial cells. Thus, it has the potential to be used in blood implantable devices [91].

2.2.3. Pharmaceutical applications of aerogels

Bio-based aerogels, mainly polysaccharides and proteins aerogels, have proven themselves as promising drug carriers due to their biocompatibility, biodegradability and the large variety of chemical functionalities [37]. The large surface area and the open pore structure, allow an effective loading of an active pharmaceutical ingredient inside the aerogel, therefore, enhance the bioavailability [35].

Incorporating a drug into the aerogel can be obtained using different strategies: (a) during the sol-gel process; (b) into the gel matrix during the solvent exchange; (c) in the gel matrix during the supercritical drying; (d) in the aerogel matrix through a supercritical impregnation. For drug delivery systems composed of biodegradable and water-soluble materials, three important factors may be involved in the drug release process; diffusion, dissolution and polymeric matrix erosion upon degradation. The subsequent drug release is also governed by the drug-aerogel interactions and the hydrophobicity of the formulations [82].

Because of its high porosity and extreme low density and therefore expected good flowability, aerogels are likely to meet the requirement of being an efficient glidant to improve the flow properties

of the tableting material. For example, the flowability of starch aerogel particles have been studied showing comparable results to other admixtures used in oral formulation like spray-dried lactose. Nevertheless, to approve such application more systematic research has to be implemented [92].

2.2.3.1. Aerogel for oral drug delivery application

Biobased aerogel drug carriers were found to meet the challenges of oral drug delivery, especially regarding the solubility limitation of drugs class II and IV, and the stability against the harsh conditions of the gastrointestinal tract including the proteolytic enzymes activity and the pH. The main strategies for improving a drug solubility or dissolution rate by aerogel technology is related to the increase in the surface area of the drug carrier, the reduction of the drug crystal size and the drug amorphization [93].

Silica aerogels were the first type of aerogels to be investigated as an oral drug carrier. And they were considered good candidates for such rout of delivery because of their large surface area, non-toxicity, versatile and well-known sol-gel chemistry as well as its possibilities of derivatization. Smirnova et al. were one of the pioneers in studying the potential of using silica aerogels as oral drug delivery system. In their study Smirnova et al. (2004), silica aerogels were prepared and loaded with several drugs by adsorption from their solutions in supercritical CO₂. It was found that the studied drugs demonstrated a high loading efficiency. Also, it was found that the drugs adsorbed on hydrophilic silica aerogels have faster dissolution rates than the corresponding crystalline drugs [64]. In a recent study of Wang et al. (2019) the authors investigated the feasibility of using silica aerogel delivery system for oral administration of the anticancer drug paclitaxel. It was found that the bioavailability and the drug effectiveness to inhibit the tumor growth were improved, as well as the side effects were reduced [65].

Aerogels derived from polysaccharides (such as starch, pectin and alginate), proteins, as well as hybrid aerogels containing silica and biopolymers were also proposed for the oral administration route. In a study of García-González et al., starch, pectin and alginate-based aerogels were investigated as drug carriers for oral administration of a poorly water soluble drugs ketoprofen and benzoic acid. A controlled drug release from pectin and alginate aerogel particles was found, the release profile fitted Gallagher-Corrigan model with different relative contribution of erosion and diffusion mechanisms depending on the matrix composition. The release from starch aerogel microspheres was driven by dissolution, fitting the first-order kinetics due to the rigid starch aerogel structure [15]. If talking about targeting the lower GI-tract, pectin is a very suitable precursor because of its stability in the stomach, so a drug carrier can be design by which the drug is mostly released in the colon where pectin is degraded by the microflora [94]. In other study citrus and apple pectin aerogels were investigated for potential pharmaceutical applications. Theophylline and nicotinic acid were used as model drugs for the dissolution study. It was found that citrus pectin aerogels have more controlled release behavior higher release rate (100 %) than apple pectin aerogels, this can be directly related to the slower degradation rate of the latter [95].

Another study compared the release behaviour of nifedipine from alginate and pectin aerogels in a simulated gastrointestinal media. It was found that around 20 % of nifedipine was released from alginate aerogels and around 30 % from pectin aerogels within the first 1-2 h in an acidic medium, while the drug release in PBS showed faster drug release reaching 100 % from both aerogels within 5 h.

Veronovski et al. (2013) investigated in there study the effect of membranes number on the release of nicotinic acid from alginate multi-membranes spherical aerogel. It was found that it is possible to increase the drug loading and to prolong the drug release by adding more membranes around

the core. Moreover, the burst drug release may be eliminated by increasing the amount of drug inside the multi-membrane spheres [96].

2.2.3.2. Aerogel for transdermal drug delivery application

Aerogels have been shown to be a potential transdermal drug delivery vehicle. Although the most studied transdermal application of aerogel is in the field of medicated wound dressing material (section 2.2.2.1), aerogels were investigated as a transdermal drug carrier for other purposes. Guenther et al. (2008) studied the Dithranol loaded silica aerogels as dermal drug delivery systems. It was found that dithranol adsorbed on hydrophilic silica aerogels exhibited superior penetration behavior compared to that of the standard ointment [13].

2.2.3.3. Aerogel for pulmonary drug delivery application

The low density and high porosity of aerogels is expected to provide them with a high air flowability, which is specifically promising for their use as a pulmonary drug carrier. By this route, drug delivery can be achieved to treat a respiratory disease, or the drug can be delivered to the systemic circulation. In the former case, the targeted drug delivery minimizes the systemic side effects, avoid the liver first pass metabolism and the offer the possibility of delivering small molecules and large proteins, while when using the lungs for systemic administration a non-invasive and painless alternative is achieved [97], [98].

So far, the only study on aerogels for pulmonary drug delivery was conducted by López-Iglesias et al., they prepared alginate aerogel particles by thermal inkjet printing technology. The prepared particles were loaded with salbutamol sulphate, as a model drug for the purpose of sustained pulmonary delivery. The used method allowed the preparation of nanoporous microparticles with

a modified salbutamol sulphate release profile and a suitable aerodynamic performance for oral inhalation purposes [19].

2.3. Challenges associated to pulmonary drug carrier

Deposition of particles in the lung depends not only on physiological factors such as airway humidity, breathing frequency, breathing rate and holding of breaths, but also on the particle properties such as the aerodynamic diameter, the morphology and geometry [99]. Drug delivery to the lung can be achieved either with liquid solutions or suspensions in nebulizers and pressurized metered-dose inhalers (pMDI), or with dry powder inhalers (DPI) (Figure 4).

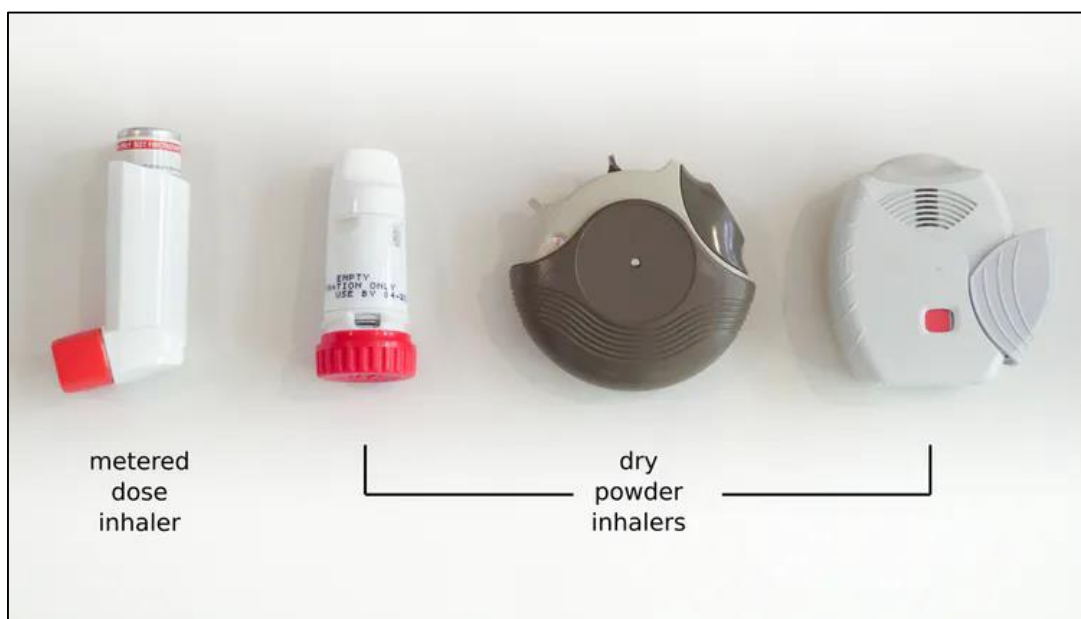


Figure 4 metered dose inhaler and dry powder inhaler [100].

Nebulizers utilize an air jet or ultrasound unit to convert a drug solution or suspension into fine droplets for inhalation, but they have the disadvantage of being relatively expensive, the contents being easily contaminated and not being portable. The pressurized metered-dose inhaler has the

limitation of a high oral deposition and a limited dose and range of drugs. In contrast, the DPI is propellant-free, portable, inexpensive, and provides better formulation stability than the liquid dosage forms [101].

In addition to the biodegradability, there is an important characteristic that must be considered in the engineering of pulmonary particles delivered by DPIs, which is the aerodynamic diameter (d_A), representing a function of the particle density and particle size. The d_A can be estimated using the following semi-empirical equation:

$$d_A = d_v \sqrt{\frac{\rho}{C_c \chi \rho_0}} \quad \text{Equation 2}$$

where d_v is the geometrical diameter, ρ_0 is the unit density, ρ is the particle true density, χ is the dynamic shape factor defined as the ratio between the drag force on a particle to the drag force on the particle volume-equivalent sphere at the same velocity, which is assumed to be that of spherical particles, i.e. $\chi=1$, and C_c is the slip correction (also = 1) for particles above 1 μm in diameter [18]. Accordingly, for the inhaled particles to achieve deep lung deposition, they need to possess low particle densities and an optimum particle geometrical size, to obtain d_A values in the range between 0.5 and 5 μm which is the requirement for pulmonary deposition [102]. With the production of large porous particles with geometric diameters greater than 5 μm and d_A less than 5 μm , the tendency for aggregation of these porous particles become much lower than that of their non-porous counterparts, because of their larger diameters and lower densities [103].

Although numerous efforts have been made to develop controlled release systems for the lungs, the currently available options in the market have mainly fast drug release behavior [104]. Thus,

the controlled drug delivery to the pulmonary system still a challenging aspect for the pharmaceutical researchers.

2.4. Future of pulmonary drug delivery by DPI

Currently, there are 100 new inhaled drugs in the pharma development pipeline have been already selected for DPI drug delivery and are expected to achieve an increasing market [105]. However, the future DPI is expected to overcome the following challenges which are summarized in table 2 [106]:

Table 2. Future challenges and objectives for DPIs [106].

| Challenge/objective | Solution |
|--|--|
| Improving patient compliance | <ul style="list-style-type: none"> • Simple, self-intuitive DPI design • Feedback on inhalation performance |
| Improving safety | <ul style="list-style-type: none"> • avoid unnecessary excipients • Disposable inhalers for special applications, such as hygroscopic drugs and vaccines |
| Improving efficacy | <ul style="list-style-type: none"> • More powerful inhaler design (balancing between interparticulate, dispersion, and deposition forces) |
| Improving patient adherence to the therapy | <ul style="list-style-type: none"> • Minimizing dose frequency • Minimal number of handling step • Simple, compact DPI design |
| Reducing patient errors | <ul style="list-style-type: none"> • Simple, self-intuitive DPI design |

| | |
|---------------------------------------|---|
| Reducing the costs of inhaled therapy | <ul style="list-style-type: none"> • Minimal number of handling steps • The same inhaler for all inhaled medication |
| Specialized inhalation | <ul style="list-style-type: none"> • Simple and cheap at the same time but effective DPI design • Simple drug formulation technologies • Patient (group) tailored DPI design |

2.5. Polysaccharides as potential drug carrier

Polysaccharides are the polymers of monosaccharides which can be derived from algal origin (e.g. alginate), plant origin (e.g. pectin, cellulose), microbial origin (e.g. dextran, xanthan gum), and animal origin (e.g. chitosan, hyaluronic acid) [107]. Polysaccharides have a wide range of molecular weight, a large number of reactive groups and a diverse chemical composition, which is reflected on the structure and in property. They can be generally divided into positively charged and negatively charged ones (alginate, hyaluronic acid, pectin, etc.). Polysaccharides are safe, non-toxic, highly stable and biodegradable [108]. Most of natural polysaccharides have hydrophilic groups such as carboxyl, hydroxyl and amino groups, which are able to form a non-covalent bond with the biological tissues [109]. Such interaction may prolong the residence time and therefore increase the drug absorbance if used as a drug carrier.

2.5.1. Chemistry of alginate

Alginates are linear acids copolymers composed of β -1,4- d-mannuronic acid and -l-guluronic acid monomers (Figure 4), forming homogenous or heterogeneous block like patterns. Alginates have

been used in the food industry, in pharmaceuticals and in medicine again because of its non-toxicity, biodegradability and biocompatibility [110]–[112]. Alginate gelation takes place in the presence of divalent cations such as Ca^{2+} , Ba^{2+} or Sr^{2+} . Several authors have reported that the physical properties of calcium alginate gel can be improved when a blend of alginate-biopolymer are used and the synergistic effects appearing due to the addition of hyaluronic acid to the gel form is expected to be prevailed in the aerogel product [113], [114]. The major shortcoming of calcium-alginate cross linked drug delivery systems is their sensitivity in the intestinal and the pulmonary regions, where Alg matrix shows high swellability and erosion, leading to fast release of drug from its matrix. Furthermore, adhesion of Alg to mucosal tissues is reduced when cross-linked with divalent ions [115]. To overcome these drawbacks, an alternative proposed is the incorporation of second biopolymer into Alg matrix, forming a homogenous blend with improved physiochemical properties as compared to pure Alg matrix, in an attempt to prolong the rates of release profile and improve mucoadhesive properties. Several authors have reported the improved properties of calcium-Alg gels when Alg-biopolymer hybrid are used [113], [114]. In this regard, Morais et al. (2013) showed that alginate-hyaluronic acid calcium hydrogel has a higher degradation rate than alginate hydrogel, processing conditions were the same for both materials. In the case of hyaluronic acid, its hydrophilic nature, prevalence and high tolerance in the lung make the biopolymer be a potential material for pulmonary drug delivery [116]–[118].

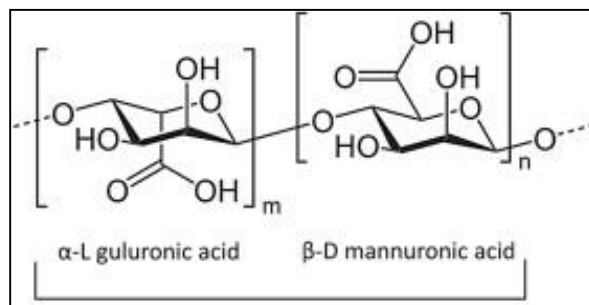


Figure 5. Alginate chemical structure.

2.5.2. Chemistry of hyaluronic Acid

Hyaluronic acid (**HA**) is a naturally occurring polysaccharide that consists of N-acetyl-d-glucosamine and -glucuronic acid (Figure 5), which was discovered for the first time in bovine vitreous humour by Meyer and Palmer in 1934. It is found in the intercellular matrix of most vertebrate connective tissues, especially skin, HA has a molecular size ranges from 1000 to 10,000,000 Da [119], [120]. In addition to its biodegradability, HA possesses mucoadhesive properties which are expected to provide much longer pulmonary retention [116]. Many studies reported the advantageous effect of HA on the drug bioavailability and release if using it in the drug delivery system [121]–[123]. In the field of pulmonary drug delivery, HA has been included as component of inhaled formulation of insulin to enhance absorption and controlled release. Morimoto et al. (2001) reported that incorporation of HA (0.1% and 0.2% w/v) to the insulin solution resulted in an enhanced pulmonary absorption [124]. Furthermore, Li et al. have reported that, because of its mucoadhesive properties, HA has prolonged the pulmonary retention to 8hr and reduced the systematic exposure of inhaled medicine [116]. Therefore, hyaluronic acid, with its biodegradability, biomucoadhesive properties; popularity in the medical field and high tolerance in lung conditions, is a potential biomaterial for pulmonary drug delivery.

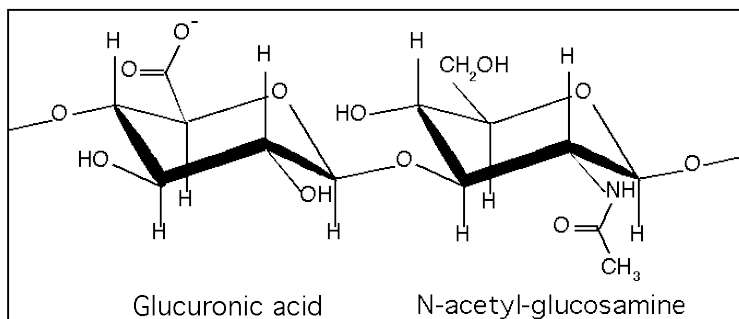


Figure 6. Chemical structure of hyaluronic acid.

2.6. Conventional methods for the production of pulmonary drug carrier

Many conventional techniques such as spray drying, freeze drying and jet milling, are available to produce DPI formulations [125]. However, these techniques have a number of limitations such as poor control over the particle size, its distribution, shape and crystallinity.

2.7. Spray drying

Spray drying has been established as a standard method to produce particles for dry powder inhalers in the lower micrometer range. In this process, the drug within an excipient solution is sprayed through a nozzle into a drying chamber where a hot air evaporates the solvent. The dried particles are collected afterward by cyclone separators [126].

Denaturation of certain proteins and lack of control over particle morphology are the major limitation of this method. The denaturation of proteins is referring to the high shear rates caused by the atomization of the liquid. Nevertheless, this denaturation may be avoided by using surfactants and excipients which stabilize the proteins during and after spray drying. The use of such surfactants and excipients might be a disadvantages as high amounts are usually needed. The morphology of particles might not be spherical because they may undergo crumpling, and buckling, which leads to the formation of convoluted surfaces, holes and voids [127].

2.7.1. Spray freeze drying

The principle of spray freeze drying (SFD), an advanced particle engineering method, was first introduced in early 1990s. It involves the atomization of a drug solution, but instead of rapid drying in hot air the drug solution is sprayed into vessel containing cold vapor over a cryogenic liquid (e.g. liquid nitrogen) as followed by lyophilization producing porous micronized or nanosized particles with a large specific surface area and high product yield (almost 100%) [128]. Temperature sensitive proteins and lipids such as insulin and plasmid DNA can also be formulated using this method [129], [130] However, the high cost of the used excipients and freezing liquid makes this method extremely expensive and restricted for only expensive drugs.

2.7.2. Jet milling

Jet milling is a very traditional method of micronization that is used at the industrial level. In this method large particles in the lower millimeters range are grinded by using a high speed jet of compressed air or inert gas (nitrogen or air). The gas fed through nozzles at high pressures, which upon exit from nozzle losses their pressure energy to kinetic energy, consequently accelerating the solid particles to sonic velocities [131]. The particles get fracture by colliding with each other or with the walls of the container. The smaller particles are removed from milling chamber by discharge gas stream, while the larger particles are moved to the walls of the milling chamber by centrifugal forces. The major limitations for this technique is the large particle size distribution, the possibility of physical and chemical degradation of the active pharmaceutical ingredients, especially of proteins [132].

2.8. Emulsion gelation and supercritical drying as novel technology for drug carrier production

From the previously mentioned techniques which are commercially used for particles production for the purpose of pulmonary drug delivery, it is apparent that each technique possesses serious disadvantages; the sphericity of the particles, the protection of the active pharmaceutical ingredient and the controlled drug release cannot be guaranteed. These problems need to be addressed in order to have a suitable pulmonary drug carrier. The drawbacks of the previously mentioned particles production techniques may be overcome by the use of the emulsion gelation technique coupled with the supercritical CO₂ technology [47], [133]. The emulsion gelation technique allows to produce spherical particles, while the supercritical CO₂ technology enables to preserve inner porous structure. Resulting in highly porous particles with low density (0.05-0.3 g/cm³) and high surface areas suitable for loading controlled amount of drug in an amorphous state using same SCF technology [15], [134].

2.8.1. Emulsion formation

An emulsion can be defined as a biphasic system whereby one immiscible liquid phase (the dispersed/inner phase) is uniformly dispersed as droplets inside a second phase (the continuous /outer phase). Since emulsions are a thermodynamically unstable system, a third agent, namely, the emulsifier is added to stabilize the system [135].

According to the structure of their system, emulsions are classified into the following types [136]:

- i. Water-in-oil (W/O) and oil-in-water O/W macroemulsions: These emulsions usually have an inner phase droplet sizes in the range of 0.1–5 μm
- ii. Multiple emulsion, it is a complex emulsion which can be water-in-oil-in-water (W/O/W) emulsion or oil-in-water-in-oil (O/W/O) emulsion

- iii. Nanoemulsions: these usually have a size range of 20–100 nm. They are only kinetically stable.
- iv. Micellar emulsions or microemulsions: they are usually in the size range of 5–50 nm. They are thermodynamically stable.

2.8.2. Forces between emulsion droplets

Generally speaking, there are three main interaction forces between emulsion droplets; van der Waals attraction, electrostatic repulsion and steric repulsion.

2.8.2.1. Van der Waals attraction

The van der Waals attraction between atoms or molecules is classified into three different types: dipole–dipole (Keesom), dipole-induced dipole (Debye), and dispersion (London) interactions; Although dipole–dipole or dipole-induced dipole attraction is large, they tend to cancel each other because of being opposed. Thus, the most important forces are the London dispersion which is a result of charge fluctuations. The London dispersion forces (G_a) is inversely proportional to the sixth power of the separation distance r between the atoms or molecules (Equation 3).

$$G_a = \frac{-\beta}{r^6} \quad \text{Equation 3}$$

where r is the separation distance and β is a London dispersion constant that is determined by measuring polarizability of the atom or molecule.

Hamaker suggested that, in case of emulsion at close distances between droplets, London dispersion interaction can be combined to give strong van der Waals attraction (G_A). For two droplets in an emulsion of equal radii R separated by distance h , the van der Waals attraction is described by following equation [137]:

$$G_A = \frac{(A_{11}^{1/2} - A_{22}^{1/2})^2 R}{12 h} \quad \text{Equation 4}$$

Where, A_{11} and A_{22} are the Hamaker constants of the inner phase droplets and the outer phase, respectively. While Hamaker constant depends on the number of atoms or molecules per unit volume q and London dispersion constant β (Equation 5)

$$A = \pi^2 q^2 \beta \quad \text{Equation 5}$$

2.8.2.2. **Electrostatic repulsion**

Electrostatic repulsion is produced if an ionic surfactant is adsorbed on the droplet with a charged surface. This layer is then neutralized by counter ions from the outer phase forming electrical double layer as illustrated in Figure 6. According to Gouy–Chapman and Stern, the surface potential decreases linearly and then exponentially with increase of distance (x) [138].

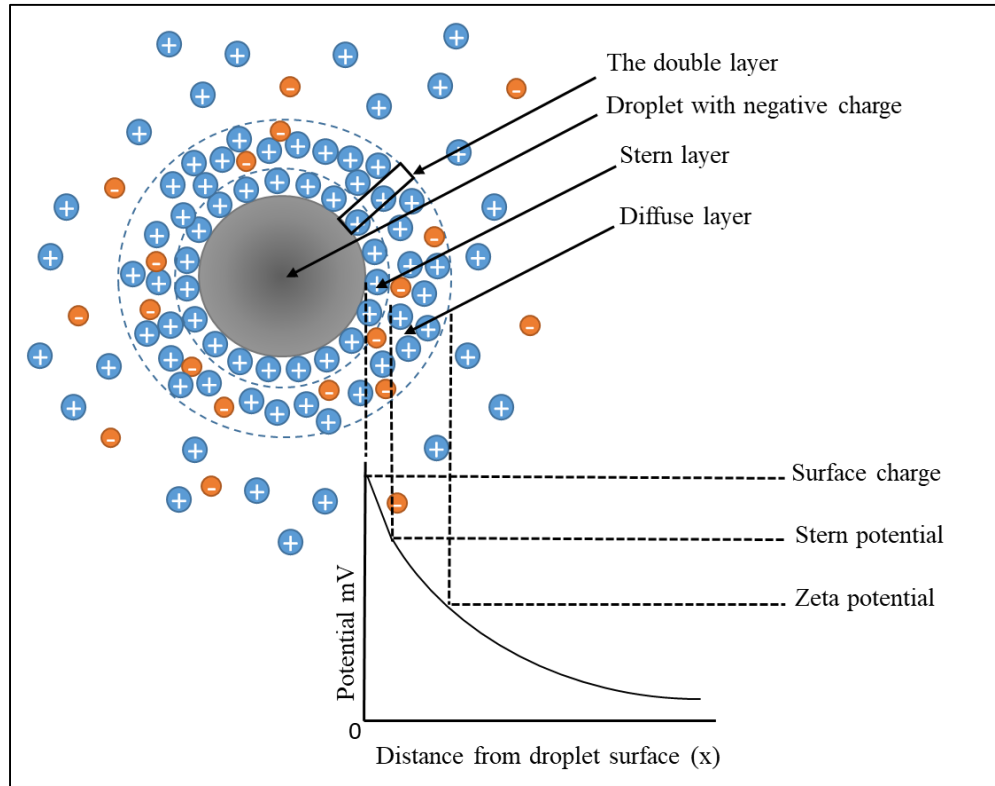


Figure 7. Schematic picture of the structure of the double layer according to Gouy–Chapman and Stern.

When charged droplets in an emulsion approach each other the double layer begins to overlap and the droplet separation distance becomes less than twice the double-layer thickness, consequently repulsion occurs. According to the expression for repulsive interaction G_{el} is given by Equation 6, the higher the value of surface potential the higher the repulsion and the weaker the flocculation [137].

$$G_{el} = 2\pi R \epsilon_r \epsilon_o \psi_o^2 \ln[1 + \exp(-kh)] \quad \text{Equation 6}$$

where, ϵ_r is the relative permittivity and ϵ_o is the permittivity of free space, ψ_o is the surface potential. k is the Debye-Hückel parameter; $1/k$ is the double layer thickness, which is given by following equation:

$$\left(\frac{1}{k}\right) = \left(\frac{\epsilon_r \epsilon_0 kT}{2n_o Z_i^2 e^2}\right) \quad \text{Equation 7}$$

where, k is the Boltzmann constant, T is the absolute temperature, n_o is the number of ions per unit volume of each type present in bulk solution, Z_i is the valency of the ions, and e is the electronic charge. Thus, the double-layer extension decreases if increase of electrolyte concentration and valency, consequently, the repulsion decreases and the flocculation may increase [136].

2.8.2.3. Steric repulsion

This type of repulsion is produced in emulsion if using nonionic surfactants. The adsorption of nonionic surfactants on the droplets produces an adsorbed layer with certain thickness (δ). This thickness can be strongly solvated by the molecules of the solvent (outer phase) when the latter is a good solvent for the surfactant. If two droplets approach to each other at a surface-to-surface distance of separation that is smaller than 2δ , the adsorbed layers can be compressed or overlapped, leading to strong repulsion [139].

2.8.3. Thermodynamics aspects of stable emulsions and destabilization mechanisms

Spontaneous stability is not a characteristic of emulsions, with the exception of microemulsions, oil and the water mixture will be eventually separated into two distinctive phases in the absence of a stabilizing material. The thermodynamics-based description of emulsions starts with the derivation of the Gibbs free energy equation [140]:

$$\Delta G = A\sigma - T\Delta S \quad \text{Equation 8}$$

where, σ is the interfacial tension, A is the interfacial area, T is the temperature and ΔS is the entropy of mixing.

The thermodynamic stability of the emulsion is determined by ΔG . If ΔG is positive the system is thermodynamically unstable and the formation of the emulsion is nonspontaneous, while if ΔG is negative a spontaneous emulsification will happen. From the above equation, there are four ways to achieve a thermodynamically stable emulsion: Increasing the temperature, increasing the entropy, reducing the surface area and reducing the interfacial tension [136].

Destabilization of an emulsion is a process in which emulsion is separated into its original component phases based on their density difference. Such separation is controlled by thermodynamics and depends mainly on the particle size distribution, any external destabilizer and the density difference between the inner phase and the outer phase. The various destabilization mechanisms in emulsions are illustrated in Figure 7. The physical phenomena involved in each breakdown process are complex, and more than one destabilization mechanism may happen simultaneously [136].

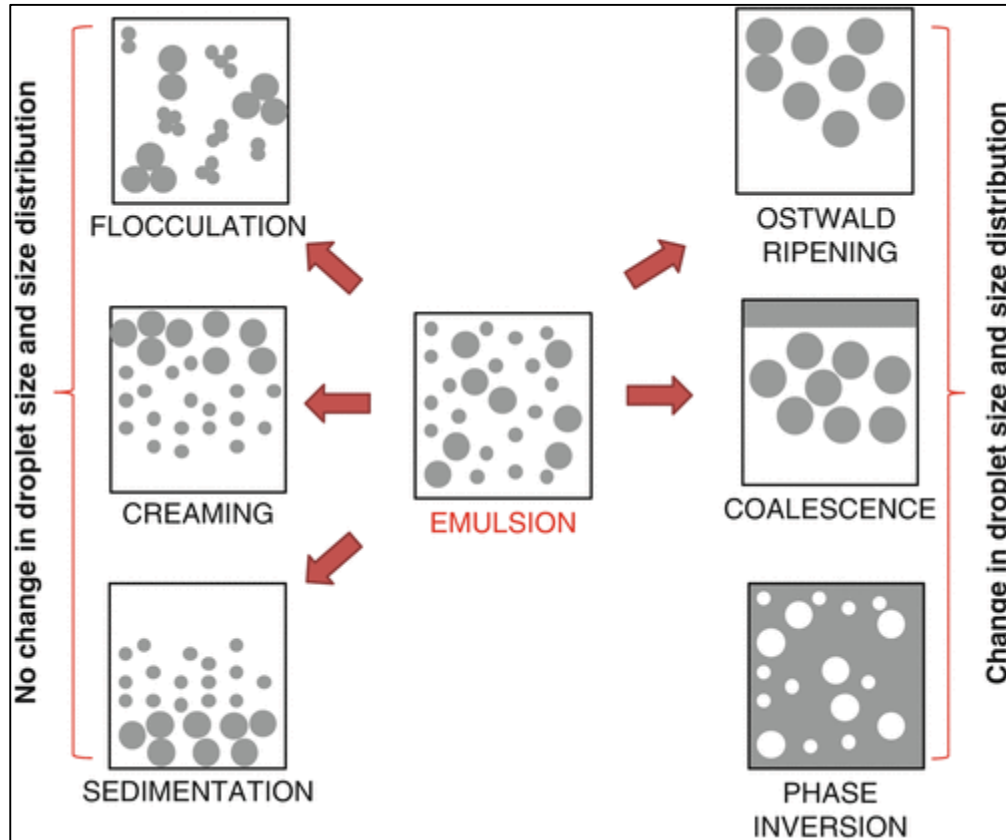


Figure 8. Schematic representation of the various destabilization mechanisms in emulsion [141].

2.8.3.1. Creaming and sedimentation

This emulsion destabilization process results from external forces, usually gravitational or centrifugal. When such forces exceed the thermal motion of the droplets (Brownian motion), a concentration gradient builds up in the system with larger drops moving faster towards top or to the bottom of the container depending on their density difference with the continuous phase. Referring to the Stokes (Equation 9), the density difference between the two phases plays a key role in the creaming phenomenon, when the density of the inner phase is higher than that of the outer phase, sedimentation occurs and the settling velocity of each droplet is an indicator to the

rate of separation of the emulsion. While creaming occurs if the inner phase density is lighter than the outer phase.

$$V_s = \frac{2r^2(\rho_p - \rho_f)g}{9\eta} \quad \text{Equation 9}$$

where V_s is the settling velocity, d is the diameter of the sphere, ρ_p is the density of the sphere, ρ_f is the density of the outer phase, g is the acceleration due to gravity and η is the viscosity of the outer phase

Such destabilization processes may be reduced by reducing density difference between the inner and the outer phases, by increasing viscosity of the outer phase and reducing the inner phase droplet sizes [136].

2.8.3.2. Flocculation

Flocculation refers to aggregation of the droplets into larger units without the interface rupture. It is a natural result of the van der Waals attraction forces, thus, it might be strong or weak, depending on the magnitude of the attractive energy involved. Such destabilization occurs when there is no sufficient repulsion to keep the droplets apart to distances [142].

In the absence of repulsion forces between emulsion droplets, flocculation might rapidly lead to produce large clusters, thus, accelerates sedimentation. To counteract flocculation, two main types of repulsion can be produced depending on the used emulsifier: Steric repulsion (resulting from the presence of adsorbed surfactant or polymer layers and electrostatic repulsion (resulting from the creation of double layers) [136].

2.8.3.3. Coalescence

Coalescence is an irreversible process by which two or more droplets in an emulsion are merged during contact forming a single daughter droplet, ending with a complete separation of the emulsion into two distinct liquid phases. This refers to the thinning of the liquid film between the droplets. The driving force for coalescence is the film fluctuations, thus, the droplets approach each other very closely, whereby the van der Waals force is strong which prevent their separation. To inhibit coalescence some approaches may be followed [143]:

- Utilize surfactants having hydrophilic groups which can be sparingly soluble in an oil phase
- Strengthen the interfacial film
- Add polymeric emulsifiers and powder materials which effectively inhibit coalescence.

2.8.3.4. Ostwald Ripening

Ostwald ripening results from the finite solubility of the liquid phases. Even liquids that are referred to be immiscible in each other often have mutual solubility that are not negligible. With emulsions, which are usually polydisperse, the smaller droplets will have larger solubility when compared with the larger ones because of curvature effects. With time, individual molecules or atoms diffuse from smaller droplets to larger droplets, and the droplet size distribution shifts to larger values [136].

2.8.3.5. Phase inversion

Phase inversion is a destabilization mechanism in which the structure of the emulsion is inverted; the continuous phase becomes dispersed phase or vice versa. This mechanism is not spontaneous,

it is driven by changes in temperature, pressure, salinity, proportion of continuous and disperse phase or the use of co-surfactant [144].

2.8.4. Emulsion stabilization

The inner phase droplets in an emulsion move continuously because of the gravitational and the thermal effects. However, emulsions may be stabilized by controlling their interface and bulk properties [145]. The most important factors affecting the stability of an emulsion are the interfacial energy and the strength of interfacial film. Lowering of interfacial tension will reduce the interfacial energy, consequently increases the stability of emulsion [146]. This can be achieved by adding a chemical substance to the emulsion namely surfactant (emulsifiers), that alters the interfacial properties if absorbed on the boundary between the two immiscible phases.

2.8.4.1. Role of surfactants in emulsion stability

To prepare an emulsion energy is required to create an interface, thus an increase in the interfacial area leads to an increase in the $A\sigma$ term (according to Equation 8). At the same time if the surface tension is reduced, the $A\sigma$ term is reduced. Therefore, the stability of the emulsion may be enhanced by adding surfactants, which sit evenly at the interfacial layer protecting the inner phase droplets and prevent them from flocculating. Usually, surfactant can be described as a structure with a hydrophilic head and hydrophobic tail. The properties of surfactants may be modified by increasing length of these two parts.

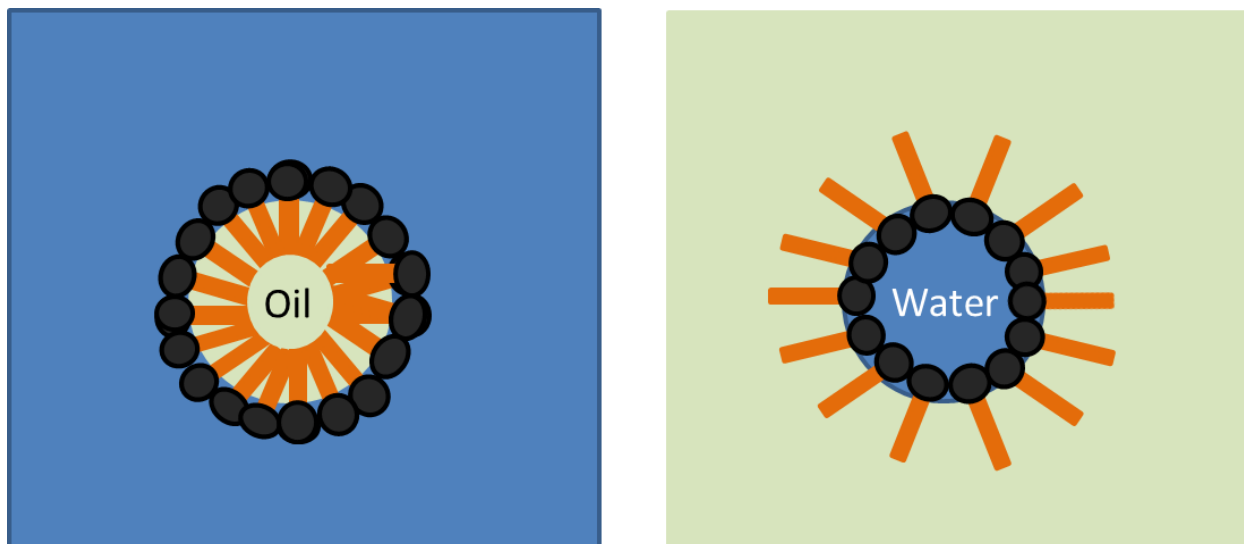


Figure 9. Graphical representation of O/W surfactant (left) and W/O surfactant (right)

In an oil in water O/W emulsion, the hydrophobic tail of a surfactant tends to move away from the water molecules as a result of the hydrophobic interaction, leading to the formation of a hydrophobic compartment surrounded with a hydrophilic shell. While in a water in oil W/O emulsion the hydrophobic chain resides in the oil phase, whereas the hydrophilic group (polar head) resides in the aqueous phase (Figure 9). Emulsions with smaller droplet size have larger interfacial area. Thus, a higher concentration of surfactant is required to cover the large interfacial area, and prevent phase separation.

2.8.4.2. Selection of the surfactant

The selection of different surfactants for different types of emulsions is often done based on an experimental basis. Though, semiempirical scale for surfactant selection was developed by Griffin, this scale called the hydrophile-lipophile balance (HLB), which express the balance of the size and strength of the hydrophilic (polar) and the lipophilic (non-polar) groups of the surfactant [147].

Water-soluble surfactant with a HLB value above 9 is required to prepare an O/W emulsion, to solubilize oils or to obtain detergent action. However, to prepare W/O emulsion, or to combine water soluble materials into an oil, an oil-soluble surfactant with a HLB value below 9 is needed. Thus, the functions of surfactant might be classified according to its HLB. Table 3 shows the classification of surfactant application depending on the HLB value. This scale (Table 3) was created based on the ratio between the hydrophilic to hydrophobic (lipophilic) groups in the surfactant molecule [136]. The surfactant selection (HLB number) depends also on the nature of the oil. Table 4 provides a guide for surfactants selection in a particular oil.

Table 3. Summary of HLB ranges and their application [136].

| HLB range | Application | Example |
|------------------|--------------------|-----------------------------|
| 3-6 | W/O emulsifier | Span 80 and Span 60 |
| 7-9 | Wetting agent | Span 20 |
| 8-18 | O/W emulsifier | Span 20 |
| 13-15 | Detergent | Tween 60 |
| 15-18 | Solubilizer | Tween 20 and Sodium Oleate, |

Table 4. Required HLB numbers to emulsify various oils [136].

| Oil type | Required HLB W/O emulsion | Required HLB O/W emulsion |
|--------------------|--------------------------------------|--------------------------------------|
| Paraffin oil | 4 | 10 |
| Beeswax | 5 | 9 |
| Linolin, anhydrous | 8 | 12 |
| Cyclohexane | - | 15 |
| Toluene | - | 15 |

2.8.5. Predicting droplet size of emulsion

To predict the size of the aerogel particles, which are produced by the emulsion gelation technique and supercritical CO₂ drying, description of the emulsion droplet size is needed. During the emulsification process, the droplets undergo shape deformation (from spherical to ellipsoidal shape), therefore, breakup of droplets because of the disruptive forces caused by stirring result in smaller droplets. Such breakup is a consequence of two opposite hydrodynamic forces acting onto the droplet: The Laplace pressure which retains the spherical shape of the droplets and the disruptive forces caused by stirring which tend to deform the droplets. Such disruptive forces mainly depend on the flow regime during emulsification. In the case of macroemulsions. The most applied theories for predicting the droplet size of an emulsion are Hinze's and Taylor's theories. Hinze's theory is created based on the assumption that the flow caused by stirring is completely turbulent during the emulsification [148]. In contrast, Taylor's theory is applied when the single

droplet breakup occurs under the laminar flow conditions (low Reynold numbers (Re)) [149]. According to Taylor, the inertial forces can be ignored, thus, particle breakup and deformation are mostly resulting from viscous shear stress. Taylor suggested that a droplet will not break unless the applied stress deforming the droplet dominates over the interfacial stress. He described his theory in the form of a dimensionless number called capillary number (Ca), displayed in Equation 10 [149]:

$$Ca = \frac{\eta_c \dot{\gamma} d}{2\sigma} \quad \text{Equation 10}$$

where η_c is the outer phase viscosity, $\dot{\gamma}$ is the shear rate in the outer phase, d is the maximum stable droplet diameter, and σ is the dynamic interfacial tension. In w/o emulsions with a high volume of the outer phase, η_c in the equation is replaced by the apparent emulsion viscosity [150]. According to Taylor, below a critical value of the Ca (Ca_{crit}) the droplet will not break regardless of its deformation. By rearranging Equation 10, the maximum stable droplet size of the emulsion can be estimated as follows:

$$d_{max} = \frac{2Ca_{crit}\sigma}{\eta_c \dot{\gamma}} \quad \text{Equation 11}$$

Taylor showed that Ca_{crit} is the function of the viscosity ratio (λ) which is the ratio between the viscosity of the inner phase and that of the outer phase. Ca_{crit} may be estimated through the five empirical parameters from Equation 12 [151].

$$\log_{10} Ca_{crit} = C_1 + \alpha \log_{10} \lambda + C_3 (\log_{10} \lambda)^2 + \frac{C_2}{\log_{10} \lambda - \log_{10} \lambda_{max}} \quad \text{Equation 12}$$

where $C_1 = -0.506$, $C_2 = -0.115$, $C_3 = 0.124$, $\alpha = -0.0994$ and $\lambda_{max} = 4.08$ (no break-up can be achieved above a viscosity ratio of 4.08 as the droplets begin to rotate rather than deform) [151].

Although Taylor's theory provides a very intuitive understanding of droplet deformation, the most widely used theory in the industry for predicting droplet sizes is Hinze's theory, because it is appropriate to the turbulent flow produced inside a homogenizer or ultrasonicator used in the industry [152].

2.9. Derivation of the objectives of the thesis based on the state of the art

Summarizing the state of the art, there is no comprehensive study bridging the engineering knowledge with the pharmaceutical science to investigate the feasibility of using the emulsion gelation technique and supercritical CO₂ drying to produce aerogel particles which are suitable to deliver active pharmaceutical ingredient to the lungs. Therefore, this work aims to fulfill this gap and to suggest the preparation process of aerogel particles of both Alg and Alg-HA, to get suitable aerodynamic diameters for lung delivery (d_A 0.5 – 5 μm).

Thereby, one of the main objectives is to optimize and control the emulsification process parameters, which are expected to directly affect the inner phase droplet sizes and consequently the final aerogel particles, namely the stirring speed and the inner phase viscosity. It is of special interest to identify the integration mechanism of HA into the matrix of the hybrid aerogel of Alg-HA, as there are no previous studies in the literature describing this system. Another major goal of the thesis is to mathematically predict the d_A of the prepared aerogel particles, and to check the feasibility of this approach by comparing the calculated d_A with the *in vitro* measurements, which were found using the cascade impactor analysis.

Further, in the literature no study has been conducted to test the safety of Alg aerogel when used as oral drug carrier, although many researchers suggested the use of Alg aerogel for such route of administration. Thus, another goal of this thesis was to explore the effect of calcium alginate aerogel on the kidney and liver, and to assess its the effect on the intestinal microbial community, as alginate is broken down in the intestines by the gut microbiota.

3. Materials and methods

3.1. Materials

For the preparation of the aerogel particles for pulmonary drug delivery applications the following materials were used: Sodium Alginate (Alg) (catalogue no. 71238), D-(+)-Gluconic acid δ -lacton (GDL) and Naproxen (CAS: 22204-52-1) were supplied by Sigma Aldrich, Germany. Hyaluronic acid (HA) sodium salt (Glucuronic acid approximately 50 %, pH (0.1 % solution): 6-7.5) of cosmetic grade was purchased from China Xi'an Trend, China. Calcium carbonate (CaCO_3) was supplied by Magnesia, Germany. Ethanol (purity: 99.8 %), methanol (purity: 99.8 %) and glacial acetic acid (purity: 100 %) were provided by Carl Roth, Germany. Span[®] 80 was obtained from Merck, USA. Rapeseed oil was purchased from Henry Lamotte Oils, Germany.

For the liver and kidney *in vivo* toxicity study of calcium alginate aerogel and its effect on the gut microbiota alginic acid (sodium salt) was supplied by BASF, Germany. Calcium chloride (CaCl_2) was purchased from Th. Geyer GmbH & Co. KG, Germany. Carbon dioxide (purity ≥ 99.5 %) was supplied by Praxair (Germany), ethanol 99.8 % was obtained from Carl Roth (Germany). All chemicals were used as received. Commercial diagnostic kits were used to measure ALP, and creatinine kits were purchased from Biostsystems S.A, Spain. The MO BIO'S PowerMax Soil DNA Isolation Kit were purchased from MO BIO Laboratories, USA. Deionized water was used throughout the study.

During the whole study, Carbon dioxide (purity: ≥ 99.5 %) was supplied by Praxair, Germany. Phosphate buffer tablets were purchased from Th. Geyer, Germany. Deionized water was used throughout the whole study.

3.2. Methods

3.2.1. Aerogel particles for pulmonary drug delivery applications

3.2.1.1. Rheological characterization for the emulsion components

3.2.1.1.1. Rheological analysis for the oil and polymers stock solutions

Viscosities as a function of shear rate for the internal and continuous phases as well as their emulsions were measured with Kinexus-pro+ rheometer (Malvern Instruments, UK), using cone and plate geometry (1° cone angle and 65 mm plate diameter) at a constant temperature 25 °C. The shear rate range for rheological measurements was set in the range of 250 - 1600 s⁻¹ for the polymers stock solutions and from 150 to 700 s⁻¹ for the oil. The viscosity of the rapeseed oil was measured at different temperature, moreover, the viscosity of the fresh rapeseed oil was measured and compared with the stored oil for 6 months.

3.2.1.1.2. Rheological study to assess polymers interaction

The possibility for polymer-polymer interaction between Alg and HA was investigated by comparing the experimental viscosity of the intrinsic solution for each polymer as well as their mixtures with their theoretically estimated viscosities which were predicted using the following equation [153]:

$$\ln \eta_{\text{theoretical}} = \phi_{\text{Al}} \ln \eta_{\text{Al}} + \phi_{\text{HA}} \ln \eta_{\text{HA}} \quad \text{Equation 13}$$

where η is the dynamic viscosity and ϕ polymer fraction.

This viscosities analysis was conducted on the solutions and mixtures of a total a total polymer concentration of 0.25 and 1 % w/w and different Alg-HA (w/w) fraction using a Kinexus-pro rheometer (Malvern Instruments, UK), using cone and plate geometry (1° cone angle and 65 mm plate diameter) at a constant temperature 25 °C.

3.2.1.1.3. **Rheological characterization to assess HA interaction with calcium**

In order to assess the HA gelation potential using calcium ions, 1 % w/w HA solution was mixed with different concentrations (0, 2, 5, 10, 15 Mm) of calcium chloride (CaCl₂). The viscosities of these mixtures were measured over time using a Kinexus-pro rheometer (Malvern Instruments, UK), using cone and plate geometry (1° cone angle and 65 mm plate diameter) at a constant temperature 25 °C.

3.2.1.2. **Gelation assessment**

3.2.1.2.1. **Gel visual assessment**

To determine the best polymers-crosslinker ratio and Alg-HA ratio which results in a stable gel formation different fractions of Alg-HA solutions of a total polymer concentration of 1% were prepared and were mixed with different amount of CaCO₃ (Table 5). Similar amounts of these mixtures were casted in cylindrical molds, and allowed to gelled by CO₂ induced gelation as described by Gurikov et al. (2015). According to this approach, the prepared dispersion of polymer solutions and calcium carbonate undergoes irreversible gelation using pressurized carbon dioxide. Therefore the prepared dispersions were left in the autoclave at 50 bar overnight at room temperature [154]. In the next day the autoclave was depressurized at a rate of 2 bar/min to avoid

bubble formation and the produced gels were visually assessed and classified into successful or failed gel.

Afterwards, the solvent exchange was performed to replace water by ethanol gradually at ambient conditions by soaking the gels overnight in different ethanol/water mixtures of 30, 60, 90 and 100 % v/v, respectively. The alcogels were consequently dried by supercritical CO₂ at 120 bar and 40 °C. The final aerogels stability was also visually evaluated in term of fragility and cracks formation. Based on this evaluation the stable aerogel with the lowest cross-linking degree and highest HA fraction (w/w) was selected for further investigation.

Table 5. Preparation conditions of different Alg- HA in the gelation assessment study.

| HA fraction (w/w) | CaCO ₃ (g) | | | |
|----------------------|-----------------------|------------------|-------------------|-----------------------------|
| | Q _{0.25} | Q _{0.5} | Q _{0.75} | Q ₁ [*] |
| 0 | 0.0456 | 0.0913 | 0.1369 | 0.1825 |
| 0.2 | 0.0365 | 0.0730 | 0.1095 | 0.1460 |
| 0.33 | 0.0306 | 0.0611 | 0.0917 | 0.1223 |
| 0.5 | 0.0228 | 0.0456 | 0.0684 | 0.0912 |
| 0.66 | 0.0155 | 0.0310 | 0.0465 | 0.0620 |
| 0.8 | 0.0091 | 0.0183 | 0.0274 | 0.0365 |

*Q₁ is corresponding to 0.1825 g CaCO₃ to each 1 g of Alg.

3.2.1.2.2. **Gel rheological assessment**

To check the reliability of the visual assessment of the gels, the successful and failed gels of the lowest Alg fraction from the previous section was evaluated rheologically. To confirm the gelation of a polymer solution during an ongoing reaction that may be a crosslinking reaction, the complex modulus; viscous (G'') and elastic (G') were measured as a function of time. Mostly, at the beginning of the crosslinking reaction both moduli are low, where the (G') is much smaller than the (G''), when the crosslinking reaction initiate, both moduli start to increase. After the gelling point the elastic modulus becomes greater than viscous modulus, this behavior is carried on as long as the cross-linking reaction is in progress till the storage and loss modulus their equilibrium values.

In this experiment, the polymer- CaCO_3 mixture was mixed with D-(+)-Gluconic acid δ -lacton (GDL) directly before start the measurement. GDL was added as a slow acidifying agent to trigger the crosslinking reaction, thus, induce a slow gelation. A specific amount of GDL powder of 2:1 (GDL: CaCO_3) molar ratio was added to the polymer blend and the measurement was started immediately after that.

Viscous (G'') and elastic (G') muduli were measured with Kinexus-pro+ rheometer (Malvern Instruments, UK) using the oscillatory shear measurement. The sequence “Single Frequency – Measure Changes in Viscoelastic Properties with Time” was carried out for three hours with a complex shear strain, 1° cone angle and 65 mm plate diameter were used and were held at 45°C for the duration of the sequence.

3.2.1.3. Preparation of Alg and hybrid Alg-HA aerogel particles and monoliths

3.2.1.3.1. Preparation of polymers stock solutions

Stock solutions of Alg and Alg-HA (1:1 % w/w) were prepared with different total polymer concentrations: 0.5, 0.75, 1, 1.5 and 2 % w/w. Certain amount of the polymers was added to distilled water to achieve the desired concentration and mixed overnight using a magnetic stirrer to obtain a homogeneous solution. The stock solutions were then stored in the refrigerator at 5 °C for maximum 1 week. Before starting the emulsion gelation step, the stock solutions were left outside the refrigerator to reach room temperature.

3.2.1.3.2. Preparation of aerogel particles by emulsion gelation and supercritical drying

To prepare the aerogel particles an internal setting method was followed, in which the polymer droplets inside the emulsion are gelled by the calcium ions, which are released slowly from its insoluble salt (CaCO_3) triggered by the addition of acetic acid. In more details (Figure 10); polymer solutions of plain Alg or Alg-HA (1:1 % w/w) were first prepared and then mixed with CaCO_3 . It was assumed that only Alg participates in the ionotropic gelation, therefore, CaCO_3 was suspended in the different mixtures at a ratio of 0.1825 g CaCO_3 : 1 g Alg (Q_1). The prepared mixture of the polymers solution and CaCO_3 was then emulsified in rapeseed oil which was premixed with 1 % w/w Span[®] 80. During emulsification, all the parameters were kept constant except the polymer concentrations (internal phase viscosity) and the emulsification speeds (shear rate). The emulsification was performed using a marine propeller (Phoenix RSO 20 A, 3.1 cm diameter) at 500, 850 and 1200 rpm. After 30 min of emulsification, the gelation of the polymer droplets inside the emulsion was induced in the emulsion by adding 1.34 g of pure glacial acetic acid. For all experiments, the stirring rates was reduced to 250 rpm after the addition of acetic acid to allow the

acetic acid to diffuse from the oil phase to the aqueous phase for a time period of 60 min. Eventually, the prepared emulsions were broken by adding excess amount (around 3 fold the emulsion's volume) of 46 % v/v ethanol/water mixture. This ratio of ethanol/water was added to reduce the washing out of HA from the particles. Although higher ethanol ratio is expected to be better in term of preserving HA content, it was not possible to break the emulsion with higher ratio of ethanol because the density of the ethanol/water mixture will be lower than the oil density, therefore, the particles will suspend in the interphases and it would be difficult to collect them. The effect of the ethanol concentration in the breaking solution on the HA content in the final aerogel particles was investigated separately in the next section.

After extraction the aqueous phase, which contains the gel particles, a centrifugation step was done to sediment the particles using Hettich-Rotina 420R centrifuge under 4500 rpm for 10 min at 25 °C. Thereafter, the collected gel particles underwent solvent exchange steps to replace water by ethanol gradually using ethanol-water mixtures of 70, 90 and 100 % v/v, respectively. At each solvent exchange step, particles were kept under shaking for at least 60 min to allow an efficient solvent exchange. Finally, the collected alcogel particles were proceeded to the supercritical CO₂ drying step.

The collected alcogel particles were packed in small filter papers and placed in the preheated autoclave (50 °C). CO₂ gas was introduced to the autoclave vessel from the top at constant flow rate (20-35 g/min) using a high pressure pump. After reaching a pressure of 120 bar, a needle valve outlet was opened and adjusted to release the extracted ethanol, while the pressure was kept at 120 bar during the drying step. After 2 h of drying, the CO₂ inlet was closed and the gas was released slowly from the autoclave by adjusting the needle valve outlet to reach a constant depressurization rate of (2-3 bar/min) at constant temperature (50 °C). When the ambient pressure is reached,

autoclave was opened and the aerogel particles were collected and stored in well-sealed containers and placed in a dry condition.

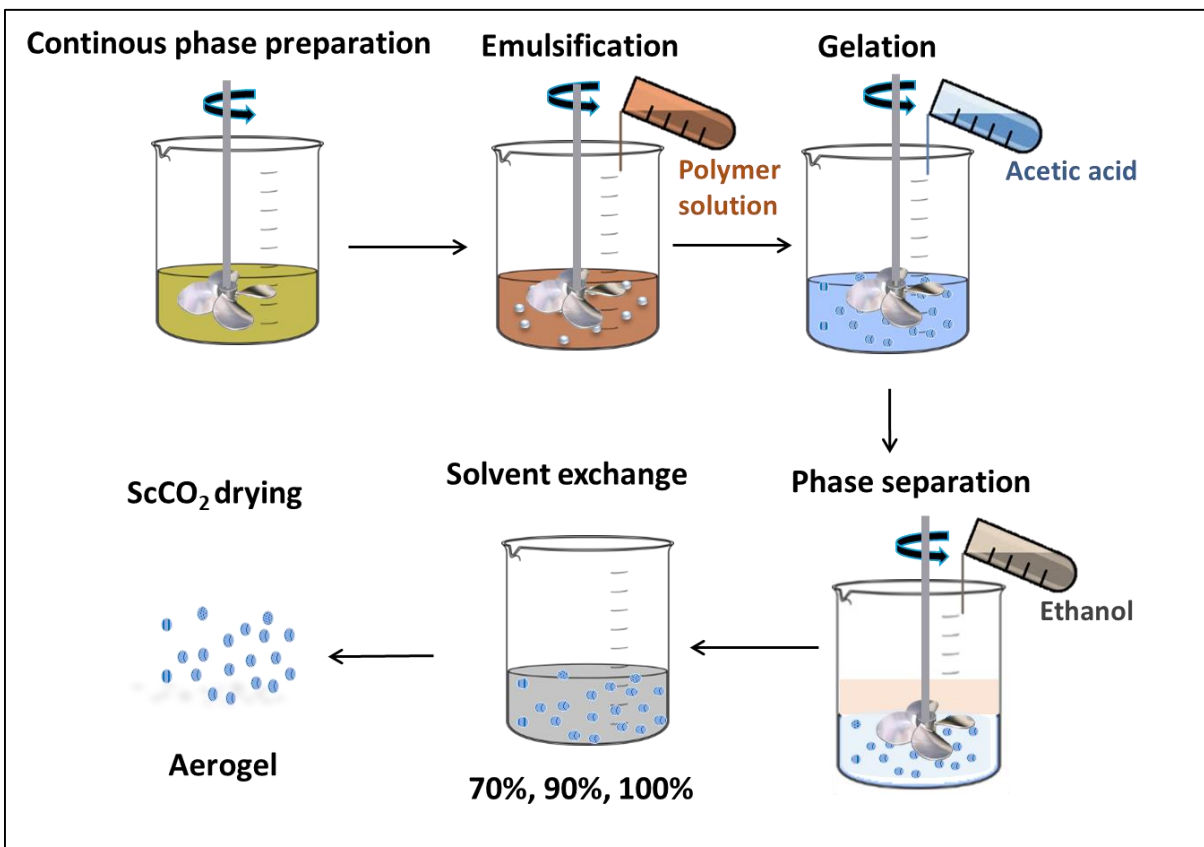


Figure 10. The preparation method of aerogel particles using the emulsion gelation and supercritical the CO₂ drying.

3.2.1.3.3. Preparation of aerogel monoliths

For characterization purposes, it was necessary to compare the density of the prepared aerogel particles with that of monoliths of the same composition. Therefore., gel monoliths were prepared and underwent the same solvent exchange and supercritical CO₂ drying that are mentioned in section (3.2.1.3.2). To prepare the gel monoliths, certain weight of Alg and Alg-HA (1:1 % w/w) was dissolved in distilled water to achieve the following polymer concentrations: 0.5, 0.75, 1, 1.5

and 2 % w/w. CaCO_3 was then suspended in the prepared polymers solutions at a ratio of 0.1825 g CaCO_3 : 1 g Alg (Q_1). GDL was then added to the previously prepared mixtures with a concentration of 6 % w/w and mixed with marine propeller (Phoenix RSO 20 A, 3.1 cm diameter) for 60 sec. This GDL concentration was used because it was found experimentally that it reduces the pH of the polymer mixture to 2.5 within 24 h, which is suitable to transform the CaCO_3 from its insoluble to soluble form. Certain volumes of the prepared mixtures were casted in cylindrical molds (~ 5 ml) and left overnight to allow gelation. In the next day, solvent exchange was initiated and finally the aerogel monoliths were dried by supercritical CO_2 (see section 3.2.1.3.2).

3.2.1.3.4. Solvent exchange and HA content uniformity in the final particles

The effect of the ethanol concentration in the initial solvent exchange step on the HA content was carried out on monoliths. Those gel monoliths were prepared following the Gurikov approach (2015) [155]. According to this approach, a suspension of calcium carbonate dispersed in the polymeric solution (2 % w/w of 1:1 Alg:HA) undergoes irreversible gelation using pressurized carbon dioxide at 5 MPa. Afterwards, the solvent exchange from water to ethanol at ambient conditions was performed by different ethanol/water mixtures (30, 46 and 70 % v/v). The volume and the scheme of the exchange solvent was kept constant (volume = 35ml) in each solvent exchange step (30, 46 or 70, followed by 90 and 100 % v/v of ethanol/water). It was expected that the HA is more susceptible for washing out in the particles than the monolith, because of the larger exposed surface area of the former. Therefore, HA content in Alg-HA particle of 2 % w/w (prepared at 850 rpm) was measured and compared with the monolith of the same concentration. The starting ethanol/water mixtures in was 30 % v/v).

Another experiment was conducted on gel monoliths of different polymer concentrations (0.5, 1, 1.5, 2 % w/w of 1:1 Alg:HA) which underwent initial solvent exchange step with 46 % v/v (ethanol/water). In this experiment, the solvent exchange solution during each solvent exchange step was also kept at a constant volume for all monoliths (35 ml). The scheme of the exchange solvent was as following: 46, 70, 90 and 100 % v/v (ethanol/water). For all experiments, the HA content in the final aerogel was evaluated through the nitrogen content in the final aerogel particles, which was determined by the elementary analyzer “vario MACRO cube” from Elementar Analysen Systeme, Germany.

3.2.1.4. **Emulsion characterization and droplet size estimation**

During the emulsion gelation process, controlling the inner phase droplet sizes is very important because the gelled particles and consequently the final aerogel particles are a result of these droplets. Thus, it is important to control the emulsion droplet sizes in order to tailor the final microsphere sizes. Droplet sizes in an emulsion can be controlled by variable emulsion parameters such as the stirring type and rate, surfactant type and concentration, outer to the inner phase ratio as well as viscosity and other parameters [156]. Thus, if aiming at preparing particles with suitable d_A for pulmonary drug delivery, the previously mentioned emulsion parameters should be taken into consideration. In this study, all the previously mentioned parameters were kept constant, while the effect of using different stirring rates and inner phase viscosities (through using different polymers concentrations) on the particles sizes and properties were studied.

During the emulsification step, capillary number calculation (Taylor’s approach) was used to estimate the largest stable droplet sizes in the emulsion (mentioned in section 2.8.5). The capillary number can be studied in two ways; either by varying the stirring speed or by varying the inner

phase viscosity [149]. Recently, Baudron et al. (2019) calculated the capillary number at a constant polymer concentration (viscosity) and at different stirring speeds [20], therefore, in this study the capillary number was calculated at a constant shear rate (stirring speed of 1200 rpm) and different concentrations (viscosities) of Alg. Thus, the following parameters were needed:

- Interfacial tension (IFT) between the dispersed and continuous phase
- Dispersed and continuous phase dynamic viscosity
- Emulsification shear rates
- Estimated critical capillary number

3.2.1.4.1. **Interfacial tension measurements**

Interfacial tension measurements were carried out using the pendant drop method. In this method, a drop of the first phase (polymer solution) was produced using a capillary and slowly grown inside the second phase (the rapeseed oil with or without surfactant). The profile of the drop was continuously monitored by image acquisition and a profile detection software (DSA4 KRÜSS[®], Germany).

3.2.1.4.2. **Viscosity of the dispersed and the continuous phase**

Viscosities as a function of shear rate of the inner phase, the outer phase and the emulsion was measured with the “Kinexus-pro+” rheometer (Malvern Instruments, UK), using cone and plate geometry (1° cone angle and 65 mm plate diameter) at a constant temperature of 25 °C. The shear rate was set in the range of the used emulsification speeds, which were calculated using Equation 14.

3.2.1.4.3. Estimation of the emulsification of shear rate at 1200 rpm

For the shear rate estimation, there are many approaches described in the literature. Some approaches estimate the average shear rate and others estimate the maximum shear rate ($\dot{\gamma}_{\max}$) which is supposed to take place near the impeller region [157]–[159]. A simple approach for the estimation of the maximum shear rate in a stirred tank has been proposed by Bowen [160], the proposed approach requires the rotational speed of the impeller and the geometrical parameters of the system, as described in the following equation :

$$\dot{\gamma}_{\max} = 9.7 N \left(\frac{D_i}{D_T} \right)^{0.3} \frac{D}{W} \quad \text{Equation 14}$$

where D_i is the impeller diameter, D_T is the tank diameter and W is the width of impeller blade. The system used in this study consists of a marine propeller ($D_i = 5.5$ cm, $W = 1.34$ cm) and a laboratory beaker ($D_T = 10.5$ cm) with no baffles. Using these geometrical parameters, the maximum shear rate that could occur inside our system was estimated.

3.2.1.4.4. The actual droplet sizes analysis in the emulsion

The actual droplet size and distribution of the Alg emulsion of different inner phase viscosities and emulsification speeds was measured by analyzing pictures taken by a light microscope with a 10 x magnification objective. Pictures from the microscope were analyzed for at least 4000 droplets using an image analysis program written in Python (Python Software Foundation). Diameter below which 90 % of the total volume of material in the sample is included ($D_{V90\%}$) was considered as the experimental value of the largest stable droplet in the studied emulsion. It was later compared with the maximum stable droplet sizes estimated from the capillary number calculations.

3.2.1.5. Aerogel particles characterization

3.2.1.5.1. Zeta potential measurements

For measuring the zeta potential, a zetasizer nanoseries from Malvern was used. The sample size for the measurement was roughly 1 ml. The sample was drawn up with a 2 mL syringe. It was important to remove any air bubbles left in the syringe. Then the sample was slowly injected in the appropriate cell (Dispersible folded capillary cell DTS1070) with the cell held upside down. As soon as the cell was filled halfway, it was turned and filled up with the rest of the sample to the maximum mark. The syringe was removed and the two open ports of the cell were closed with two plastic blockers. The measurements were carried out at a temperature of 25 °C and the temperature.

3.2.1.5.2. Fourier transform infrared

Fourier transform infrared (FTIR) spectra were recorded with a Bruker VERTEX 70, Germany spectrometer in the 4000–400 cm^{-1} region with a resolution of 2 cm^{-1} ; the samples were analyzed in attenuated total reflectance (ATR) mode using a diamond crystal.

3.2.1.5.3. Scanning electron microscopy

Scanning electron microscope (SEM) photographs of the particles were performed (Supra VP 55 microscope, Zeiss, Germany) at an acceleration voltage of 3 kV and a working distance of 9-9.4 mm.

3.2.1.5.4. Particle size and distribution

Particle sizes of the aerogel particles were calculated from the particle size distribution data measured with a Camsizer XT (Retsch, Germany), and was calculated using equation 15 [161]:

$$d_v = e^{0.01 \sum p_3 \cdot \ln(d_m)} \quad \text{Equation 15}$$

where d_m is the interval mean size and p_3 is the volume fraction for each particle size class.

3.2.1.5.5. Particle density and porosity and BET surface area

True particle density (ρ_{part}) was estimated using the tapped density (ρ_{tap}) by equation 16 [162]:

$$\rho_{\text{part}} = \rho_{\text{tap}} / 0.794 \quad \text{Equation 16}$$

Overall porosity (ε) of aerogel particles was determined using the following equation 17 [163]:

$$\varepsilon (\%) = \left(1 - \frac{\rho_{\text{bulk}}}{\rho_{\text{sket}}} \right) \cdot 100 \quad \text{Equation 17}$$

where ρ_{bulk} is the bulk density and ρ_{sket} is the skeletal density measured by helium pycnometry (Multivolume 1305, Micrometrics, USA). The aerodynamic properties were estimated by the d_A using equation 2, while d_v of the aerogel particles was calculated from the particle size distribution data measured with a Camsizer XT (Retsch, Germany), and was calculated using equation 15. For comparison purposes, monoliths of Alg and Alg-HA was prepared according to section (3.2.1.3.3) and their bulk densities were measured according to the following equation:

$$\rho_{\text{bulk.monolith}} = \frac{M_{\text{monolith}}}{V_{\text{bulk.monolith}}} \quad \text{Equation 18}$$

where $\rho_{\text{bulk.monolith}}$ is the bulk density of the aerogel monolith, M_{monolith} is the mass of the aerogel monolith and $V_{\text{bulk.monolith}}$ is the bulk volume of the aerogel monolith which is calculated according to the following equation:

$$V = \pi r^2 h \quad \text{Equation 19}$$

where r is the radius of the circular end of the cylinder and h is the height of the cylinder.

The Brunauer–Emmett–Teller specific surface area (BET) was analyzed by low temperature nitrogen adsorption/desorption (Nova 4000e surface area analyzer, Quantachrome instruments, Germany).

3.2.1.6. Analysis of aerodynamic diameter

The European Pharmacopoeia (Ph.Eur.) Method Chapter 2.9.18 currently specifies one twin and three multi-stage impactors for the aerodynamic assessment of fine particles in both metered dose inhalers (MDIs) and DPIs. While The United States Pharmacopoeia (USP) Test Chapter 601 specifies six impactors suitable for aerodynamic size distribution:

- USP Apparatus 1 for MDIs: Andersen Cascade Impactor (ACI)
- USP Apparatus 2 for DPIs: MarpleMiller Impactor (MMI)
- USP Apparatus 3 for DPIs: Andersen Cascade Impactor (ACI) + Preseparator
- USP Apparatus 4 for DPIs: Multi-Stage Liquid Impinger (MSLI)
- USP Apparatus 5 for DPIs: Next Generation Impactor (NGI) + Preseparator
- USP Apparatus 6 for MDIs: Next Generation Impactor (NGI)

Currently only three impactors appear in both Ph.Eur. and USP: Multi-Stage Liquid Impinger (MSLI), Andersen Cascade Impactor (ACI) and Next Generation Impactor (NGI). Both Pharmacopoeias specify test methods for all three impactors for use with DPIs and for the NGI for nebulizers.

In this study, the aerodynamic assessment of prepared aerogel particles was conducted using an Andersen Cascade Impactor (Copley Scientific, UK). To simulate pulmonary adhesiveness, the cascade impactor stages were coated with a 1% w/v mixture of Span[®] 80 and cyclohexane, to allow for the attachment of floating particles and to mimic the surface humidity of the airways. The flow rate was set to 30 L/min by a vacuum pump (high-capacity pump model HCP5, attached to the critical flow controller TPK and connected to the flowmeter DFM 2000, all from Copley Scientific, UK). For each run; three parallel measurements were done, using 3 capsules each to be ‘inhaled’ at the appropriate flow rate. A Breezhaler[®] DPI device was used for the inhalations, each investigated capsule containing 10 mg of aerogel particles.

3.2.1.7. Supercritical drug impregnation and in-vitro release from the particles

For incorporating the drug into the produced particles, the supercritical CO₂ impregnation method was used, in which aerogel particles and naproxen (Table 6) were wrapped separately in filter paper, then the aerogel cartridge was placed at the bottom of the preheated autoclave (50 °C) and the drug on the top. Later, supercritical CO₂ -assisted impregnation was initiated by injecting the CO₂ into the upper part of the autoclave. Impregnation conditions were kept constant (50 °C, 200 bar) under magnetic stirring for 48 h.

Table 6. Microsphere mass (g) and corresponding drug mass (g) used during the supercritical CO₂ impregnation method.

| Sample | Particles mass (g) | Drug mass (g) |
|---------------|---------------------------|----------------------|
| 0.75 % Alg | 0.138 | 0.138 |
| 0.75 % Alg-HA | 0.076 | 0.076 |

The loading capacity (LC %) study was conducted using methanol, because the studied drug has higher solubility in methanol than in phosphate buffer saline (PBS). Therefore, to study the loading capacity (LC %) it was necessary to determine the calibration curve of naproxen in methanol, whereas to study the drug release profile it was needed to prepare the calibration curve in PBS (pH = 7.4±0.05). The calibration curves were plotted using absorbance data from an ultraviolet (UV) spectrophotometer at a wavelength of 318 nm and at different concentrations of the drug solution in methanol and in phosphate buffer solution, the different solutions were prepared by series dilution.

To study the release of naproxen from the impregnated particles, the LC % was considered the 100 % value in the release profile. Therefore, a certain amount of impregnated particles was soaked in 25 ml of methanol and kept under stirring for 24 h. In next day; the solution was filtered through a 0.2 µm filter and the naproxen concentration was determined with an UV spectrophotometer at 318 nm. The particles recovered from the first supernatant were again transferred to 25 ml fresh methanol to recover any possible residual drug and this process was repeated three times in total

to ensure the entire recovery of the drug present inside the microsphere samples. The LC % was calculated using the following equation:

$$\text{LC \%} = \left(\frac{\text{Mass of naproxen in the methanol supernatant}}{\text{Mass of naproxen-loaded particles}} \right) \times 100 \quad \text{Equation 20}$$

There are no current pharmacopoeial methods available for dissolution testing of powders designed for pulmonary drug delivery [164]. For instance, USP paddle systems are not suitable for determining release profiles that are expected in the pulmonary system [165]. The *in vitro* release of naproxen from particles was studied using a dialysis tubing technique, this method were previously used in the literature [166]–[168]. In more detail, 12.3 mg of naproxen-loaded particles were transferred into a dialysis membrane bag and were immersed in a 200 ml of freshly prepared PBS (pH = 7.4 ± 0.05) present in a laboratory bottle. The bottles were placed in a shaking water bath at 100 rpm and at 37 °C. Samples were collected and passed through a filter of 0.2 µm at different time intervals (5, 10, 15, 20, 30, 60, 90, 120, 150 and 180 min). All drug release experiments were conducted in triplicate.

3.2.2. The liver and kidney *in vivo* toxicity study of calcium alginate aerogel and its effect on the gut microbiota

This part of the study was conducted in Jordan as a collaboration with the Applied Science Private University. All experimental protocols were approved by the animal care and use committee of Applied Science Private University, Jordan.

3.2.2.1. Preparation of aerogel particles for the in vivo toxicity and microbiota shift studies

The first step in the preparation of the aerogel particles was to prepare the stock solution, for that, Alg was added to distilled water in a concentration of 1 % w/w and was kept under magnetic stirring overnight at room temperature. To prepare hydrogel particles, Preibisch et al. (2018) approach was followed and Jet Cutter Type S from geniaLab, Braunschweig, Germany was used. During Jet Cutting the biopolymer solution was ejected via a nozzle (350 μm diameter) in a jet form, the solution ejection was driven by compressed air (1 - 3 bar) which was tuned with a pressure-regulating valve. The jet cutting process was carried out using the following parameters: mass flow rate of 1 g/sec, 40 wire/100 μm of wire diameter of cutting discs, cylinder ratio of 5. After cutting, polymer solution fell downwards into the gelation bath which contains CaCl_2 solution of 5 g/l. To avoid gel agglomeration, the volume of the gelation bath was at least four times the total volume of the processed biopolymer solution and the content of the baths was stirred with a magnetic bar for 60. The separation distance between the nozzle and the gelation bath was kept between 50- 70 cm. After finishing the jet cutting, the stirring was continued for 60 min to ensure complete gelation of particles and to avoid agglomeration. Gelled particles were then collected by from the gelation bath via filtering, and were proceeded for the solvent exchange. Solvent exchange (water to ethanol) was performed on the collected particles stepwise (30, 60, 90, 100 % v/v ethanol). The ethanol content of the soaking liquid after the last solvent exchange step measured through its density using a density meter (DMA4500, Anton Paar Company, Austria). Alcolgel particles were packed into a filter paper, and dried with supercritical CO_2 in an autoclave at a constant temperature of 50 $^\circ\text{C}$ and a pressure of 120 bar. Continuous flow of CO_2 (20 – 80 g/min) was set until complete extraction of ethanol was done. Afterwards, slow depressurization of the autoclave (1 – 3 bar/min) was performed. When the ambient pressure is reached, autoclave

was opened and the aerogel particles were collected and stored in well-sealed containers in dry conditions.

3.2.2.2. The in vivo toxicity of Alg aerogel as a potential oral drug carrier

The toxicity study was divided into two parts: a sighting study aiming at selecting the safest dose for the second part of the toxicity study. In the second part of the study, the animals were exposed to a fixed dose (selected based on the first part of this study) for a longer period of time. Regarding age and weight variations and husbandry conditions during this study, the Organization for Economic Cooperation and Development (OECD) guidelines were followed

3.2.2.2.1. Animals

In both short term and long term studies, ten-week old, healthy Wistar Rats with an average weight of 240 ± 37 g were housed in a temperature (21 - 23 °C) and humidity (35 % - 70 %) in controlled rooms with 12 h light-12 h dark cycles. Rats were identified and placed individually in clear-sided cages for ease of observation without disturbing their behavior. Wood shavings were used as bedding. Rats were fed a commercially available diet (Local Supplier, Jordan) and fresh water was offered.

3.2.2.2.2. Short-term toxicity (Sighting study)

The aim of this study was to find the highest possible dose of calcium alginate (Ca-Alg) aerogel that would not cause morbidity nor mortality to the tested animals. Therefore, a repeated oral dose for a one-week duration was performed to define the safest dose of aerogels in Wistar rats. Five dose levels were examined individually by administering Ca-Alg aerogel orally: 25, 50, 100, 250, 500 mg dosages of aerogels, corresponding to the average dose levels of 100, 200, 400, 1000, and

2000 mg/Kg (aerogel/body weight), respectively. The results were compared with two control groups that were given pristine sodium alginate (Na-Alg) in two different concentrations: 50 and 500 mg, corresponding to the average doses of 200 and 2000 mg/Kg (Na-Alg/body weight), respectively. Eventually, all the previous groups of Ca-Alg aerogel and Na-Alg treatments were referenced to a control group who did not receive any treatment, but only the phosphate buffer (placebo).

In all experiments, each treatment group was consisted of 4 rats/group (two females and two males/group). The solid powders of Ca-Alg aerogel or Na-Alg were suspended in phosphate buffer (pH 7.4) and mixed well directly before the oral administration, because the rats refused to eat them in the dry state. For all groups, administration to rats was initiated at the same time everyday using an oral gavage.

3.2.2.2.3. **Long-term toxicity study (15 days repeated dose study)**

Based on the results of the previous section, the dose of 250 mg of Ca-Alg aerogel was selected to be further evaluated for the long term (15 days) toxicity test. Wistar rats were used and were observed for any immediate or delayed renal and/or hepatic adverse effects that might occur. This study was basically branched into two parts, the first one is to evaluate the toxicity of Ca-Alg aerogel and the second part is to evaluate the toxicity of Na-Alg. Each of these studies was consisted of three groups: control, treatment and a satellite group. The control group consisted of 6 Wistar rats/group (3 males and 3 females), while the treatment and satellite groups consisted of 10 Wistar rats/group (5 males and 5 females). The Wistar rats in the treatment groups received the daily dosage of 250 mg of the test substances (Ca-Alg aerogel or Na-Alg) for 15 days, and they were sacrificed on the day 16. While the satellite groups were treated exactly the same as the

treatment groups, but were not sacrificed on the day 16, but they were rather kept under observation for further 15 days after stopping the treatment, and they were sacrificed on the day 30.

It worth to mention that it was not possible to conduct the two studies of Ca-Alg aerogel and Na-Alg in parallel. For this reason, it was not convenient to use one control group for both. These control groups received oral phosphate buffer for 15 days and were subsequently monitored for a further 14 days. As the short-term experiment, the solid powders of Ca-Alg aerogel and Na-Alg were also suspended in a phosphate buffer (pH 7.4) and mixed well directly before the oral administration. For all groups, administration to rats was initiated at the same time everyday using an oral gavage.

3.2.2.2.4. **Clinical and behavioral observation**

In accordance with the OECD guidelines 407, animals were monitored daily for any abnormal clinical signs or changes in the behavior for the duration of the study period, with special attention at the first four hours after the administration of the test substance. Animals in the satellite groups were further observed for an additional 15 days without treatment administration to allow for detection of any late-occurring clinical signs indicative of hepatotoxicity and/or nephrotoxicity hepatic toxicity through measuring the of Alkaline Phosphatase (ALP) and creatinine levels.

3.2.2.2.5. **Serum biochemistry and feces analyses**

In the short-term sighting study, blood samples were collected every second day to measure levels of (ALP) and creatinine, using commercial diagnostic kits from Biostsystems S.A, Spain. Feces samples were also collected every second day to investigate the change in microbial community structure. The feces were gathered in a clean sterile 15 ml-screw -capped tubes, and they were

directly kept at -20 °C until all the samples were collected. For the 15-days repeated dose study, only blood samples were collected on a weekly basis to measure levels of Alkaline Phosphatase (ALP) and creatinine, that is on day 0, day 7, day 14, day 21 and day 30 (day 21 and day 30 applied for the control and satellite group only).

3.2.2.3. Intestinal microbial community analysis

DNA extraction from the collected feces samples was performed using MO BIO'S PowerMax Soil DNA Isolation Kit (MO BIO Laboratories, USA), following the manufacturer instruction. Polymerase Chain Reaction (PCR) purification, and sequencing of genomic DNA (gDNA) were then conducted using Mr. DNA Lab (Molecular Research LP, USA). PCR amplification of the 16S rRNA gene and its subsequent sequencing was done using Illumina. The 16S rRNA gene V4 variable region PCR primers *ill27F mod* (AGRGTTCGATCMTGGCTCAG)/ *ill519R mod* (GTNTTACNGCGGCKGCTG) with barcode on the forward primer were used in 30 cycles using the HotStarTaq Plus Master Mix Kit (Qiagen, USA). After amplification, PCR products are checked in 2 % agarose gel to determine the success of amplification and the relative intensity of bands.

Then the pooled and purified PCR product were used to prepare Illumina DNA library. Sequencing was performed with MR DNA on a microbiome sequencing (MiSeq) following the manufacturer's guidelines. Sequenced data were processed using MR DNA analysis pipeline. In brief, sequences were joined then were depleted of barcodes, after that, sequences < 150 bp as well as sequences with ambiguous base calls were removed. Sequences were denoised and operational taxonomic units (OUTs) were generated and chimeras removed. OTUs were defined by clustering at 3 % divergence (97 % similarity). Final OTUs were taxonomically classified using BLASTn against a

curated database derived from RDP-II and NCBI. A package of different statistical analyses included in “R” software was used for hierarchical clustering (version 3.5.1, vegan Package).

4. Result and discussion

4.1. Rheological characterization for the emulsion components

The emulsion gelation method was used to prepare the aerogel particles. In this method, the rheological properties of the emulsion components are directly influencing the droplet size of the emulsion, and consequently the final aerogel particle size. Therefore, it was necessary to study the rheological properties of the polymers stock solutions (Alg and Alg-HA) and their emulsion in the rapeseeds oil, as well as the rapeseeds oil.

4.1.1. Rheological analysis for the oil and polymers stock solutions

The concentration dependence of the intrinsic viscosity of Alg and HA in water at 25 °C is illustrated in figures 11 and 12 respectively. Both polymers are soluble in water and, if dissolved, forms a viscous solution in which the viscosity is increasing with increasing the concentration and/or the molecular weight. As the latter was fixed in this study, the viscosity was increasing with the concentration as expected. It is clear from the results that the viscosity of HA solution is much higher than the corresponding concentration of Alg solution. The high viscosity of HA solution is related to its ability to form an entangled network in solutions. Many researchers have studied the conformation of HA in its solution using the space-filling molecular models and computer simulations as well as nuclear magnetic resonance (NMR). Specifically, Scott and co-workers who published extensively on this topic [169]–[173] proposed that HA incorporating in multiple hydrogen bonds forming a 2-fold, “tape-like” single helix. Also, they suggest that “a series of overlapping interactions in which each HA molecule associates with and binds to antiparallel

molecules ahead and behind. Each HA molecule thus links to other HA molecules on either side of the HA ambidextran by secondary valencies [169].

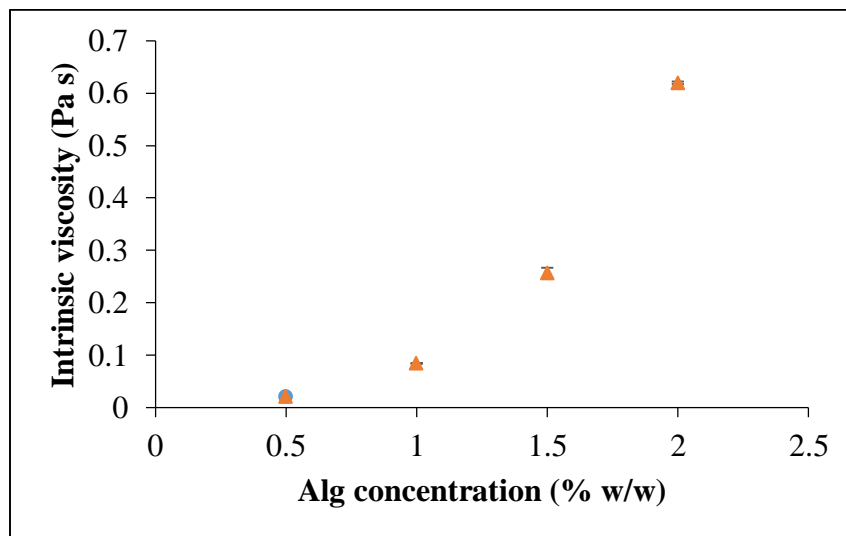


Figure 11. Concentration dependence of the intrinsic viscosity of Alg in water at 25 °C.

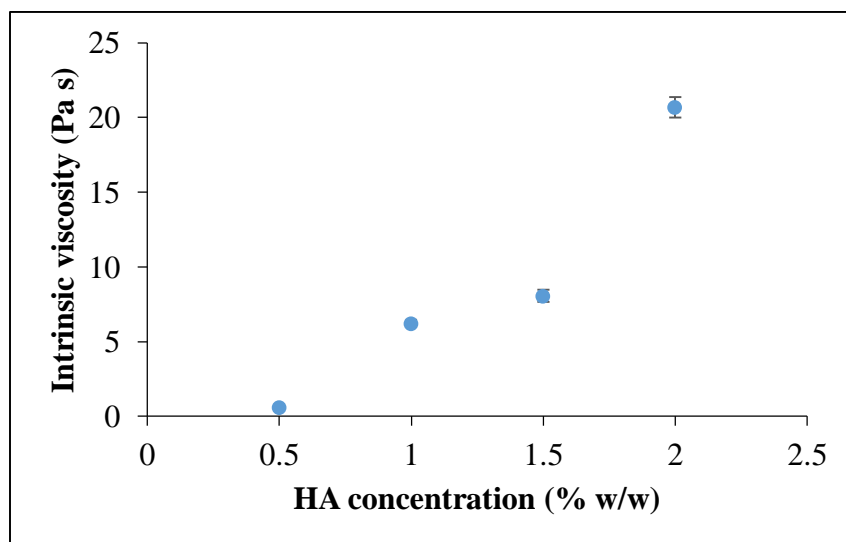


Figure 12. Concentration dependence of the intrinsic viscosity of HA in water at 25 °C.

As expected, rapeseed oil shows Newtonian behavior (Figure13). It was found that the viscosity of rapeseed oil is not only affected by the temperature but also by the storage time. As the rapeseed

oil contain unsaturated fatty acids which is susceptible to autoxidation, and therefore its viscosity is expected to increase during storage.

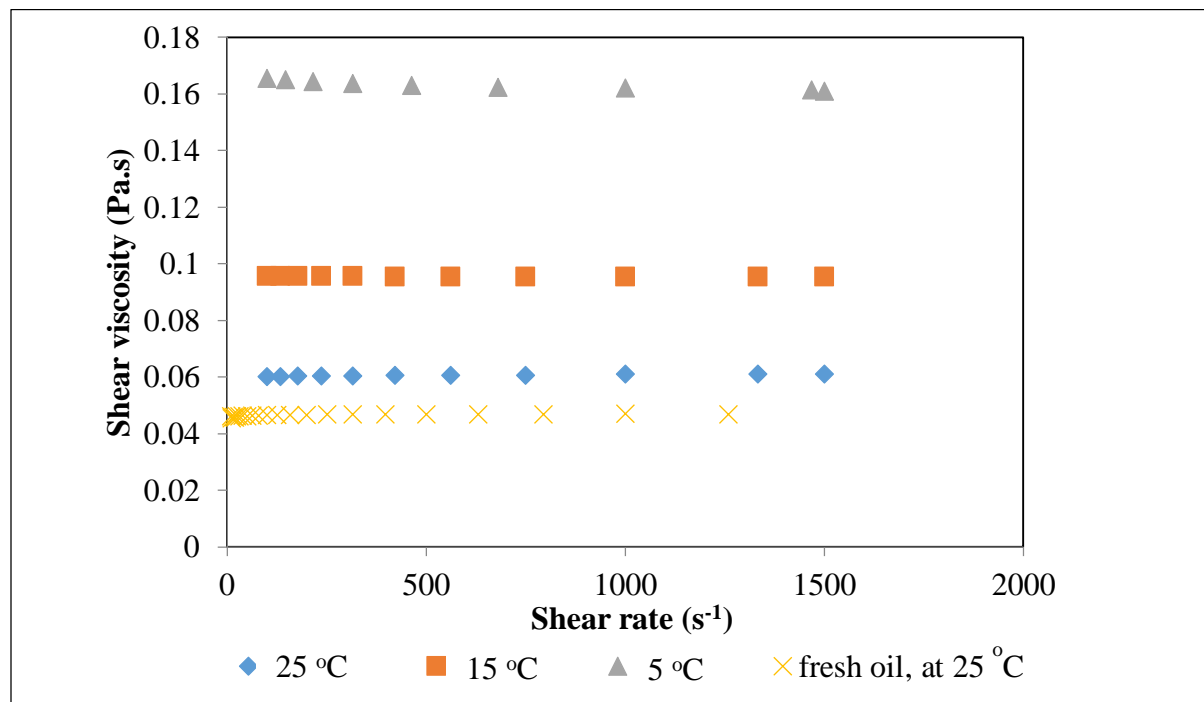


Figure 13. Effect of shear rate and temperature on the viscosity of rapeseed oil.

Figures 14 and 15 show the viscosity profile of different solutions of Alg and Alg-HA (respectively) as a function of the shear rate. It was found that both Alg and Alg-HA solutions show shear thinning behavior (except for the 0.5 % and 0.75 % Alg solutions, show Newtonian behavior). Therefore, the viscosity is expected to decrease during the emulsification process, thus, the apparent viscosities should be taken into account if using the viscosity ratio in the capillary number calculations.

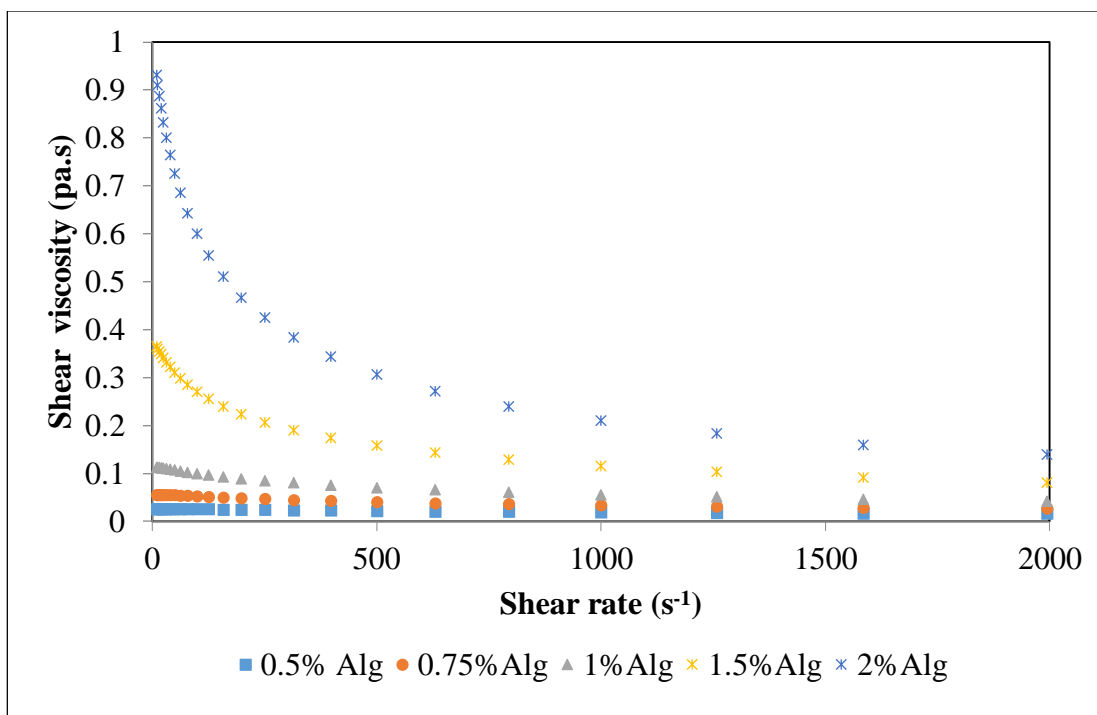


Figure 14. Effect of shear rate on the viscosity of different Alg solutions at room temperature.

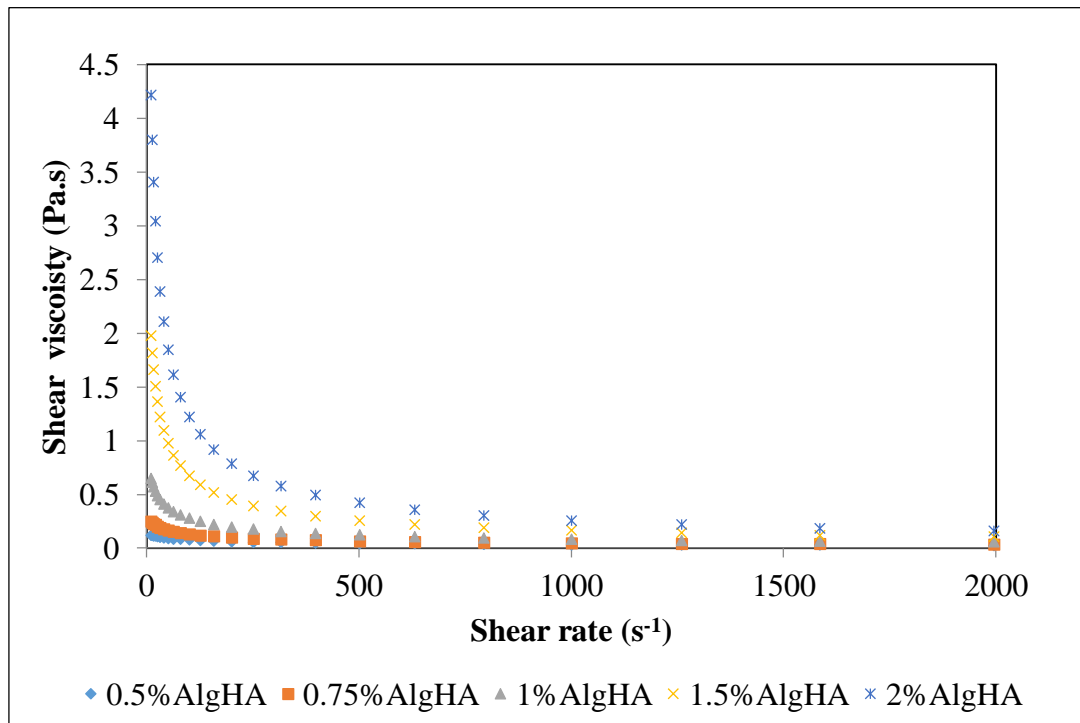


Figure 15. Effect of shear rate on the viscosity of different Alg-HA solutions at room temperature.

The apparent viscosities (η_{app}) of the polymers solutions and their emulsions in oil were analyzed and fitted to the power law model (Equation 21):

$$\eta_{app} = K \dot{\gamma}^{n-1} \quad \text{Equation 21}$$

where K is the flow consistency index, $\dot{\gamma}$ is the shear rate, and n is the flow behavior index. For the purpose of capillary number calculation, the apparent viscosity ratio between the inner phase and the emulsion at the shear rate which was applied during emulsification process was calculated as follows:

$$\lambda_{app} = \frac{K_{inner} \dot{\gamma}^{n_{inner}-1}}{K_{emulsion} \dot{\gamma}^{n_{emulsion}-1}} \quad \text{Equation 22}$$

For higher viscous liquid, K is higher, while n indicates the degree of non-Newtonian behavior of the liquid; if the liquid becomes more shear-thinning, the value of n decreases. For Newtonian liquids $n = 1$. The parameters n and K which were obtained after power law fitting are shown in Table 7. It was found that n decreases with increasing polymer concentration of the Alg and the Alg-HA solutions, and it is always lower in the polymer solutions than in their corresponding emulsions. This decrease in the n value refers to the high fraction of the oil in the emulsion, that allows the rheological properties of the oil to be predominant. As expected, higher K values were noticed if adding HA and if increasing the polymer concentration in the inner phase.

It was also found that emulsions prepared with low polymer concentrations in the inner phase are more viscous and with more pronounced non-Newtonian behavior comparing to emulsions of medium polymer concentrations. Such emulsions with low polymer concentrations in the inner phase are expected to be fine emulsions because of their small droplet size. Therefore they show

much higher viscosities, and they exhibit more non-Newtonian behavior as well as a much stronger shear-thinning effect [174].

Table 7. Power law parameters of Alg and Alg-HA (of a weight ratio 1:1) solutions and their corresponding emulsions.

| Polymer concentration | K | n | Polymer concentration | K | n |
|------------------------------|----------|----------|------------------------------|----------|----------|
| Solution | | | Solution | | |
| 0.5 % Alg-HA | 0.055 | 0.578 | 0.5 % Alg | 0.067 | 0.818 |
| 0.75 % Alg-HA | 1.312 | 0.515 | 0.75 % Alg | 0.198 | 0.743 |
| 1 % Alg-HA | 3.802 | 0.443 | 1 % Alg | 0.530 | 0.673 |
| 1.5 % Alg-HA | 14.280 | 0.351 | 1.5 % Alg | 2.450 | 0.557 |
| 2 % Alg-HA | 33.790 | 0.293 | 2 % Alg | 8.197 | 0.469 |
| Emulsion | | | Emulsion | | |
| 0.5 % Alg-HA | 0.231 | 0.866 | 0.5 % Alg | 0.045 | 1.000 |
| 0.75 % Alg-HA | 0.187 | 0.864 | 0.75 % Alg | 0.216 | 0.887 |
| 1 % Alg-HA | 0.139 | 0.924 | 1 % Alg | 0.159 | 0.905 |
| 1.5 % Alg-HA | 0.148 | 0.916 | 1.5 % Alg | 0.138 | 0.940 |
| 2 % Alg-HA | 0.194 | 0.892 | 2 % Alg | 0.340 | 0.801 |

4.1.2. Rheological study to assess the polymers interactions

Unfortunately, there is no clear understanding of the mechanism of interaction between HA and Ca^{2+} . Therefore, it was proposed that the gel of Alg-HA is formed by obtaining a semi-interpenetrating polymeric network structure, in which the Alg network is ionically crosslinked by Ca^{2+} ions to provide a structural reinforcement, while the HA network is expected to be integrated into this structure on the molecular scale but without covalent bond formation [175]. To prove this hypothesis, it is necessary to examine the potential interactions between Alg and HA.

The theoretical viscosity of polymer mixtures was estimated using equation 13 and plotted as a function of the Alg-HA composition, which is expressed as the weight fraction of HA. In resulting curves (Figure 16), it can be noticed that the theoretical viscosity deviated positively from the experimental viscosity, which suggesting some kind of interaction between the two polymers resulting in decreasing their water solubility and, consequently, their viscosity [176].

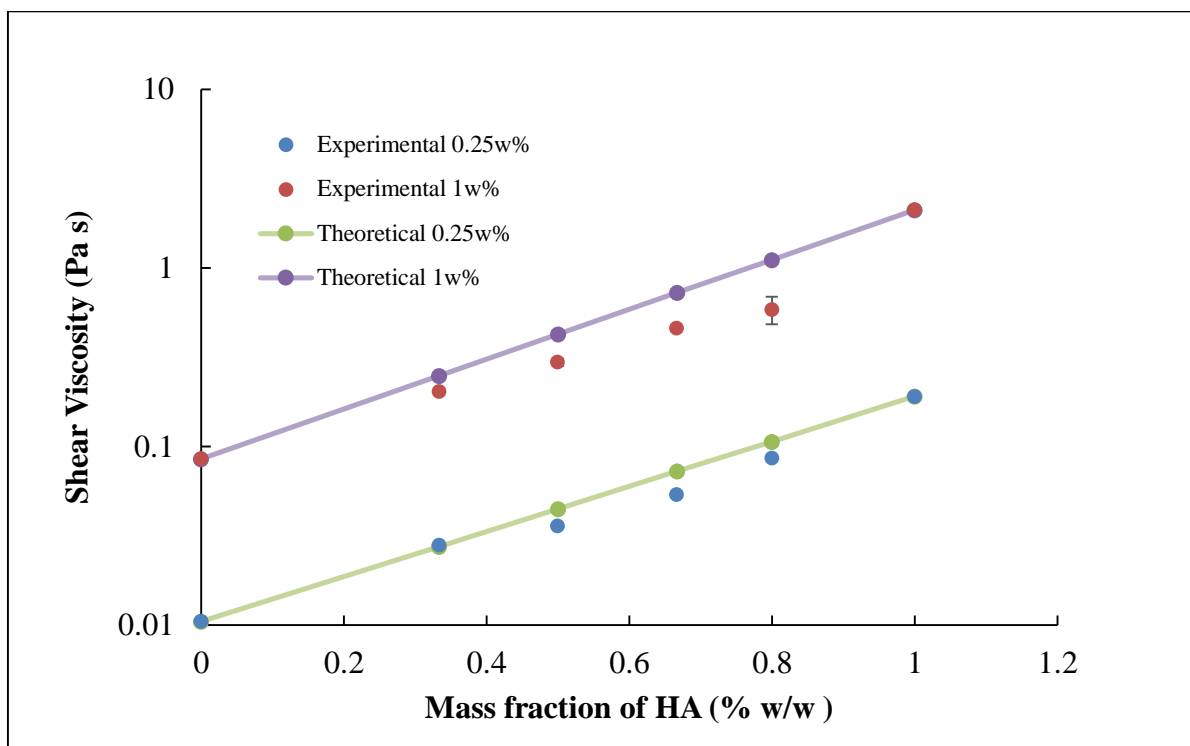


Figure 16. Results of the viscosity of the Alg-HA solutions with different mass ratios and total polymer concentrations of 0.25 and 1 % w/w at a shear rate of 5 s^{-1} . Means \pm SD, $n = 3$.

In the aqueous solution of HA, water molecules form a hydrogen bridging between the amide of the N-acetyl-D-glucosamine and the carboxylate groups of the D-glucuronic acid [169]. Such interaction is also expected to decrease the pKa of the carboxylate group below its intrinsic value and thus, the carboxylate charge is stabilized by an additional intra- or intermolecular interaction, i.e. hydrogen bond [177]. Accordingly, hydrogen bond formation between the carboxylate groups of Alg and the amide of the N-acetyl-D-glucosamine in HA) is expected, which might explain the observed rheological behaviour of Alg-HA mixtures.

4.1.3. Rheological characterization to assess HA interaction with calcium

The gelation of Alg by divalent cations (Ca^{2+}) is well known, and can be described by forming ionic bonds between the Ca^{2+} and the G-residues of the alginate polymer chains in the so-called “egg-box” mechanism [178]. However, the interaction between Ca^{2+} and the HA which was used in this study has to be defined. This can be done by studying the effect of Ca^{2+} on the viscosity of HA solution.

Figure 17 shows the viscosity profile of HA solution with the addition of calcium chloride. It is clear that the viscosity of the HA solution decreases with increasing CaCl_2 concentration, as Ca^{2+} tends to destabilize the HA secondary structure [179].

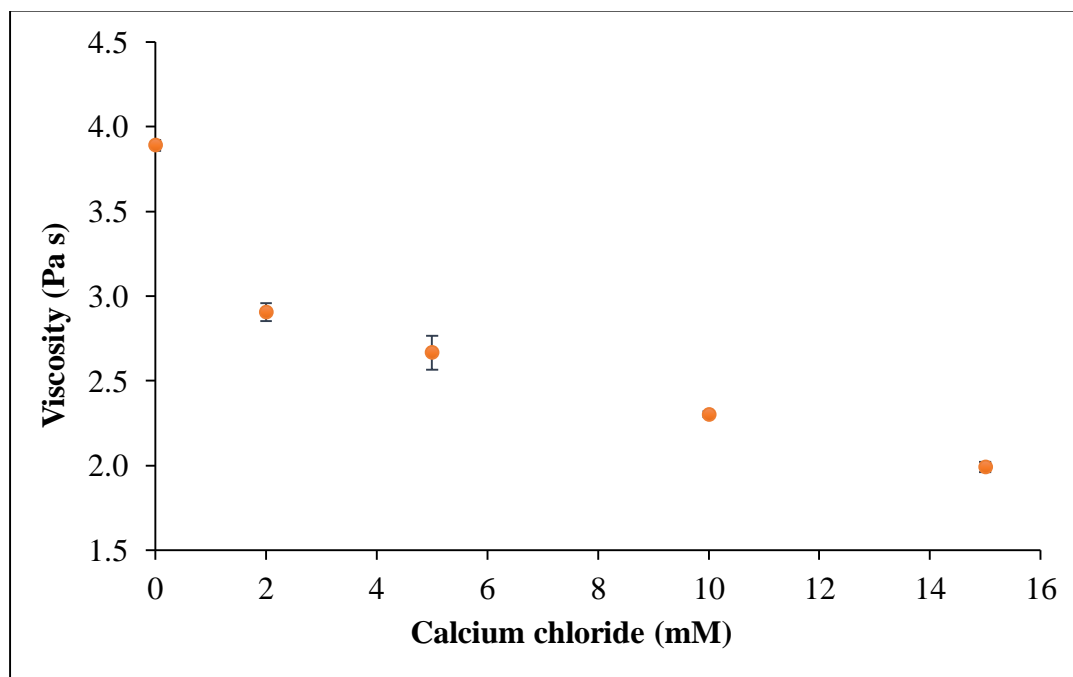


Figure 17. Change of the HA solution (1 % w/w) viscosity upon addition of calcium chloride.

Means \pm SD, n = 3.

4.2. Gelation assessment

4.2.1. Gel visual assessment

Gels visual assessments were conducted to visually characterize the samples in term of gelation process and their physical appearance as well as mechanical strength. Figure 18 demonstrate a dot plot of the different prepared hydrogels and their ultimate gelation status after the CO₂ induced gelation. The results show that all the gels of a total polymer concentration of 1% w/w prepared with a wt. fraction of Alg above 0.2 and CaCO₃ content above $Q = 0.25$ (0.0456 g) were characterize as stable gels. Moreover, it was noticed that if increasing the Alg ratio, the corresponding aerogel (after drying) became more stable, which support the proposed hypothesis that the crosslinked Alg network provides the structural reinforcement for the gel. It was also noticed that the final aerogels corresponding to the HA content above 0.5 % w/w fraction in the gel were found to be more mucoadhesive, more fragile and contain more cracks. Therefore, aerogel of 1:1 % w/w of HA:Alg was considered for the preparation of the particles.

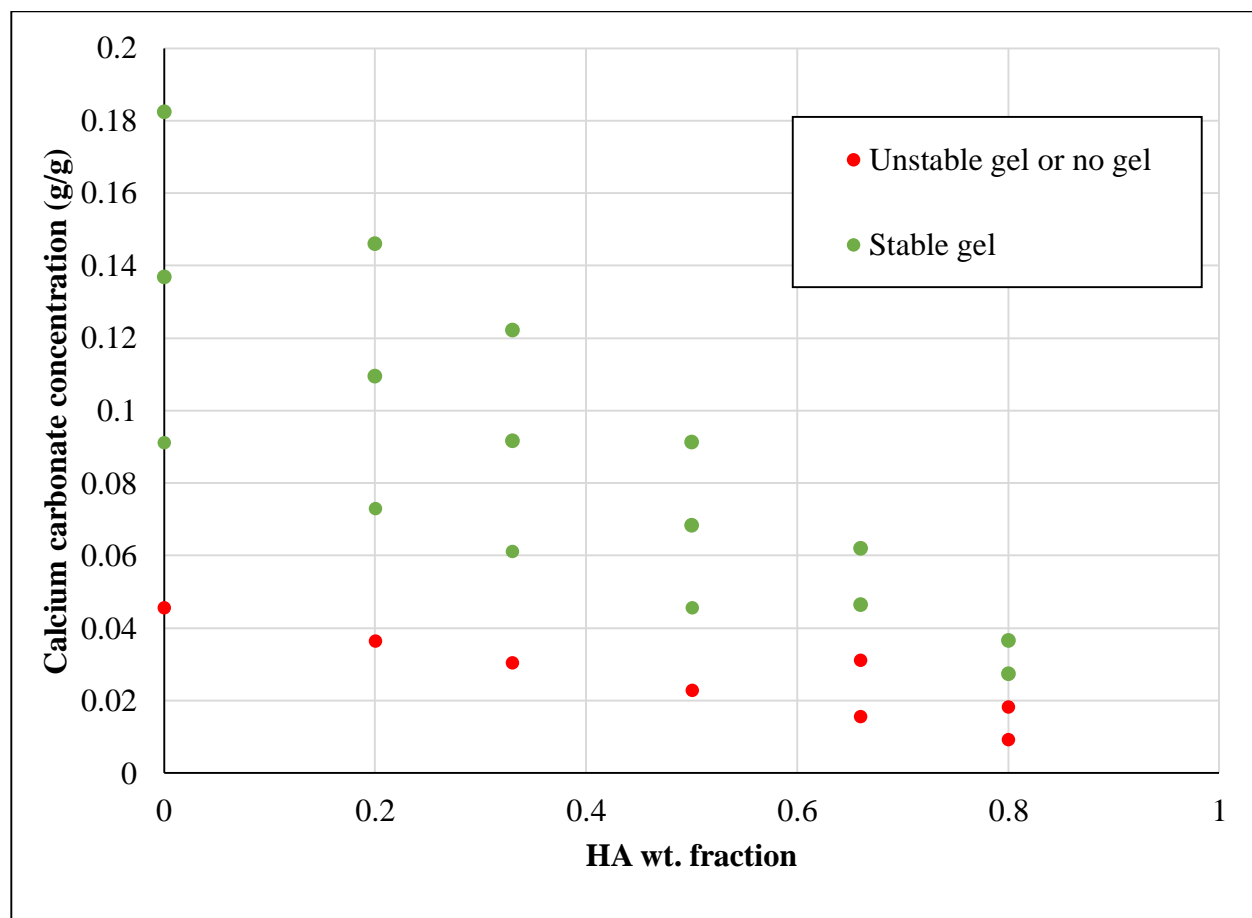


Figure 18. Dot plot of the different prepared hydrogels and their ultimate gelation status after the CO₂ induced gelation.

4.2.2. Gel rheological assessment

To check the reliability of the previous results regarding the gel visual assessment, the hydrogels which were considered stable or unstable at the lowest Alg content were evaluated rheologically. Those were the gels made at following conditions: of Alg 0.2 wt. fraction and $Q = 0.5$ of CaCO₃ (corresponding to 0.01825 g of CaCO₃ to each 1g of Alg), and the gel made of Alg 0.2 wt. fraction and $Q = 0.75$ of CaCO₃ (corresponding to 0.02738 g of CaCO₃ to each 1g of Alg), of 1 % w/w total polymer concentration for both. It was found that it was not possible to form a gel with 0.2

wt. fraction Alg and $Q = 0.5$ CaCO_3 , as the G' didn't exceed the G'' during the analysis time (Figure 19). While the gel made of the same wt. fraction of Alg but with higher amount of CaCO_3 (of $Q = 0.75$, corresponding to 0.02738 g of CaCO_3 to each 1g of Alg) was stable as illustrated in figure 20, where G' exceed G'' after 2500 second of starting the gelation process. Thus, it can be concluded that the lowest Alg wt. fraction among the investigated formulations that can be used to prepare a successful hybrid gel of Alg-HA is 0.2 with calcium carbonate $\geq Q = 0.75$.

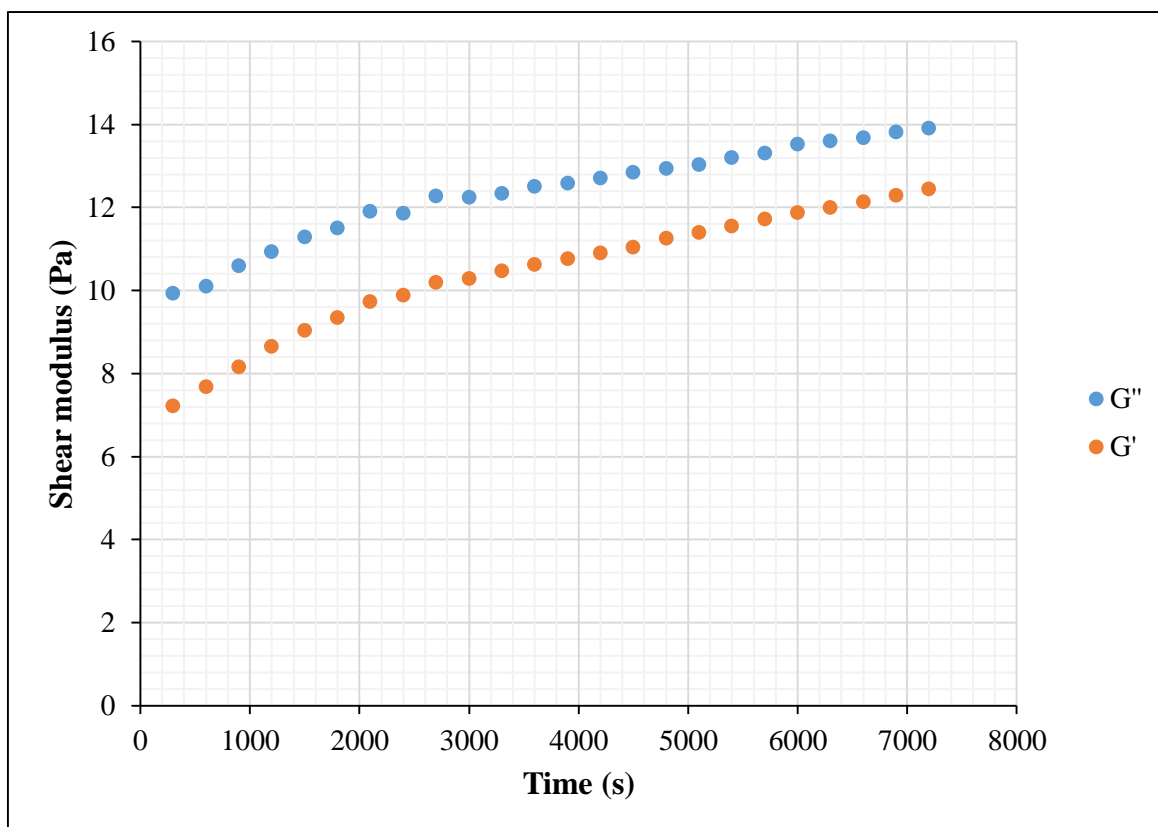


Figure 19. Gelation over time for a 1 % w/w polymer blend made of HA 0.8 fraction and $Q = 0.5$ CaCO_3 (corresponding to 0.01825 g of CaCO_3 to each 1g of Alg).

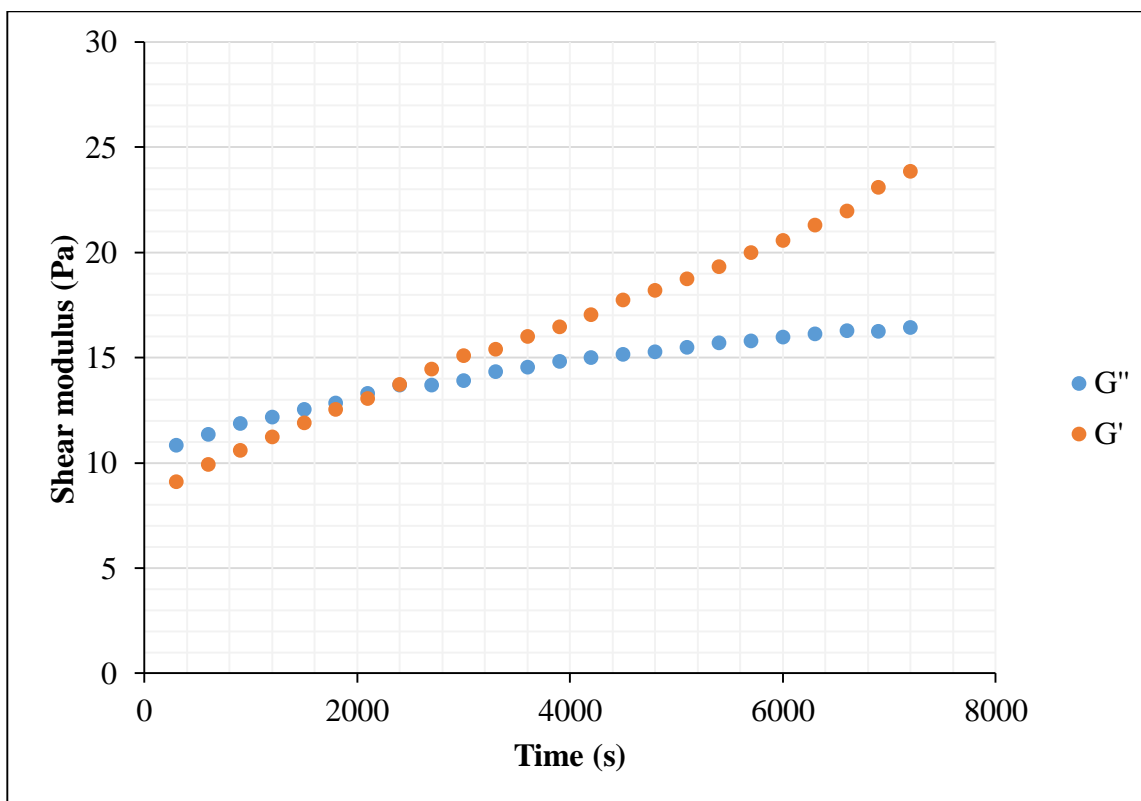


Figure 20. Gelation over time for a 1 % w/w of Alg-HA polymer solution made 0.8 fraction of HA, 0.2 fraction of Alg and $Q = 0.75$ CaCO_3 (corresponding to 0.02737 g of CaCO_3 to each 1 g of Alg).

4.3. Determining the conditions of solvent exchange under consideration of Solve

From the previous results of the rheological analysis, it was suggested that HA is not participating in the crosslinking mechanism of the hybrid Alg-HA aerogel, nevertheless, it is expected to be bound within the Alg network by forming hydrogen bonding between the free groups present within the structure of both polymers (the carboxyl group of Alg and the amine group of HA). Therefore, it is expected to be washed out of the gel significantly during the solvent exchange process, especially at the first step at which the water concentration is high (~ 70 % v/v) as the HA is soluble in alcohol-water mixtures up to an ethanol concentration of approximately 50 % v/v

[180]. As can be seen from Table 8, the washing out of HA was reduced remarkably if starting the solvent exchange step with higher ethanol concentration. The elemental analysis shows that the residual HA content (from the original amount of HA added to form the hydrogel) increased from 26 to 68 % w/w when changing the starting solvent exchange content from 30 to 70 % v/v ethanol/water.

Table 8. The effect of the ethanol concentration on the residual HA during the solvent exchange steps as performed with Alg-HA monoliths (2 % w/w of 1:1 Alg:HA).

| Ethanol concentrations of the solvent exchange steps [% v/v] | Weight loss [mg] | Residual HA [% w/w] |
|---|-------------------------|----------------------------|
| 30, 60, 90, 100, 100 | 57.2 ± 1.0 | 26 |
| 60, 90, 100, 100 | 44.7 ± 3.0 | 50 |
| 75, 90, 100, 100 | 30.4 ± 1.5 | 68 |

Nevertheless, it was not possible to conduct the solvent exchange step for the particles with such a high ethanol concentration because of a density limitation: the density of 70 % v/v ethanol/water mixture is lower than the rapeseed oil's density. Thus, the particles are suspended at the interface between the oil and the ethanol/water mixture, consequently, it is difficult to collect them. Therefore, the initial solvent exchange step for the particles was carried out using ethanol/water mixture of 46 % v/v. This concentration was determined experimentally as the mixture with the highest ethanol concentration that has a density above that of the used oil.

To confirm these conditions, another experiment was conducted on gel monoliths which underwent initial solvent exchange step with 46 % (see chapter methods, section 3.2.1.3.4). The results (Figure 21) show that the HA content was kept almost constant with a residual HA amount between 40 – 50 % w/w.

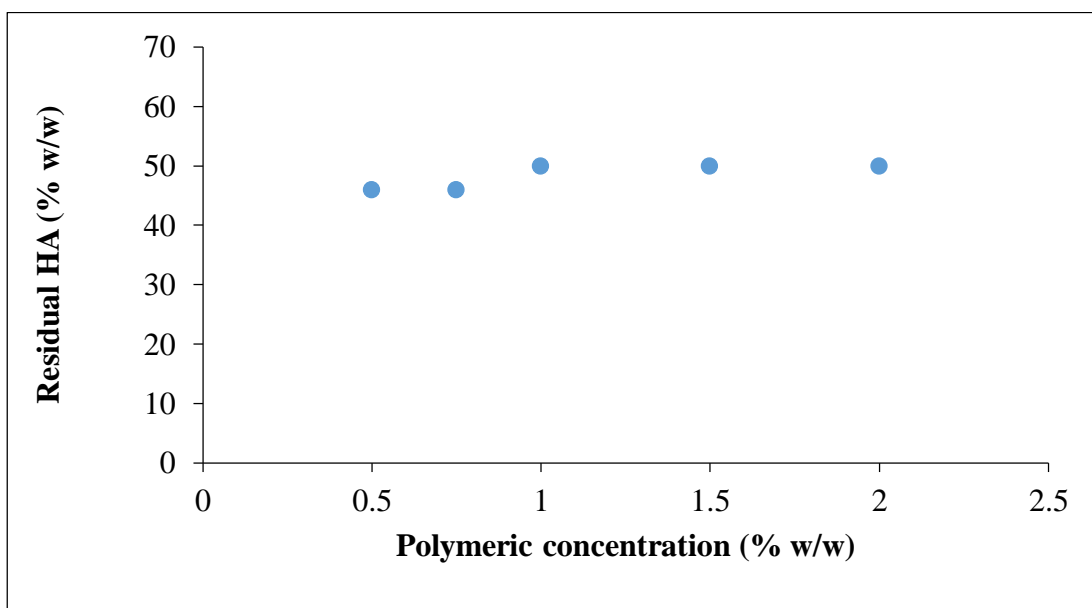


Figure 21. Residual HA content in the gel after the solvent exchange if using a starting ethanol concentration of 46% w/w.

The content of HA in in Alg-HA particle of 2 % w/w (prepared at 850 rpm) was measured and compared with the monolith of the same concentration. The results revealed that the remaining % w/w of HA in the particles was 17, while in the monolith of the same concentration it was 26. This was explained by the larger exposed surface area of the particles than that of monoliths, which allows the HA to be dissolved in the solvent exchange mixture in a higher degree.

These findings suggest that it is possible to control the HA content in the hybrid aerogels through controlling the ethanol concentration in the solvent exchange solution. Based on these results,

during the preparation of all particles the initial ethanol concentration was set to 46 % v/v in the first step of the solvent exchange (breaking the emulsion).

4.4. Emulsion characterization and droplet size estimation

4.4.1. Surface tension measurements

Interfacial tension (IFT) measurements were conducted at different concentrations of Alg and Alg-HA solutions to study the effect of polymer and surfactant concentration on the IFT. Also, the IFT value is necessary as an input to calculate the capillary number (Equation 10).

The IFT was determined after 2100 s which represent the emulsification time. Figures 22 and 23 show that in the absence of span 80, the IFT decreases with time from an initial value of 32 mN/m to 12 mN/m for Alg, and from 44 mN/m to 16 mN/m for Alg-HA of 1:1 % w/w. Similar findings for Alg solution were reported by Bourden et al. (2019) for Alg and by Haug et al. (1964) for Alg and other polysaccharides solutions [181], [182].

It was also noticed that not only solutions of Alg-HA possess higher dynamic IFT values than Alg solutions, the same trends were also noticed for the equilibrium interfacial tensions values between Alg and Alg-HA polymer solutions and rapeseed oil in the presence of surfactant (Figure 24). Such higher IFT values might be referred to the hydration layer of HA which is expected to be formed around the hybrid droplet because of the high water affinity of HA, that may hinder the surfactant adsorption and, therefore, lead to a higher IFT value. Also, the surface charge on Alg-HA droplets because of the presence of HA may increase the repulsion between droplets and/ or cause a resistance to the surfactant adsorption. The results of the Zeta potential analysis will be introduced later in (section 4.5.1).

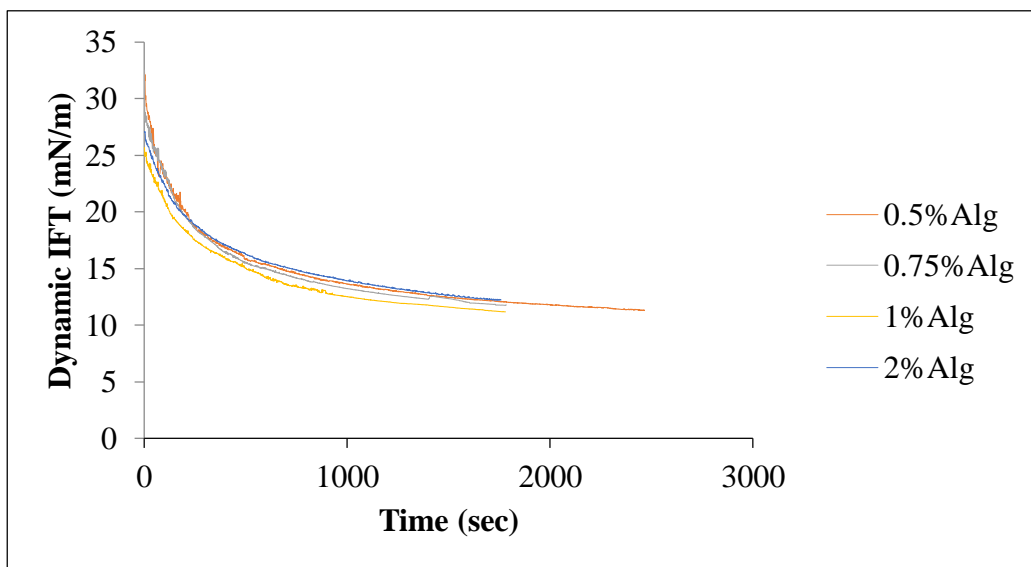


Figure 22. The dynamic interfacial tensions between Alg polymer solutions and rapeseed oil in the absence of surfactant.

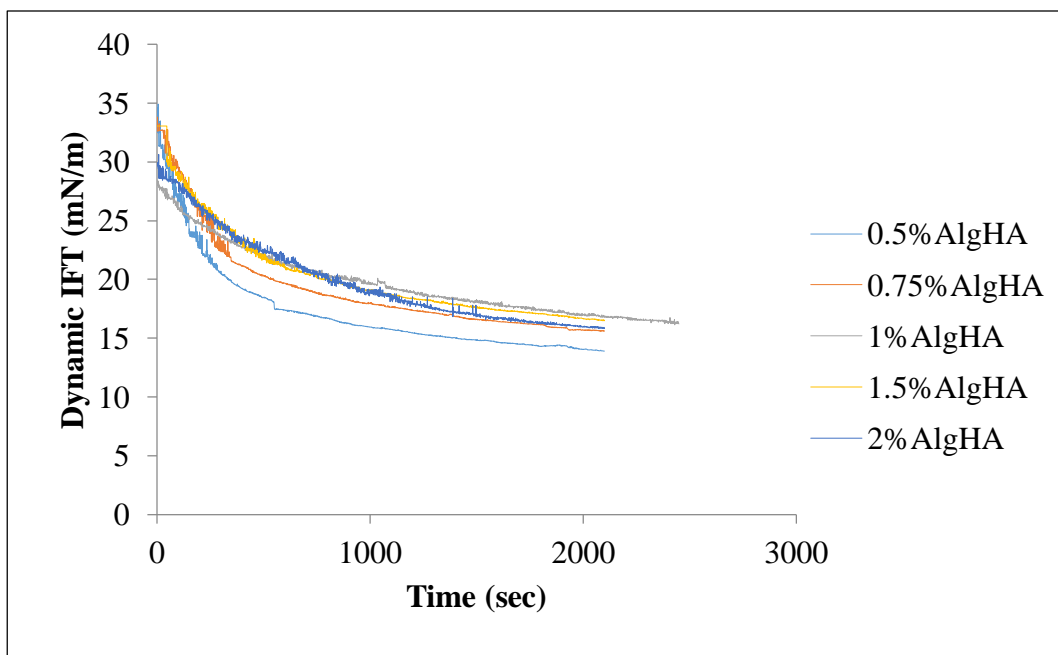


Figure 23. The dynamic interfacial tensions between Alg-HA polymer solutions and rapeseed oil in the absence of surfactant.

Regarding to the effect of polymer concentration on the IFT, it was observed that for both Alg and Alg-HA, the polymer concentration has no significant effect on the value of IFT for both polymer phases in rapeseed oil at different polymer concentrations as shown in figure 24.

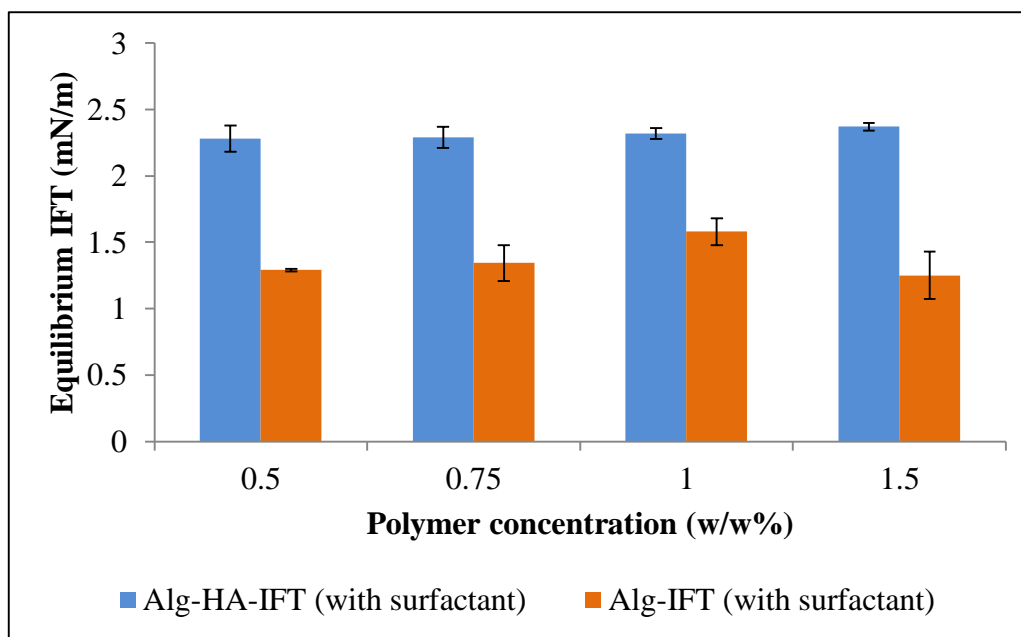


Figure 24. Equilibrium interfacial tensions between Alg and Alg-HA polymer solutions and rapeseed oil in the presence of 1 % w/w surfactant (Span[®] 80); means \pm SD, n = 3.

The time progression of the interfacial tensions between Alg and Alg-HA polymer solutions of 0.75 % w/w and rapeseed oil in the presence of 1 % w/w surfactant (Span[®] 80) is illustrated in figure 25 (as a representative example of the results). According to the results, if Span[®] 80 is added to the rapeseed oil at a 1 % w/w, the IFT dropped to the saturation to reach 1.3 mN/m for Alg solution (0.75 % w/w) in about 300 s. Also, for the Alg-HA solution (0.75 % w/w) the IFT dropped to the saturation in about 300 s to reach 2.3 mN/m.

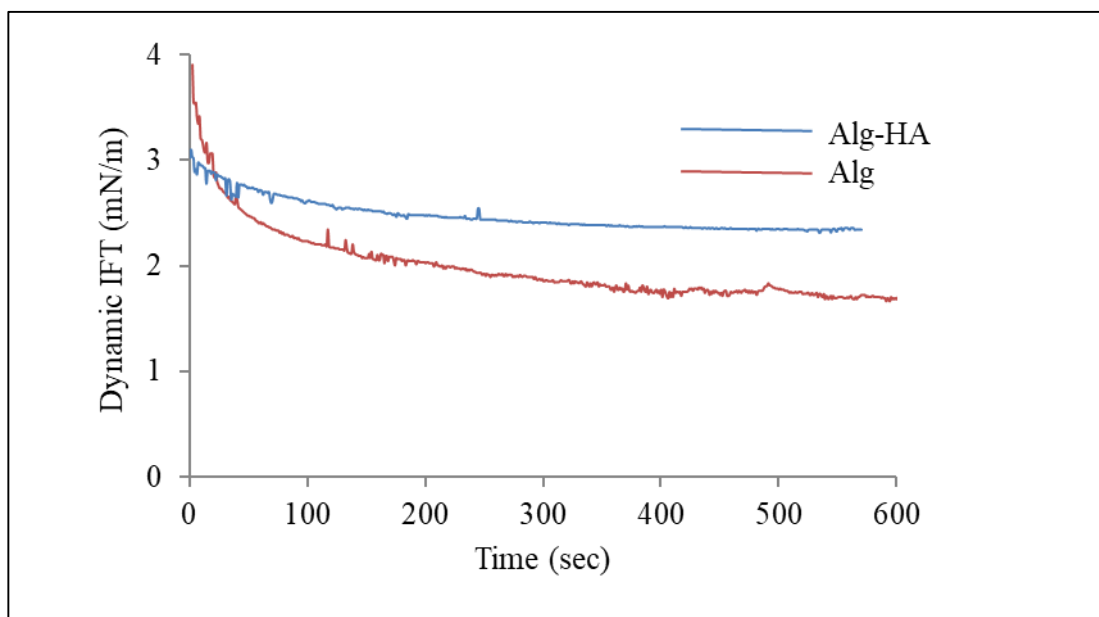


Figure 25. The dynamic interfacial tensions between both Alg and Alg-HA (0.75 % w/w) polymer solutions and rapeseed oil in the presence of 1 % w/w surfactant (Span[®] 80).

4.4.2. Estimation of the emulsification shear rate

The drop break-up in the emulsion happens if the applied shear stress is transferred effectively by the outer phase to the inner phase droplets. The estimated shear rate at different stirrer revolutions were calculated using equation 14 and given in table 9. The shear rate at 1200 rpm (656 s^{-1}) was used later in the capillary number calculation. This particular value was selected because the smallest particle sizes of aerogels were obtained at this shear rate.

Table 9. Estimated maximum shear rate using correlation from Bowen [160].

| Stirrer revolution (rpm) | Shear rate (s⁻¹) |
|---------------------------------|------------------------------------|
| 500 | 273 |
| 800 | 437 |
| 1200 | 656 |

4.4.3. Viscosity of the dispersed and the continuous phase

After estimating the shear rate at the stirring speed of 1200 rpm, the apparent viscosities of the investigated emulsions and their inner phases at the corresponding shear were derived from the experimental rheological measurements (section 4.1.1). Subsequently, the apparent viscosity ratios (λ_{app}) of the investigated emulsions were calculated and eventually used later for the estimation of the critical capillary number using Equation 12 (Table 10).

Table 10. The apparent viscosities of the investigated Alg in rapeseed oil emulsions, their inner phases and the corresponding viscosity ratio and at emulsification speed of 1200 rpm corresponding to a shear rate of 655.86 s^{-1} .

| Polymer concentrations (% w/w) | $\eta_{\text{app, inner}}$ (mPa·s) | $\eta_{\text{app, emulsion}}$ (mPa·s) | λ_{app} (-) |
|-----------------------------------|---------------------------------------|--|-------------------------------|
| 0.5 % | 20.67 | 45.00 | 0.46 |
| 0.75 % | 37.39 | 103.79 | 0.36 |
| 1.0 % | 63.56 | 85.86 | 0.74 |
| 1.5 % | 138.46 | 93.51 | 1.48 |
| 2.0 % | 261.78 | 93.53 | 2.80 |

4.4.4. Capillary number calculation and droplet size estimation

The critical capillary number values were calculated using Equation 12 and were used along with the emulsion viscosity and equilibrium IFT values to estimate the largest stable droplet size in the emulsions using Equation 11. It was noted that the critical capillary number value increased rapidly from 0.55 at 1.5 % w/w of the Alg concentration to 1.5 at 2 % w/w of the Alg concentration (Figure 26). Consequently, more energy is expected to be required to break up the droplet [151].

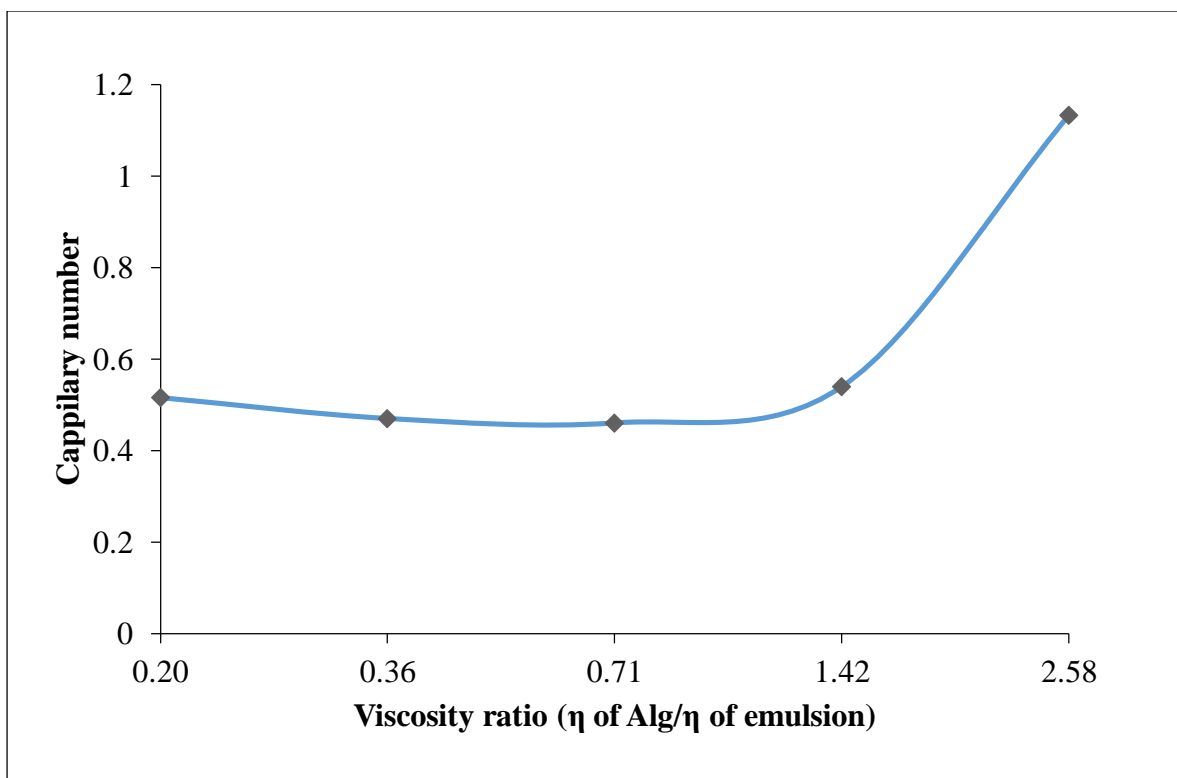


Figure 26. The calculated critical capillary number values using Equation 12 for Alg in rapeseed oil emulsions, at different viscosity ratio and at emulsification speed of 1200 rpm corresponding to a shear rate of 655.86 s^{-1} .

After applying the experimental finding of the equilibrium IFT values as well as the rheological data in Equation 11, and estimating the maximum stable droplet size in the studied emulsion, the resulting values were compared with the actual droplet sizes ($dv_{90\%}$) obtained by the microscope (Table 11). The method of droplet size analysis was described in section (3.2.1.4.4). The results revealed that the largest stable droplet size in the studied emulsion is well estimated using the critical capillary number equation, which indicates the reliability of this approach in predicting the inner phase droplet size in an emulsion prepared at lab scale.

Table 11. The estimated largest stable droplet sizes in the emulsions using Equation 11 compared to the actual droplet sizes ($d_{v90\%}$) obtained by the microscope for the emulsion prepared at a stirring rate of 1200 rpm corresponding to a shear rate of 655.86 s^{-1} .

| Polymer concentrations (% w/w) | Ca_{crit} (-) | Actual $d_{v90\%}$ (μm) | Estimated d_v (μm) |
|--|--------------------------------------|---|--|
| 0.5 % | 0.46 | 41 ± 2 | 42 |
| 0.75 % | 0.47 | 18 ± 2 | 19 |
| 1.0 % | 0.46 | 25 ± 2 | 22 |
| 1.5 % | 0.55 | 24 ± 0 | 24 |
| 2.0 % | 1.50 | 68 ± 0 | 67 |

4.5. Aerogel particles characterization

After conducting the gelation and the solvent exchange steps, the gel particles were dried by the supercritical CO_2 and the produced particles were characterized.

4.5.1. Zeta potential analysis

It was noticed that aerogel particles of Alg were more agglomerated than aerogel particles of Alg-HA of the same concentration. Since the agglomeration behavior is directly related to the surface charge, zeta potential analysis was conducted for the final aerogel particles (chapter methods, section 3.2.1.5.1). The results revealed that the zeta potential value of the tested Alg-HA was -37.1

mv which is much higher than zeta potential value of pure Alginate (-11.8 mv). This might be attributed to the presence of HA which is an anionic polymer or to the lower amount of Ca^{2+} in the Alg-HA particles. The findings of the current study are consistent with those of Chiesa et al. who reported a similar influence of HA on increasing the zeta potential value of HA- chitosan- based nanoparticle [183]. In a recent paper, López-Iglesias et al. prepared Alg aerogel particles for pulmonary drug application in the size range of the particles prepared in this study, they reported a negative zeta potential of -4.4 ± 0.4 mV. Such higher value was referred to the Ca^{2+} cations used extensively (concentration of 0.5 M) for the gelation of the Alg which partially compensate the negatively charged molecular chains of Alg.

4.5.2. Fourier transform infrared analysis for the aerogel particles

The Fourier transform infrared analysis (FTIR) was conducted on the final aerogel particles to check the possible interaction between Alg and HA. The FTIR spectra of plane Alg, plane HA and the physically mixed Alg-HA powder were analyzed and compared to the Alg-HA aerogel particles (Figure 27). In the FTIR spectrum of the plane Alg powder, a broad peak appears around 3252 cm^{-1} refers to the O-H stretching vibration. While the peak near 1598 cm^{-1} is related to the $\text{C}=\text{O}$ asymmetric stretching of the carboxyl group and the peak at 1407 cm^{-1} refers to the symmetric COO^- stretching vibration.

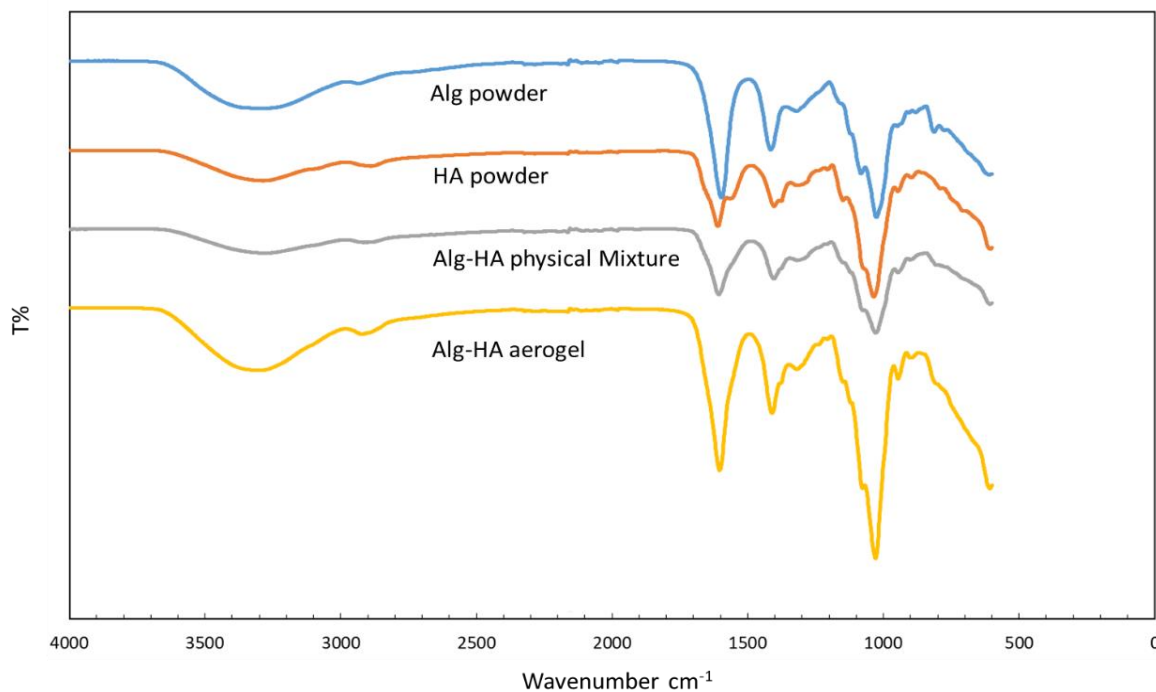


Figure 27. FTIR spectra of plain Alg, plain HA, Alg-HA powder and Alg-HA aerogel.

In the FTIR spectrum of plain HA, the peak appearing at around 1609 cm^{-1} with a shoulder at 1566 cm^{-1} corresponding to the C=O asymmetric stretching of the amide group. While a hydroxyl group O-H broad peak appearing around 3284 cm^{-1} , refers to the carboxyl group asymmetric stretching. The peak at 1403 cm^{-1} is related to the symmetric stretching of the carboxyl group COO^- . The peak at 1380 cm^{-1} is associated with a C-N stretching vibration of the aromatic amine [184], [185]. If comparing the FTIR spectra of the physically mixed Alg-HA powders with the corresponding aerogels, it seems that the spectra are almost unchanged, except a slight difference in the height and width of the COO^- bands. Also, with the hybrid Alg-HA aerogel it was noticed that the shoulder at 1566 cm^{-1} representing the amide C=O asymmetric stretching disappeared, which might be the result of hydrogen bond formation between the two polymers or of the dilution of HA in the aerogel.

4.5.3. Scanning electron microscopy

In the SEM micrographs (Figure 28) the external morphology of some particles are shown. different sizes and size distributions of the particles were found depending on the composition of polymer solutions, and the stirring rate during the emulsion gelation step. Comparing Alg with Alg-HA particles, the latter showed higher sphericity which might be referred to the stronger cross-linked network and more pronounced agglomeration tendency than the hybrid particles.

This behavior is less prominent for the Alg-HA particles, most probably because of the incorporation of HA which is expected to increase the surface charge of the particles and therefore increases repulsion and reduces agglomeration. The previously mentioned Zeta potential analysis supports this explanation.

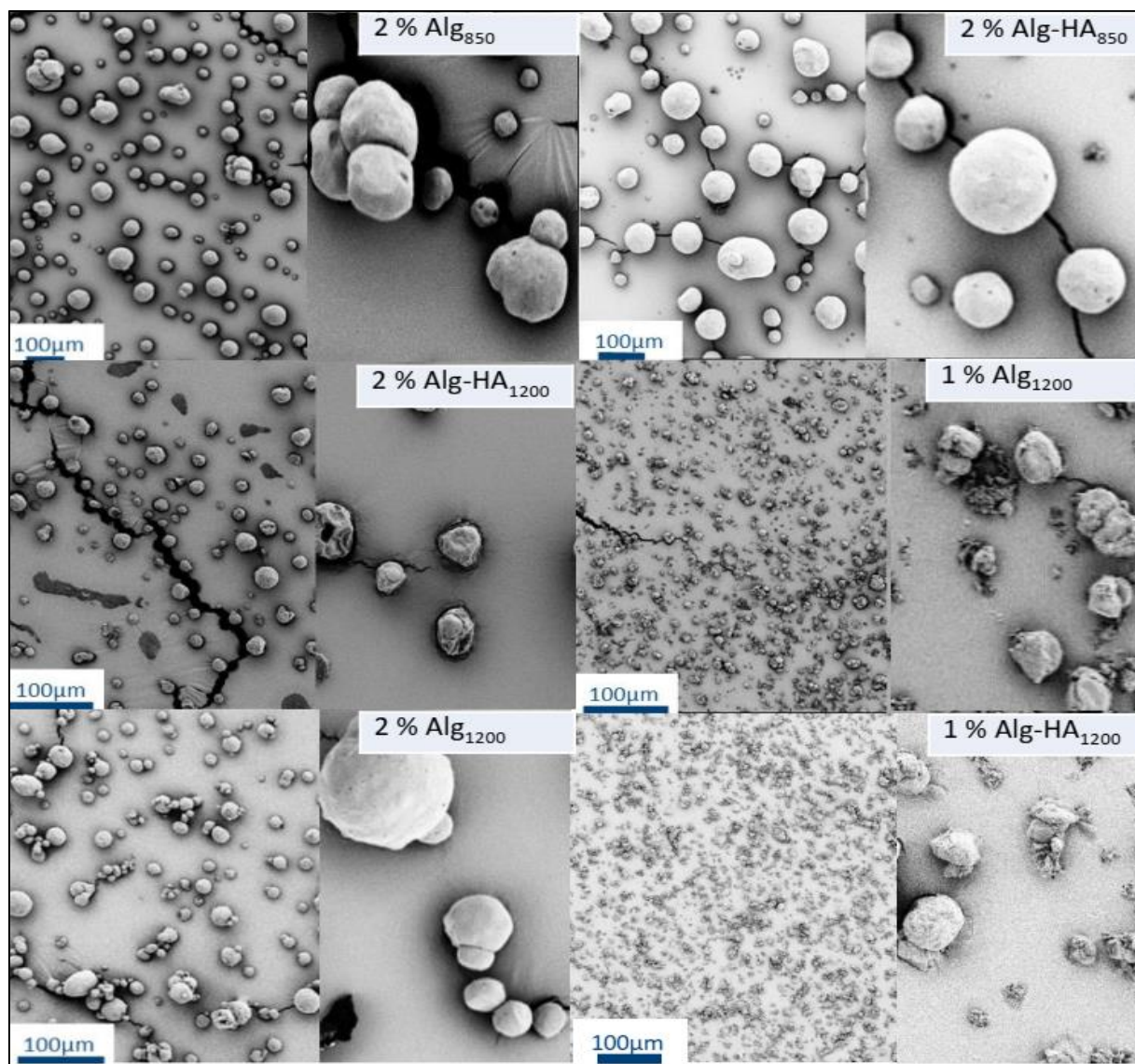


Figure 28. Scanning electron micrographs of different Alg and Alg-HA particles which were prepared by an emulsion gelation process with a subsequent drying step by supercritical CO₂ (the right side of each picture is a magnified part taken from the left side).

4.5.4. Particle size analysis

The particle size distribution of aerogel particles was measured by Camsizer XT (Retsch, Germany) (see chapter methods, 3.2.1.5.4) and presented in Table 12. The produced Alg and Alg-HA particles showed d_v values ranging from 1 - 365 μm . It is apparent from the table that the d_v values and consequently the size of the aerogel particles increased if increasing the viscosity of the polymer solution (by increasing its concentration). If the viscosity of the inner phase is increased and the emulsification speed is kept constant, more energy is required to create an interfacial area, which subsequently leads to produce larger particles [186]. Furthermore, it was noticed that d_v decreased if increasing the emulsification speed, which is directly attributed to the high energy input which splits the droplets apart. Such effect of the emulsification rate on the final aerogel particles prepared by the emulsion gelation technique has already been reported by Chen et al. (2017) and Alnaief et al. (2011) [187], [188].

If comparing the size of the Alg-HA particles with that of the plain Alg, it was unexpectedly found that the latter showed larger sizes at low polymer concentrations although it has a lower viscosity. This might be referred to the shrinkage of the gel during the preparation resulting from the low robustness of the gel because of the low Alg content. Therefore, less crosslinking points promoted the shrinkage and consequently smaller microsphere sizes are obtained. The density results reported in the next section support this explanation.

Table 12. d_v values of Alg and Alg-HA (1:1) aerogel particles (means \pm SD, n = 3).

| Emulsification rate | 500 rpm | 800 rpm | 1200 rpm |
|-------------------------------------|-----------------|-------------|------------|
| d_v | (μm) | | |
| Initial Alg concentration | | | |
| 0.5 % | 61* | 52 \pm 2 | 44 \pm 5 |
| 0.75 % | 47 \pm 1 | 40 \pm 2 | 28 \pm 6 |
| 1 % | 53.9 \pm 0.7 | 44 \pm 3 | 36 \pm 3 |
| 1.5 % | 78 \pm 9 | 53 \pm 2 | 45 \pm 5 |
| 2 % | 97 \pm 6 | 69 \pm 10 | 61 \pm 6 |
| Initial Alg-HA concentration | | | |
| 0.5 % | 72* | 42* | 34 \pm 3 |
| 0.75 % | 47 \pm 2 | 34 \pm 3 | 27 \pm 6 |
| 1 % | 53.0 \pm 0.8 | 37 \pm 3 | 31 \pm 2 |
| 1.5 % | 108 \pm 14 | 45 \pm 8 | 38 \pm 1 |
| 2 % | 179 \pm 11 | 63 \pm 8 | 54 \pm 1 |

*Measurement from single batch only: the yield of the prepared particles was not enough to be analyzed in triplicate.

Alnaief et al. (2011) also prepared Alg aerogel particle using the emulsion gelation method [156], the resulted particles were found to have d_{50} values of $491 \pm 41 \mu\text{m}$. Although in current study the same polymer and surfactant concentrations were used, smaller microsphere diameters (28 ± 6) were reached after modifying the emulsification process parameters (viscosity of the continuous

phase and aqueous phase/oil phase ratio). Furthermore, a positive effect was achieved by hybridization of Alg with HA in term of decreasing of particles agglomeration. Moreover, the biodegradability of such particles is expected to be improved.

4.5.5. Particle density, porosity and BET surface area

All the aerogel particles showed ultra-high porosities of 97.5 - 99.8 %, as well as high BET specific surface areas and low particle true densities in the range of 0.0087 - 0.0634 g/cm³. The BET specific surface areas of the prepared aerogel particles are ranging between 354 ± 16 and 759 ± 22 m²/g (Table 13). Such high surface areas for polysaccharide based aerogels, dried by the supercritical fluid technology, were also reported by various researchers [12], [39], [156], confirming that supercritical drying is a method of choice to preserve the gel structure as revealed by the high surface areas and porosities. Generally, the hybrid particles show lower BET surface area than the pure Alg particles of the same concentration. This might be because the HA is not participating in the crosslinking mechanisms, but is entrapped within the pores formed by the crosslinked Alg to form an interpenetrating network. The results of Quraishi et al. (2015) support this explanation [89]. They prepared calcium crosslinked alginate-lignin hybrid aerogel in a form of interpenetrating hybrid network in which Alg is forming the ionic network with calcium ion and noticed that the higher the lignin ratio in the hybrid aerogels the lower the BET surface area [89].

Table 13. BET surface areas of the investigated aerogel particles; means \pm SD, n = 3.

| Stirring speed | 500 rpm | 800 rpm | 1200 rpm |
|-------------------------------------|--|--|--|
| Sample | S_{BET} (m²/g) | S_{BET} (m²/g) | S_{BET} (m²/g) |
| Initial Alg concentration | | | |
| 0.5 % | 560** | 567 \pm 3 | 759 \pm 22 |
| 0.75 % | 687 \pm 44 | 681 \pm 42 | 678 \pm 55 |
| 1 % | 687 \pm 5 | 654 \pm 7 | 581 \pm 50 |
| 1.5 % | 644 \pm 33 | 657 \pm 9 | 620 \pm 9 |
| 2 % | 596 \pm 72 | 622 \pm 8 | 611 \pm 49 |
| Initial Alg-HA concentration | | | |
| 0.5 % | 527 \pm 5 | -* | 696 \pm 68 |
| 0.75 % | 623 \pm 106 | 531 \pm 28 | 607 \pm 8 |
| 1 % | 625 \pm 37 | 510 \pm 24 | 575 \pm 50 |
| 1.5 % | 649 \pm 19 | 562 \pm 32 | 561 \pm 20 |
| 2 % | 699 \pm 20 | 637 \pm 22 | 538 \pm 29 |

*The tested amount was too small

**single measurement was done due to the low yield

By comparing the results of tables 14 and 15, which present the density values of the prepared aerogel particles, it can be noticed that most of Alg-HA particles showed lower particle densities than the Alg particles of the same initial polymer concentration. Such decrease can be explained by the mass loss of HA because of the washing out of HA from the hybrid gel during the solvent exchange process. Thus, after drying more spaces inside the aerogel is expected to be created. In this sense HA is acting similar to templates using for production of porous particles.

The particle densities and surface areas are supposed to reveal no clear dependence on the stirring speed, as the textural properties is influenced by the three-dimensional structure of the initial gel, that is mainly affected by the degree of crosslinking, as well as by the solvent exchange sequence, the solvent type and the drying conditions [189], which were all retained constant. This was obvious for Alg particles, the density was not affected by the emulsification speed, but rather by the polymer concentration. As Table 5 shows, when the polymer concentration is increased from 0.5 to 2 % w/w (at emulsification speed of 500 rpm) the density increased from 0.0254 to 0.0620 (g/cm³). If comparing the densities of the particles prepared from 0.5 % w/w Alg at different emulsification rates the densities are almost similar.

Table 14. Densities (g/cm^3) of the prepared plain Alg aerogel particles (g/cm^3); means \pm SD, $n = 3$.

| Concentration %w/w | 0.5 % | 0.75 % | 1 % | 1.5 % | 2 % |
|-------------------------|------------------------|------------------------|------------------------|----------------------|------------------------|
| Stirring speed | 500 rpm | | | | |
| Tap density | 0.0202 \pm 0.0007 | 0.0240 \pm 0.0003 | 0.029 \pm 0.002 | 0.041 \pm 0.005 | 0.0492 \pm 0.0000 |
| Particle density | 0.0254 \pm 0.0009 | 0.0303 \pm 0.0004 | 0.037 \pm 0.003 | 0.052 \pm 0.007 | 0.0620 \pm 0.0001 |
| Stirring speed | 800 rpm | | | | |
| Tap density | 0.02 \pm 0.01 | 0.0235 \pm 0.0002 | 0.0299 \pm 0.0005 | 0.040 \pm 0.001 | 0.050 \pm 0.002 |
| Particle density | 0.0278 \pm 0.0002 | 0.0295 \pm 0.0003 | 0.0376 \pm 0.0007 | 0.051 \pm 0.001 | 0.063 \pm 0.003 |
| Stirring speed | 1200 rpm | | | | |
| Tap density | 0.0199 \pm 0.0004 | 0.0254 \pm 0.0005 | 0.028 \pm 0.001 | 0.039 \pm 0.003 | 0.050 \pm 0.001 |
| Particle density | 0.0251 \pm 0.0005 | 0.0320 \pm 0.0006 | 0.036 \pm 0.002 | 0.049 \pm 0.003 | 0.063 \pm 0.001 |

Surprisingly the hybrid particles show a different trend than the Alg particles, as the particle density decreased first with an increase in the polymer concentration from 0.5 to 1 % w/w and then increased (Table 15).

Table 15. Densities (g/cm^3) of the prepared Alg-HA aerogel particles; means \pm SD, n = 3.

| Concentration %w/w | 0.5 % | 0.75 % | 1 % | 1.5 % | 2 % |
|-------------------------|------------------------|------------------------|------------------------|------------------------|------------------------|
| Stirring speed | 500 rpm | | | | |
| Tap density | 0.0167 \pm 0.0004 | 0.0132 \pm 0.0004 | 0.0122 \pm 0.0009 | 0.0228 \pm 0.0003 | 0.0269 \pm 0.0002 |
| Particle density | 0.0210 \pm 0.0005 | 0.0166 \pm 0.0005 | 0.0150 \pm 0.001 | 0.0288 \pm 0.0003 | 0.0338 \pm 0.0002 |
| Stirring speed | 800 rpm | | | | |
| Tap density | 0.0220 \pm 0.006 | 0.0145 \pm 0.0002 | 0.0129 \pm 0.0008 | 0.0214 \pm 0.0004 | 0.0272 \pm 0.0007 |
| Particle density | 0.0270 \pm 0.008 | 0.0183 \pm 0.0002 | 0.016 \pm 0.001 | 0.0269 \pm 0.0006 | 0.0342 \pm 0.0009 |
| Stirring speed | 1200 rpm | | | | |
| Tap density | 0.0110 \pm 0.002 | 0.0069 \pm 0.0001 | 0.0123 \pm 0.0000 | 0.0208 \pm 0.0004 | 0.0267 \pm 0.0000 |
| Particle density | 0.013 \pm 0.002 | 0.0087 \pm 0.0001 | 0.0155 \pm 0.0000 | 0.0261 \pm 0.0005 | 0.0336 \pm 0.0001 |

To exclude the effect of particle size distribution on calculating the density, aerogels monoliths (cylinder in shape with volume range 2 - 8 cm³) of Alg and Alg-HA were prepared with exactly the same polymers and calcium concentrations of the particles and their densities were compared to each other (see section 3.2.1.3.3). Figures 29 and 30 shows the particle true densities of the Alg and Alg-HA particles respectively, prepared at different concentrations (0.5 %, 0.75 %, 1 %, 1.5 %, and 2 %) compared to the true (bulk) density of the monoliths prepared at the same polymer concentrations. The plot of the densities versus the Alg concentration of the particles agrees with the monoliths, resulting in an R² value > 0.99 for the particles results. Accordingly, it might be possible to predict the true density of Alg aerogel (particles or monoliths) within the same experimental condition of this study.

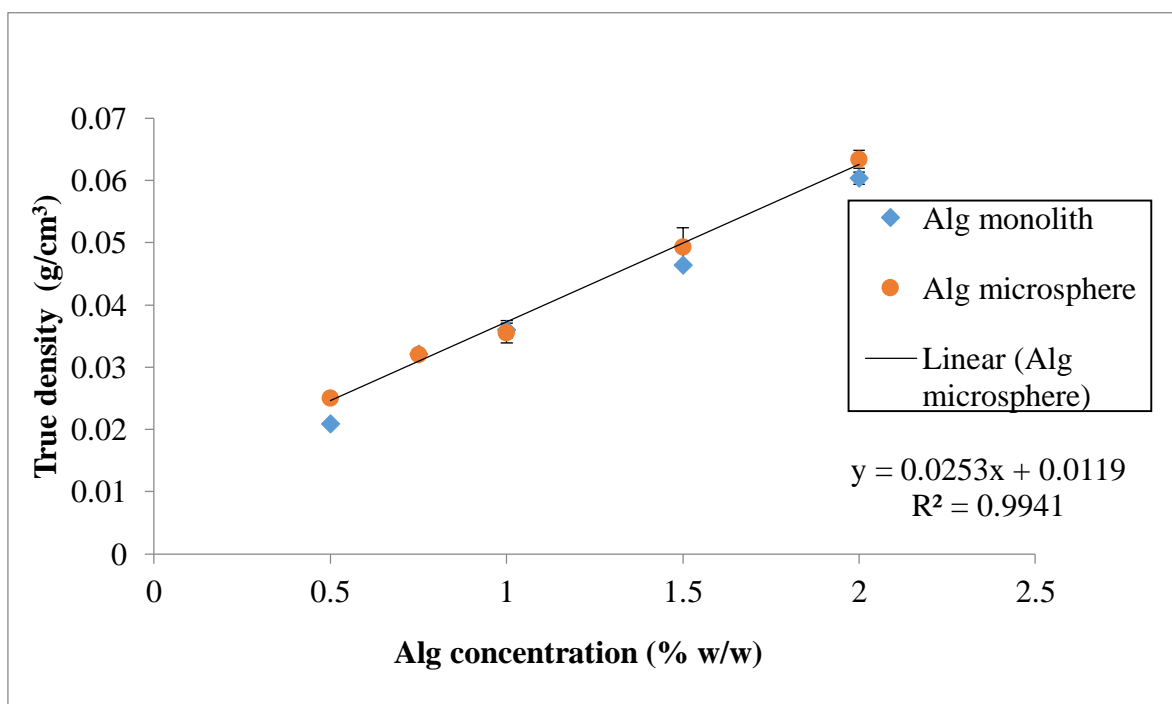


Figure 29. True density of Alg particles (prepared at 1200 rpm) compared to the true density of monoliths prepared at various concentrations of Alg; means \pm SD, n = 3.

It was observed that the true density of an Alg microsphere is comparable to the monolith's true density. However, in the case of Alg-HA (Figure 30), monoliths showed higher densities in comparison to the true density of the particles at the corresponding polymer concentrations. This behavior might be associated with the difference in mass loss of HA between the particles and the monoliths, because of their different exposed surface area, which is expected to be more pronounced in microparticles than in monoliths.

It was previously said, the density of Alg-HA particles decreased with an increase in the polymer concentration from 0.5 to 1 % w/w and then started to increase again. Interestingly, the same trend was also observed for monoliths (Figure 30). Thus, it is likely that the gel size and shape are not responsible for this effect, but rather the mechanical strength of the gel. In this study, Alg was cross-linked with Ca^{2+} ions providing the gel robustness: the higher the amount of Alg, the stronger the gel structure and the lower the shrinkage [190]. Keeping in mind that 0.5 % Alg-HA mixture corresponds only to 0.25 % Alg, the structure of the gel is expected to be weak and susceptible to a more pronounced shrinkage in comparison to the 0.75 % Alg-HA, leading to condenser gel network and consequently to higher true densities. The same explanation is proposed to the fact, that the density of the 0.75 % Alg-HA aerogels is higher than that of the 1 % Alg-HA aerogels. Nevertheless, this effect of shrinkage is diminished at higher polymer concentrations above 1 % of Alg-HA (containing 0.5 % Alg), because the greater degree of crosslinking is higher, and, therefore, the structure becomes stronger and less susceptible to shrinkage. Accordingly, in this research, the 1 % polymer concentration of the Alg-HA aerogel may be considered as the critical polymer concentration, above which the aerogel is strong enough and its density is proportional to the polymer concentration similar to the trend observed with the Alg aerogels.

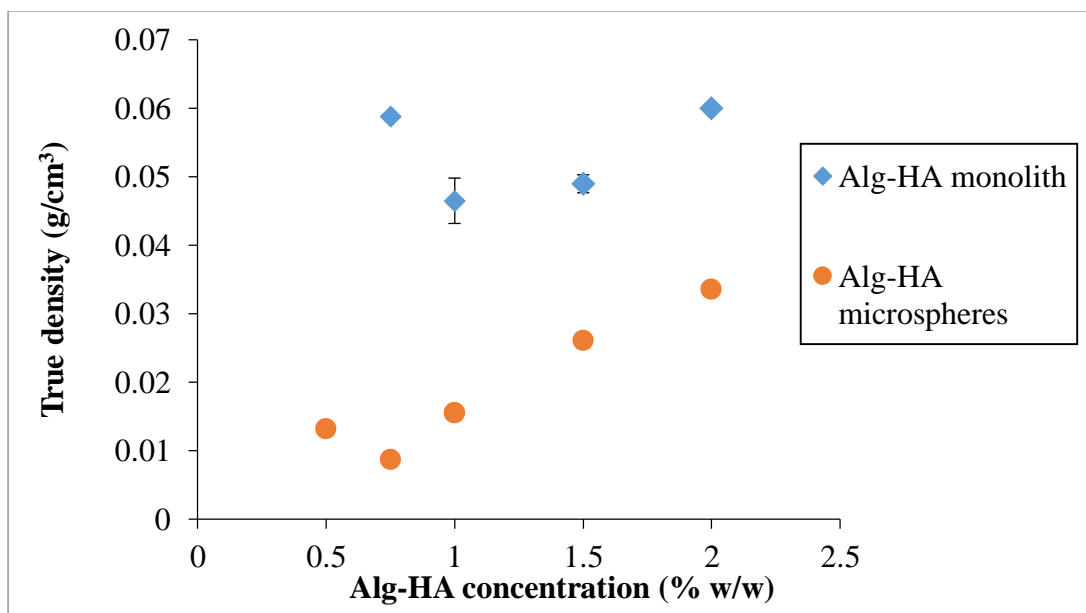


Figure 30. True density of Alg-HA particles (prepared at 1200 rpm) compared to the true density of monoliths prepared at various concentrations of Alg-HA, means \pm SD, $n = 3$.

The previous findings were used together with the particles size results to estimate the aerodynamic diameters (d_A) of Alg and Alg-HA aerogel particles.

4.5.6. Analysis of aerodynamic diameter

The geometrical diameters (d_v) and the densities of the prepared particles were applied in equation 2 to estimate the aerodynamic diameters (d_A) of Alg and Alg-HA particles, the results are illustrated in table 16. It was found that to attain aerodynamic diameter in the range of (0.5-5 μm) that is suitable for pulmonary drug delivery, the d_v of the prepared particles should be < 30 μm for Alg, and < 34 μm for the Alg-HA.

It can be noticed that for the Alg-HA particles it was possible to reach d_A in the range of (0.5-5 μm) for five samples (0.5 % at 1200 rpm, 0.75 and 1 % at 800 rpm, and 0.75 and 1 % at 800 rpm), whereas for the Alg particles it was not possible to reach low range of d_A even at high

emulsification rates and at low viscosities (concentrations). This was referred to the effect of HA in term of reducing the agglomeration and lowering the density of the aerogel particles.

Table 16. The estimated d_A values of Alg and Alg-HA (of a wt. ratio 1:1) particles aerogel particles prepared by the emulsion gelation technique at different conditions

(means \pm SD, n = 3).

| Emulsification rate | 500 rpm | 800 rpm | 1200 rpm |
|-------------------------------------|-------------------|-----------------|---------------|
| d_A | (μm) | | |
| Initial Alg concentration | | | |
| 0.5 % | 9.7* | 8.6 \pm 0.3 | 7.0 \pm 0.9 |
| 0.75 % | 8.2 \pm 0.2 | 6.9 \pm 0.3 | 5 \pm 1 |
| 1 % | 10.4 \pm 0.1 | 8.5 \pm 0.5 | 6.8 \pm 0.5 |
| 1.5 % | 18 \pm 2 | 12.0 \pm 0.4 | 10 \pm 1 |
| 2 % | 24 \pm 2 | 17 \pm 2 | 15 \pm 2 |
| Initial Alg-HA concentration | | | |
| 0.5 % | 10.4* | 7.0* | 3.9 \pm 0.3 |
| 0.75 % | 6.0 \pm 0.3 | 4.6 \pm 0.4 | 2.6 \pm 0.6 |
| 1 % | 6.55 \pm 0.09 | 4.7 \pm 0.3 | 3.8 \pm 0.3 |
| 1.5 % | 18 \pm 3 | 7.33 \pm 0.06 | 6.1 \pm 0.2 |
| 2 % | 33 \pm 2 | 12 \pm 2 | 9.9 \pm 0.2 |

*Measurement from single batch only, because the yield of the prepared particles was not enough to be analyzed in triplicate.

Using the cascade impactor, the *in vitro* d_A of selected samples of the prepared particles were measured and were compared with their estimated values. It was found that the estimated d_A values were in agreement with the experimental values (Figure 31). The *in vitro* d_A values for most of the tested samples were in the range which is suitable for deep lung deposition (0.5 - 5 μm). For most of the tested particles, the *in vitro* d_A values were higher than the calculated value and this may be referred to the hygroscopic nature of HA: as the cascade impactor stages were mimicking the airways humidity, particles containing HA are expected to absorb moisture during passing through its stages, which increases their weight and consequently their d_A values.

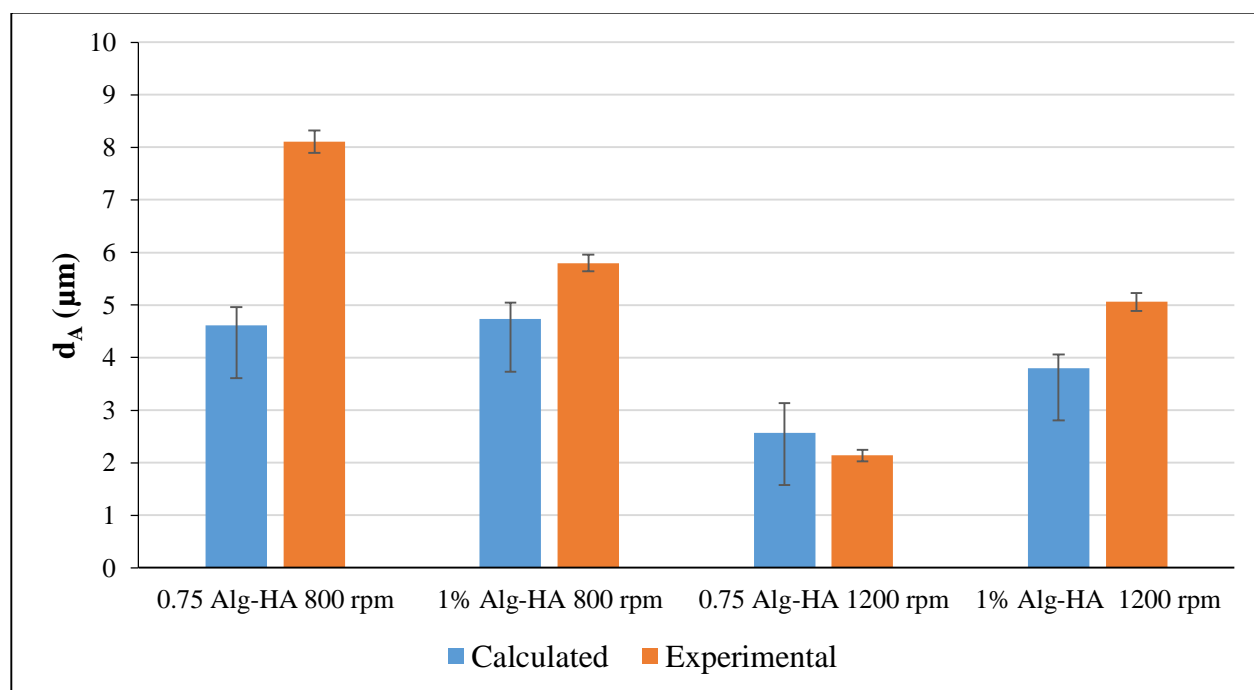


Figure 31. Aerodynamic diameter (d_A) of selected samples of the Alg-HA particles which were prepared by the emulsion gelation technique with a subsequent drying step by supercritical CO_2 (means \pm SD, $n = 3$).

Sample 0.75 % Alg-HA₁₂₀₀ shows the lowest experimental and calculated d_A values (2.6 and 2.1 μm respectively). Such diameter allows the particles to be deposited in the lower respiratory tract. So far, only one recent study was found in the literature regarding the evaluation of the aerodynamic properties of aerogel microparticles. López-Iglesias et al. (2019) prepared Alg particles by thermal inkjet printing combined with supercritical CO₂ drying [32]. Comparing the two results, the same d_A values were found in this work as those obtained by the mentioned researchers. Nevertheless, the emulsion gelation technique shows clear advantages with flexibility to use broader range of viscosities and higher polymer concentrations as well as to produce larger amount of particles in a shorter time. Furthermore, the emulsion gelation technique can be established in a continuous mode [181], allowing for an easy scale-up of the production of aerogel particles.

Based on the previous results, particles produced at 1200 rpm with a polymer concentration of 0.75 % Alg and Alg-HA, respectively, were chosen for the *in vitro* drug release studies.

Summarizing, the present findings confirm the feasibility of using the emulsion gelation process with the supercritical CO₂ drying to prepare spherical aerogel particles of Alg and Alg-HA. The latter particles fulfil the requirement of deep lung deposition in term of aerodynamic properties. Such low d_A is mainly referred to the positive effect of HA addition, that reduces the particle density and lowers the agglomeration tendency.

4.6. Supercritical drug impregnation and *in-vitro* release from the particles

Although the prepared aerogel particles were found to be able to reach the deep lung, they cannot be considered a successful pulmonary drug carrier unless they are able to carry a significant amount of the drug to the cite of action. At the same time to be able to release loaded drug in the

lung. Therefore, it was necessary to evaluate the drug loading efficiency of the prepared aerogel particles, as well as the drug release under the physiological lung conditions. Also, it was important to figure out the influence of HA addition on the release of naproxen from the aerogel particles. Thus, the drug release from Alg aerogel particles and that from Alg-HA was investigated.

The drug loading from a supercritical CO₂ into an aerogel carrier may be considered as a tunable process, as it can be controlled by the depressurization rate, the time of impregnation or the supercritical CO₂ density (and consequently the drug solubility in it) by adjusting its pressure and temperature [191], [192]. In addition to the process parameters, drug impregnation into an aerogel by supercritical CO₂ depends mainly on the surface chemistry and the textural properties of the aerogel carrier (e.g. pore size and surface area), in addition to the drug-carrier interactions and the chemistry of the loaded drug. Thus, the drug loading capacity increases if the surface area and pore size of the aerogel are increased [189]. Table 17 show the loading efficiency results of naproxen into Alg and Alg-HA based particles.

Table 17. Loading efficiency and pore properties of the loaded aerogel particles of Alg and Alg-HA prepared at 1200 rpm of polymer concentration 0.75 % w/w.

| Sample name | particle diameter (μm) | Loading efficiency (g/g) | Loading efficiency (mg/m ²) | Total pore size (cm ³ /g) |
|-----------------------------------|------------------------|--------------------------|---|--------------------------------------|
| 0.75 % Alg _{1200 rpm} | 28 | 0.21 | 0.29 | 7.9 |
| 0.75 % Alg-HA _{1200 rpm} | 27 | 0.20 | 0.33 | 6.4 |

There were no significant differences between the drug loading of plain Alg and in the Alg-HA aerogels. This can be related to their comparable surface area (678 ± 55 and 607 ± 8 m²/g for the Alg and Alg-HA particles, respectively) and pore sizes.

To compare the previous results with the literature, it was important to find studies in which the supercritical CO₂ drug impregnation was conducted under the same parameter (pressure, temperature and time) of the current study. Also it was necessary to compare the loading efficiency of naproxen with a drug of similar molecular structure and solubility in supercritical CO₂. Therefore, few studies have been found under these restrictions. Gonçalves et al. (2016) prepared Alg aerogel microparticles by the same technique of the current study and were impregnated with ketoprofen by adsorption from supercritical CO₂. The prepared Alg microparticles showed a BET surface area of 330 m²/g and a loading efficiency of 0.22 g/g, which is corresponding to 0.7 mg/m². This considerable loading was referred by the authors to the ketoprofen – Alg aerogel interaction. As the formation of hydrogen bonds between OH- and COOH- groups of the Alg and carboxylic and carbonyl group of ketoprofen is expected [72]. In another study, García-González et al. (2015) prepared Alg particles by emulsion gelation technique. Their results revealed that the prepared aerogel particles have a specific surface area of 524 ± 26.4 m²/g and a loading efficiencies for benzoic acid of 0.23 g/g (0.43 g/m²), which is comparable with the current results [12].

There is no standard method in the pharmacopoeia for the evaluation of the drug release from a pulmonary drug carrier which simulates the drug release in the respiratory tract [164], so it was not possible to simulate the biological conditions in the lung. Therefore, the drug release experiment used in the present study was conducted mainly to explore the differences in the drug release between Alg and Alg-HA aerogel particles.

After obtaining the calibration curve of naproxen in PBS (pH 7.4), the in vitro release profiles of naproxen from Alg and Alg-HA particles was investigated (see chapter methods, section 3.2.1.7), results are illustrated in Figure 32. If taking into account the overlapping error bars, no significant differences can be noticed between the release profiles of Alg and Alg-HA particles. Both of them showed a fast initial release rate at the first 30 min followed by a slow release up to 180 min. Such fast release is expected from the Alg and Alg-HA aerogel particles, as it was reported by Garcia et al. that hydrophilic aerogels show burst release and hydrophobic aerogels show sustained release [11]. Although it was expected to observe a faster drug release from the Alg-HA than the Alg particles, because of the lower crosslinker concentration and the lower polymeric concentration (due to the mass loss of HA). But apparently, those factors were somehow compensated, maybe by the polymer-polymer interaction which was found between the Alg and HA, that strengthened the polymeric network and delay the dissolution. Or it might be related to the effect of HA, that is expected to swell and form a viscous matrix inside the Alg network, thus, naproxen is likely take

longer time to pass through this pathway. Nevertheless, more research is inquired to investigate this behavior and to check the previous hypotheses.

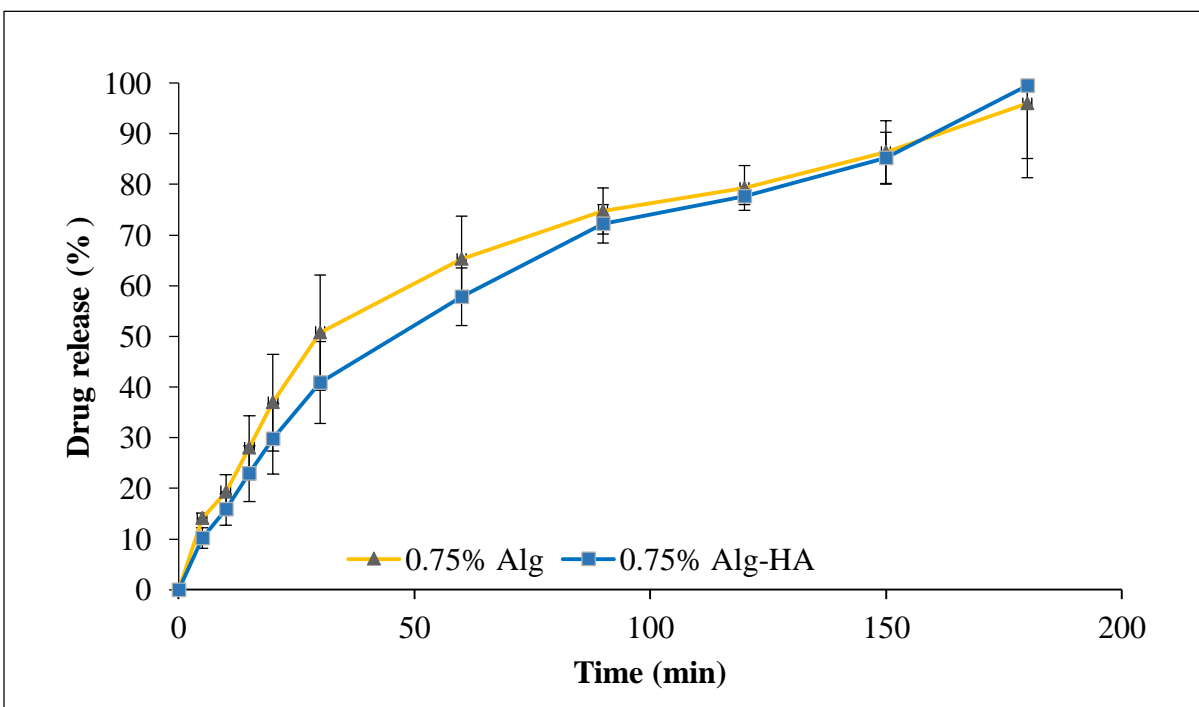


Figure 32. In vitro release profile of sodium naproxen from 0.75 % Alg and Alg-HA microspheres. Study was conducted in phosphate buffer solution ($\text{pH } 7.4 \pm 0.05$) at 100 rpm in a shaking water bath at 37°C , means \pm SD, $n = 3$.

To study the release kinetics, Ritger–Peppas and Korsmeyer–Peppas semiempirical model - the so-called power law - (Equation 23) was applied, which was developed by Korsmeyer, Gurny, Doelker, Buri, and Peppas (1983) and Ritger and Peppas (1987). This semi-empirical model can be used to describe the drug release kinetics from a polymer matrix, when the release mechanism is unknown or when more than one type of phenomenon of drug release is expected to be involved [193], [194].

$$M_t/M_\infty = kt^n$$

Equation 23

where M_∞ is the amount of drug at the equilibrium state, M_t is the amount of drug released over time t , k is a constant reflecting the structural and geometric characteristics of the delivery system, and n is a release exponent the value of which is related to the underlying mechanism(s) of drug release (related to the drug release mechanism). The value of the exponent n obtained from the fitting of the equation 23 to the first 60 % drug release of the experimental data is an indicative of the release mechanism (Table 18).

Table 18. Values of the exponent n in Equation 23 and the corresponding release mechanisms from a delivery system of various geometries [196].

| Exponent n for a sphere | Drug release mechanism |
|---------------------------|--|
| 0.43 | Fickian diffusion |
| $0.43 < n < 0.85$ | Anomalous transport (combination of Fickian diffusion and Case II transport) |
| 0.85 | Case II transport (zero-order kinetics) |

The results below 60 % of the release data were fitted to this model, the R^2 values were found to be 0.99 and 0.97 for the Alg-HA and Alg particles, respectively. The n value was found to be 0.66 for the Alg particles and 0.73 for the Alg-HA particles, this suggest a non-Fickian or anomalous transport model, in which the mechanism of drug release is controlled by diffusion and swelling equally. Comparing the results to the literature, Mehling et al. (2009) studied the release profile of ibuprofen from Alg aerogel in PBS at pH 7.2, the studied aerogel was crosslinked with CaCO_3 and

impregnated with the drug by the supercritical adsorption method. The results were found comparable with the current study, as 50 % of the ibuprofen was released in around 30 min. They also reported that the release profile of ibuprofen is dependent on the kind of the matrix, since the drug is absorbed at a molecular level [37]. In another study of López-Iglesias et al. (2019), Alg aerogel particles were prepared by Inkjet printing technique and loaded with salbutamol sulphate. Their results showed more sustained drug release profile than the current study, which was expected because the Alg network in the mentioned study has much higher crosslinking degree [32].

The insignificant differences between the release profiles of Alg and Alg-HA particles can be considered as another advantages of the hybridization of Alg with HA. Because the release behavior and kinetics of Alg particles stayed almost constant, although the crosslinking degree was reduced to the half. In case of lower crosslinking, higher biodegradation rate is expected for those hybrid particles, not only due to the presence of HA, but also because of encompassing less crosslinker amount.

Summarizing the results obtained in this study some general conclusions for aerogel application as pulmonary drug delivery can be drawn. Pulmonary drug delivery methods have mainly two strategies: (i) the use of controlled release polymeric systems to improve the duration and effectiveness of inhaled drugs, for both local and systemic action and (ii) the use of mixtures of dry drug particulates with dry carrier particles (mainly composed of sugars) to deliver drug quickly to the bloodstream or local tissue to treatment asthma and pain relief [195]. Using aerogel technology, the properties of the pulmonary carrier can be tailored in a way allowing to control the drug release in a degree ranging from fast drug release to prolonged one, based on the selected polymer and crosslinking type and/or degree. Regarding to the aerogel particles of this study, if

the in vivo drug release kinetics was similar to the previous in vitro finding, the prepared aerogel carrier might be more suitable to deliver drug quickly (to treat asthma or to relief pain). Nevertheless, the release profile may be sustained for a longer time period by increasing the polymer concentration and/or the crosslinking degree of the aerogels, taking into consideration the biodegradation issues.

4.7. *In vivo* toxicity study of calcium alginate aerogel

Alg has been widely used in food products and pharmaceutical additives (such as gelling agent and tablet disintegrant) [196], [197], as well as in biomedical applications, including drug delivery and tissue engineering [198]. Like other edible dietary fibers, Alg and its oligomer derivatives are resistant to the digestion by the human endogenous enzymes. However, it can be digested significantly by the human gut microbiota [199]. Despite its importance, little is known about such gut microbiota that is responsible for the degradation of Alg.

The European Food Safety Authority (EFSA) has declared the safety of alginic acid and its salts as well as the fermentation products from alginic acid and its salts. As the *in vivo* test for the absorption and excretion of the aqueous solution or suspension of alginic acid and its salts in animals were investigated. The results showed its inability to be absorbed or metabolized by enzymes present in the gastrointestinal tract regardless of the form administered. However, they would be partially degraded by fermentation during their passage through the large intestine by the action of the anaerobic intestinal microbiota causing caecal enlargement which was considered by the EFSA as an adaptive process related to the high doses tested as food additives [200]. Nevertheless, no previous *in vivo* studies have examined the effect of calcium alginate aerogel (Ca-Alg) on the liver, kidney or the bacterial community in the intestines.

Gut microbiota are very essential components of the human digestive system, as they help in the degradation of the ingested food, especially those that human body doesn't have the required enzymes for [201], [202]. Gut microbiota can also inhibit the blooming of pathogenic microorganisms through competing them on the nutrients resources, or by producing chemical substances to inhibit their growth. However, it has been shown that degradation of the ingested digestible fibers such as Alg occurs mainly by fermented bacteria in the colon [203]. The products

of this process are short-chain fatty acids (SCFA), which are beneficial for colon inflammation and act as anticancer. Brownlee et al. reported in their paper that the incubation of Alg and human fecal microflora demonstrated that most of Alg degradation is accompanied by change in the gut microbiota. Also, such incubation leads to the production of SCFA and gas after 24 hours [203].

Part of the goal of this thesis is to assess the safety of Ca- Alg aerogel through studying its effect on the kidney and liver, as it has been proposed widely in the literature for drug delivery applications. Besides, as Alg is degraded in the intestinal by the gut microbiota, it is also crucial to study the effect of Ca-Alg aerogel on the intestinal microbial community.

4.7.1. Short-term toxicity (Sighting study)

The short-term toxicity experiments were basically designed to detect the highest safe dose of Ca-Alg aerogel associated aerogels application as oral drug carrier if used for short-term treatment intervals, e.g. antibiotics, this was done through tracking the liver and kidneys enzymes. Five dosage levels were applied to specify the highest possible dosage of aerogels that can be used safely. One rat from the group of the highest dosage of 500 mg aerogels passed away on day 2. Upon necropsy examination of this group, the rats of this group were found to have swollen GI (Figure 33) that might be referred to a physical blockage of the digestive track because of the undigested Ca-Alg aerogel and the gases produced by its fermentation.



Figure 33. Two examples on the swelling of the gastro-intestinal tract of the rats belonging to the group of 500 mg aerogels.

4.7.1.1. ALP level analysis

ALP blood level was used as an indicator for liver toxicity. A baseline for the normal ALP level was established using the ALP readings for all the animals on day 0 (n = 35). The average of the established ALP level was $0.84 \pm 0.36 \mu\text{Kat/L}$, and the median was $0.74 \mu\text{Kat/L}$ with a range of (0.28 – 1.98 $\mu\text{Kat/L}$). When comparing the ALP levels independently between each individual treatment group and the control group (Figure 34), no significant differences were detected in the ALP levels at the beginning of the study on day 0. However, there was a significant difference ($p < 0.05$) in three groups on day 7, namely the treatment groups taking 500 mg of Ca-Alg aerogel and 50 and 500 mg of Na-Alg. On day 3 and day 5 the only significant difference in the ALP levels was detected between the control group and the treatment group who were administered the 500 mg dosage of alginate.

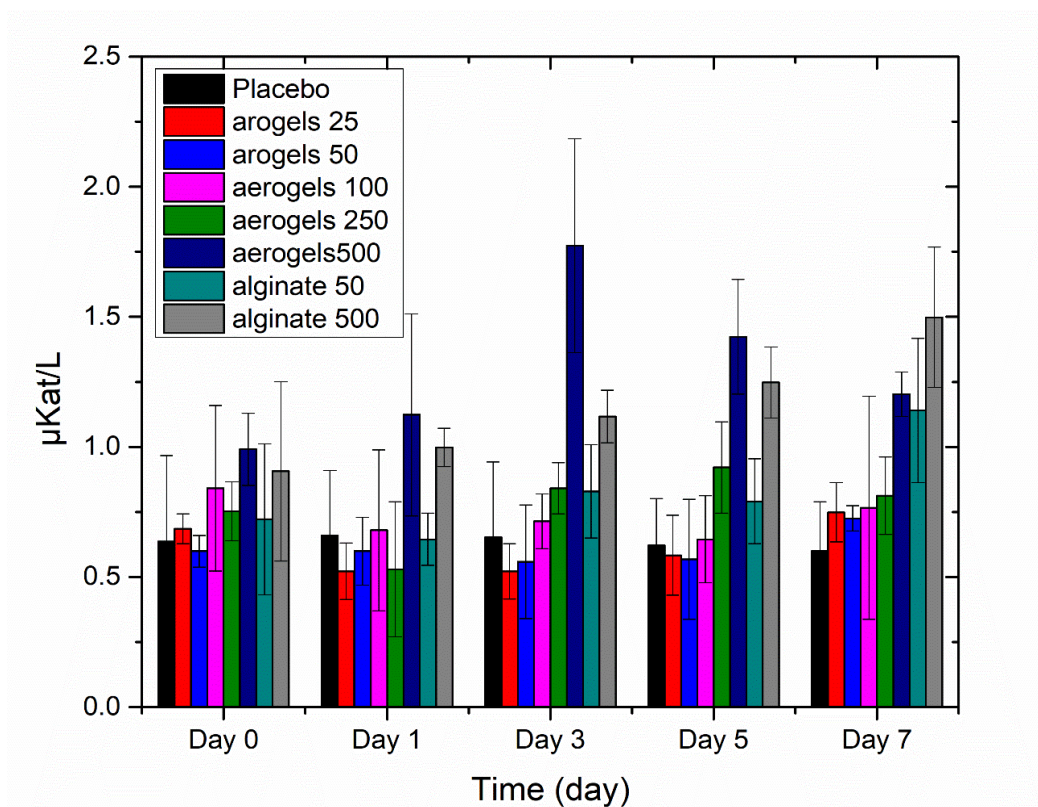


Figure 34. Short term analysis for the effect of different doses of calcium alginate aerogels and sodium alginate on ALP serum levels (aerogel corresponding to Ca-Alg aerogel and alginate corresponding to Na-Alg).

Overall, the average ALP levels for the different treatment groups of Ca-Alg aerogel and Na-Alg aerogel did not exceed neither the highest level of the normal range established at baseline nor the stated value in the literature (113.8 ± 4.7 IU/L = 1.93 μ kat/L) [204]. It is well known however that the raise in the ALP values could be referred to the stress factors that the rats might be experienced during taking the blood sample and /or giving them the assigned dose of the treatment [205].

4.7.1.2. Creatinine level analysis

Creatinine blood level was used as an indicator for kidney toxicity. The baseline for the normal creatinine level was also established using the readings for all the animals on day 0 (n = 35). The average of the established creatinine level was 0.38 mg/dl with a median of 0.32 mg/dl and a range of (0.09 – 1.47 mg/dl). When comparing the creatinine levels for the control group with the levels of each treatment group independently, no significant differences were detected in the creatinine levels for the 7-days duration of the study.

In the short-term treatment, creatinine levels of 100 mg group (Figure 35B) increased slightly from 0.3 mg/dl at day 0 to 0.625 mg/dl at day 7. While in the group of 250 mg (Figure 35C) creatinine levels increased from 0.5 mg/dl to 0.72 mg/dl on day 1. Then, they returned gradually to 0.5 mg/dl on day 7. With respect to the groups of rats treated with the following doses; 50 mg Ca-Alg aerogel (Figure 35A), 500 mg Ca-Alg aerogel (Figure 35D), 50 mg Na-Alg (Figure 35E) and 500 mg Na-Alg (Figure 35F), creatinine levels stayed within the range of (0.2 mg/dl to 0.5 mg/dl) from day 0 to day 7. During this part of the study, the average of the creatinine level in all groups did not exceed neither the upper limit of the established baseline nor the normal level of creatinine in rats (0.25–3.09 mg/d) [206].

Based on the results obtained from the short term sighting study, including clinical observations and blood biochemistry, the dosage level of 250 mg aerogels (dose ~ 1000 mg/kg) was selected to be further investigated in the second part of the toxicity study.

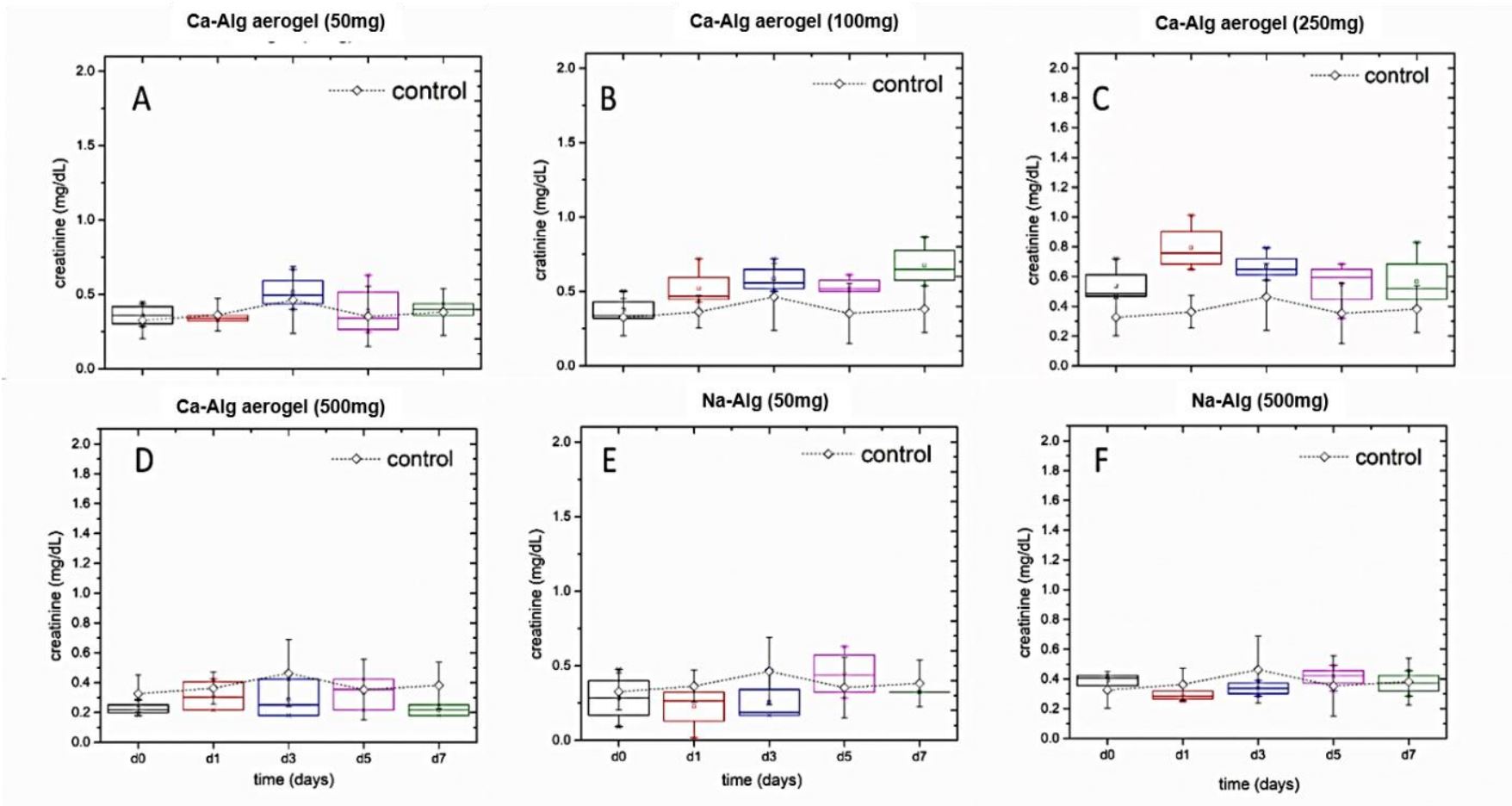


Figure 35. Box-plot for the in vivo serum creatinine level analysis that was done for the different doses of the aerogels and the alginate.

The dotted lines in all the panels represent the creatinine values for all the control groups.

4.7.2. Long-term toxicity study

4.7.2.1. ALP level analysis

In Figure 36A, the long-term experiment results for the ALP measurements of the Ca-Alg aerogel in comparison to the control group are illustrated. It was found that the average ALP level of the treatment group did not exceed neither the control ALP levels nor the normal level of ALP in rats. Also, there was no significant differences between the measurements before cutting the Ca-Alg aerogel (day 14) and after that.

Similarly, the average ALP level of the Na-Alg group (Figure 36B) were found to be within the normal ranges, though, it was noticed that the average level of ALP in the Na-Alg group is increasing gradually after cutting the treatment (day 14) till the end of the study time (but still in the normal levels), although the ALP level in control of this group has an opposite trend. However, further investigations and longer experiment is needed to check the sustainability of this trend. Accordingly, it can be said that Na-Alg and its crosslinked aerogel (Ca-Alg) don't appear to have toxic effect on the liver if used according to this study conditions (for a duration of day 14 and a daily dose of 250 mg). However, its safety may be dose dependents (especially for Na-Alg).

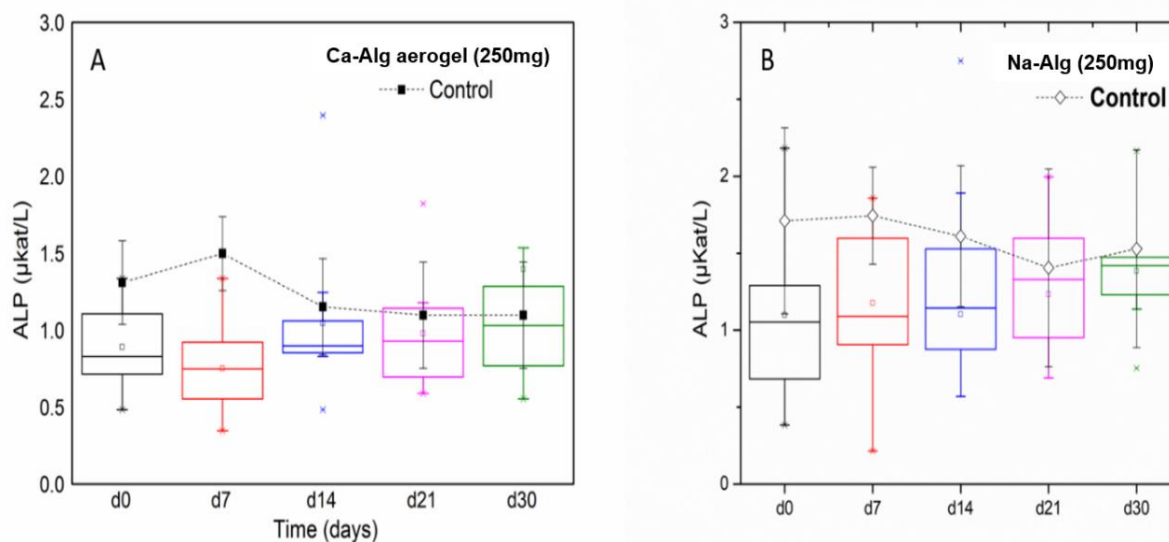


Figure 36. Box-plot for ALP test that was done for the 250 mg Ca-Alg aerogels (A) and Na-Alg (B) during a long-term experiment. The dotted lines in all the panels represent the ALP values for all the control groups.

4.7.2.2. Creatinine level analysis

In the long-term treatment group, creatinine values in the groups treated with Ca-Alg aerogel and Na-Alg was evaluated at day 0 and these values were used to establish the baselines for the readings. In long term treatment (Figure 37), both Ca-Alg aerogel and Na-Alg groups showed no toxic effect on the kidney, with a maximum serum creatinine in Ca-Alg aerogel group reaches 1.6 mg/dl at day 14. Remarkably, the creatinine levels of Na-Alg group were almost the half of those measured when treating the rats with Ca-Alg aerogels. This slight increase in the creatinine (which still within the normal ranges) might not be significant because of the high error bars, which refer to the individual variation in rats and the small sample size of this study. Nevertheless, such increase is expected due to the presence of calcium in the aerogel, as it was reported by Barry et

al. (2014) that daily calcium supplement causes a small increase in the blood creatinine, and they refer this increase to the effect of calcium on renal function, or to the mild vasoconstriction due to increased calciuria or induction of natriuresis by calcium, which can cause mild dehydration, or possibly increased calcification of the glomeruli [207], [208].

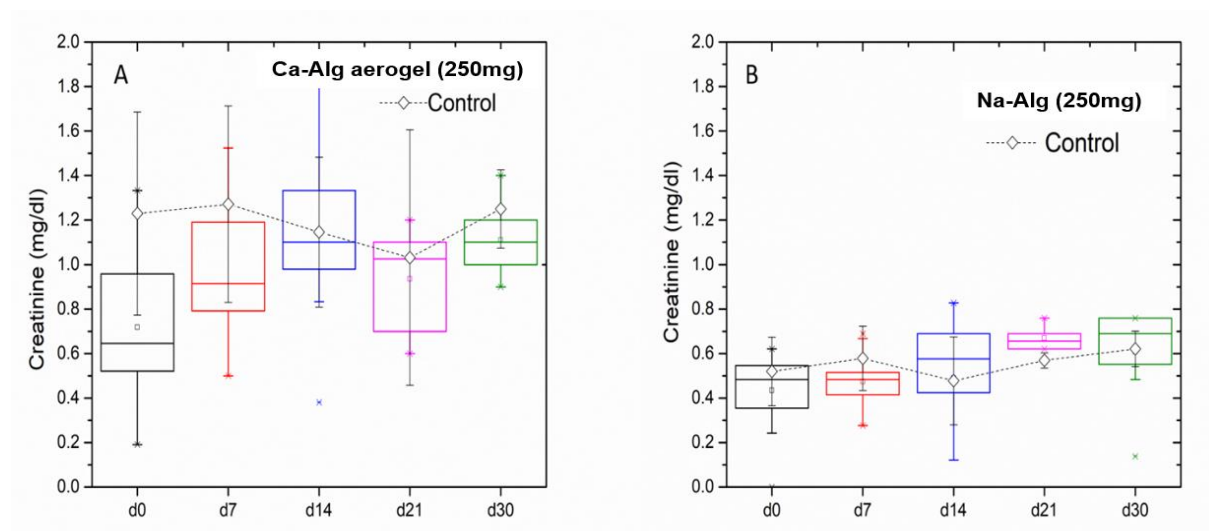


Figure 37. In vivo serum creatinine analysis, for the 250 mg calcium alginate aerogels (A) and sodium alginate (B) during a long-term experiment.

The findings of this part of the thesis provide an evidence that neither immediate nor delayed renal toxicity is recognizable when given aerogels at a dose of 250 mg (approx. 1000 mg/KG) for 15 days. However, delayed renal toxicity cannot be totally ruled out in the case of Ca-Alg aerogel, and further laboratory evaluation are needed.

4.7.3. Shift in gut microbiota

Gut microbiota are active partners in the body health and gut metabolism of their host. The by-products of Alg digestion might result in products that inhibit colon cancer [209]. They are responsible for providing up to 15 % of total caloric intake because they participate in polysaccharide digestion, as well as vitamins, short- fatty acids and other nutrients production for their hosts [210]. Therefore, it is important to study the effect of calcium alginate aerogel on the gut microbiota when assessing its safety.

The remarkable results for the gut microbial study are summarized in Figure 38, which was obtained by analyzing the 16S rRNA gene sequencing. In the gut of the untreated rats and the rats before giving the Ca-Alg aerogel, the highest abundance of the bacterial members belonged to the class Bacilli, while members of the classes Clostridia, Bacteroidia, Erysipelotrichia, and Candidatus saccharibacteria were represented in lower relative abundances (control and rats at d0, Figure 38). In response to feeding rats with Ca-Alg aerogel, gut microbiota showed different patterns; the relative abundance of certain groups of bacteria increased during the Ca-Alg aerogel regime and continued to increase after cutting it (from d23 - d30) such as Clostridia and Bacteroidia. While members of another groups (i.e., Erysipelotrichia, and Candidatus saccharibacteria) increased during Ca-Alg aerogel treatment and then decreased again at d30. Members of the class Bacilli showed unique trend, that is after being the most abundant group at

d0 (63 %), the relative abundance decreased dramatically until reaching < 5 % even after stopping aerogel treatment.

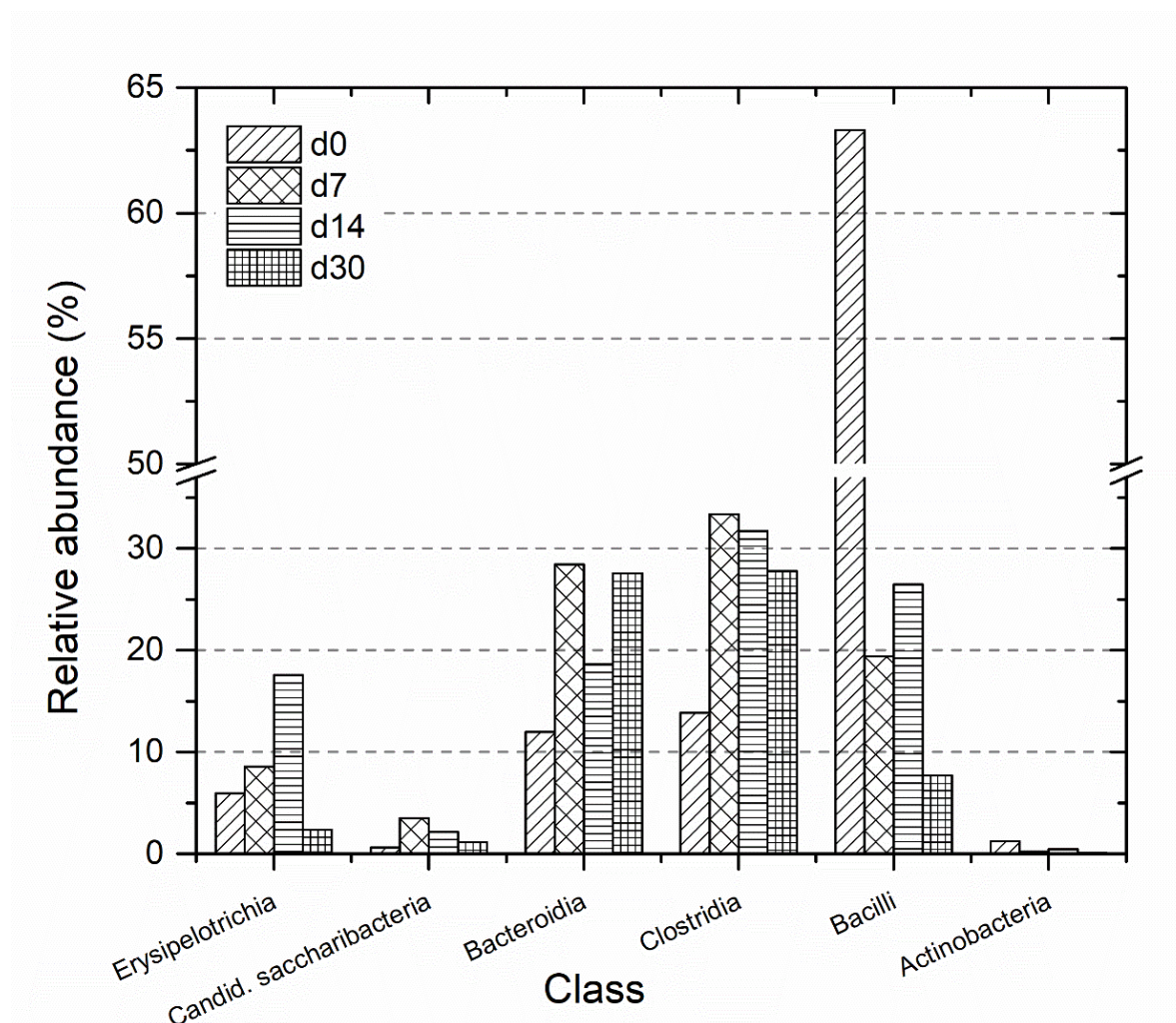


Figure 38. Microbial community structure of the gut at the class level in rats treated with Ca-Alg aerogel.

On the species level (Figure 39A and B), gut microbiota showed similar response to that noticed at the class level, with either reversible or irreversible abundances at d30 (after stopping Ca-Alg aerogel treatment). This response can be categorized into 5 distinctive trends based on the

increase/decrease or disappearance of certain species in response to the treatment. The first one is when the relative abundance of the bacteria increased in response to aerogel treatment and then decreased back to the normal or close to the normal value. These include *Romboutsia ilealis*, *Turicibacter spp.*, *Barnesiella spp.*, *Allobaculum stercoricanis*, *Eubacterium spp.*, *Clostridium spp.* and *Barnesiella spp.* This behavior may refer to the ability of such bacteria to digest calcium alginate aerogel, although to confirm this hypothesis, more experiments should be conducted. However, the current findings are in agreement with the previous results of Li et al. (2016), as they reported the capability of different species of Bacteroides to utilize alginate and its oligosaccharides [211].

The second trend (Figure 39A) is represented by some species such as *Anaerobiospirillum* that showed an irreversible massive increased abundance (from 1 % at d0 to 24 % after stopping aerogel). Such increase might induce diarrhea: it was reported in the literature that this kind of bacteria was isolated from patients suffering from diarrhea [212], [213]. Also, it was noticed when collecting the feces of rats treated with Ca-Alg aerogel that the feces was softer, lighter in color, and smaller in size compared to untreated rats, which might support such effect of raising the relative abundances of *Anaerobiospirillum*. It is also expected to have acetic acid and succinic acid as major byproducts of *Anaerobiospirillum* as well as a trace of lactic acid [214], which in its role may alter the intestinal pH. Such alteration may have an impact on the interaction between lactate-producing and lactate-consuming communities [215]. Moreover, Pereira and Gibson (2002) reported in their clinical studies that lactic-acid-producing bacteria exert beneficial effects on host health, such as promoting cholesterol absorption. Therefore, such pH alteration may have an effect on the cholesterol absorption in the host intestine [216]. Another explanation for such irreversible massive increased abundance is increasing the fermentability with time. Brownlee et al (2005)

reported that the fermentability of Alg appear to be slightly lower in rats than that in human within 24 hours (64 % in rats compared to 80 % in human). However, the fermentability in rats increases with continuous feeding of Alg (more than 4 weeks). Thus, feeding with alginate aerogel over time is expected to raise the number of the colonic microflora that ferment alginate [203].

The third trend that was observed in Figure 39A and B, is the decrease in bacterial growth with time during feeding with Ca-Alg aerogels and continue decreasing even after cutting it. Examples on these species are *Lactobacillus johnsonii* (acidophilus), *Akkermansia muciniphila* and *Holdemanella eubacterium biforme*. Such behavior might be attributed to the overgrowth of other types of bacteria, which were blooming during the period when the aerogels were abundant.

The fourth trend displayed total loss of the bacteria species after cutting the Ca-Alg aerogel treatment, this trend was related to some species such as *Staphylococcus lentus* and *lactobacillus intestinalis* (Figure 39A and B). However, the findings of the current study do not support the previous research findings by Wang et al. (2006), in which they reported that Alg oligosaccharide prepared through enzymatic hydrolysis of Na-Alg enhanced the growth of intestinal *bifidobacteria* and *lactobacilli* of male Wistarrats after feeding for two weeks [217]. Bereswill et al. (2017) investigated the potential of a murine commensal intestinal *L. johnsonii* (acidophilus) strain to reduce intestinal pathogenic burdens and to alleviate pro-inflammatory immune responses upon *C. jejuni* infection *in vivo* [218]. Bifidobacteria and lactobacilli are known to directly inhibit the growth of pathogenic bacteria, such as certain species of *Clostridia* (i.e., *Clostridium difficile* and *Clostridium perfringens*) and pathogenic Enterobacteriaceae, through the production of short-chain fatty acids, lowering of colonic pH, production of antimicrobial compounds, and competition for growth substrates and adhesion sites [219]–[221].

The last trend showed a decrease during the treatment with Ca-Alg aerogel and after stopping it there was a surprising blooming of the bacteria. This trend is shown in *Anaerobiospirillum sp.* and in *Prevotella copri* (Figure 39A). Such sudden increase in the relative abundances may be referred to certain byproducts resulted from the degradation of Ca-Alg aerogel, which might inhibit the growth of *Anaerobiospirillum sp.* and in *Prevotella copri*. Due to ceasing the production of these by-products (after cutting the Ca-Alg aerogel) these two species started to bloom again. Another assumption could be that due to the resulted by-products of Ca-Alg aerogel degradation. However, such assumptions need further studies to be confirmed.

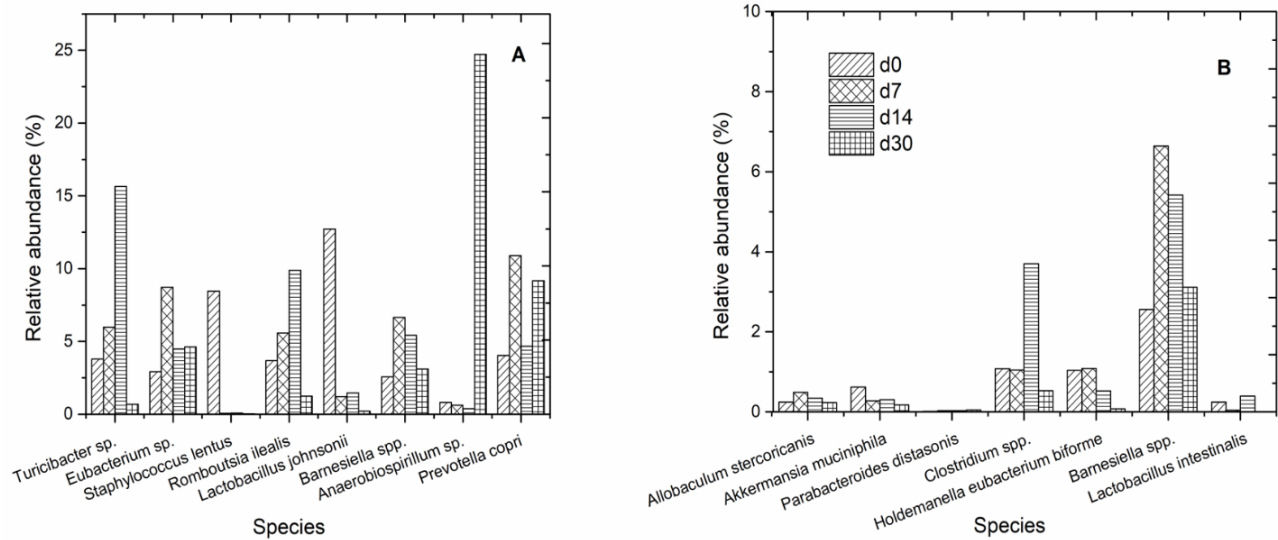


Figure 39. Temporal shift in gut microbiota in response to the Ca-Alg aerogel exposure, representing the species that increased, decreased, or totally disappeared due to the treatment.

5. Conclusion

In the first part of this work, aerogel particles based on Alg and on hybrid Alg-HA, were successfully obtained by an emulsion gelation process with subsequent drying using supercritical CO₂. Thereby Alg-HA aerogels were reported for the first time. Combing these two approaches, spherical gel particles of Alg and Alg-HA were prepared, exhibiting highly porous structure, high BET-specific surface and low density. The rheological study suggests an interaction between Alg and HA in hybrid gels. This suggestion was supported by the FTIR result that indicated a possible hydrogen bond formation between the carboxylate groups of Alg and the amide of the N-acetyl-D-glucosamine in the hybrid aerogel occurred, preventing the separation of the components in the microsphere matrix. In addition to the expected improvement in the biodegradation, hybridization of Alg with HA showed positive effect in term of reducing the particles density and agglomeration. Therefore, the aerodynamic diameter of the Alg-HA particles is generally lower than that of the Alg particles. It demonstrates again, that hybrid aerogels are very promising, since their properties can be tailored more flexible and in a broader range, as those of plain polymer aerogels.

Predicting, controlling and preparing of Alg and Alg-HA aerogel particles suitable for pulmonary drug delivery were the main goals of this research that were successfully achieved. The prepared Alg-HA aerogel particles in this study achieved the requirement regarding the d_A values in the range of 0.5 - 5 μm . In addition to the possibility for adjusting the microsphere diameters by controlling the emulsification rate and the inner phase viscosity, it was also possible to predict the microsphere diameters using the capillary number calculations. A limitation of this study is that the evaluation of the drug release under simulated pulmonary conditions were not conducted because there has been no recommended method in the pharmacopeia so far. Nevertheless, it was

possible to explore the differences in the drug release between the Alg and the Alg-HA particles. The results revealed no significant changes in the release profiles and in the extent of release, which may be considered as another advantages of HA, since the release behavior and kinetics were similar to that of Alg particles, although the crosslinking degree was significantly reduced (to the half of the initial value). This reduction in the calcium-crosslinked Alg is expected to improve the biodegradation. Potentially, other release profiles of the particles (e.g. more sustained) may be achieved if increasing the polymer concentration and/or the crosslinking degree of the aerogels, taking into account the particle size and biodegradation issues.

Moreover, further research is needed to evaluate the *in vivo* degradation of the prepared aerogel particles as well as the *in vivo* drug release kinetics.

Overall, the present study provides an evidence that aerogels may be considered a potential material to deliver pharmaceutical active ingredients to the pulmonary system.

In the second part of the thesis, the aim was to assess the effect of calcium-crosslinked alginate aerogel on the gut microbial community, liver and kidney (through their enzyme: ALP and creatinine) which would further support their potential as drug delivery system. The results revealed that neither immediate nor delayed renal or liver toxicity were identified when calcium-crosslinked alginate aerogel is given to the Wistar rats for 14 days with a daily dose of 250 mg. However, the progress of delayed renal toxicity cannot be entirely excluded in this case and further investigations are still needed. Regarding the microbial community before and after the treatment with calcium-crosslinked alginate aerogel, gut microbiota showed different behaviors: Clostridia and Bacteroidia groups increased during the aerogels regime and continued to increase after aerogel was stopped, while another groups such as Erysipelotrichia, and Candidatus saccharibacteria increased during aerogels treatment and then decreased again after one month.

The blooming of some species appeared to have a suppression impact on others such as Bacilli, even after cutting the treatment with alginate aerogel. As a consequence of abundant increases of some bacteria, intestinal pH might be altered and such alteration may have an impact on the absorption of cholesterol. The increased abundance of some bacteria in response to aerogel treatment and then the decreased abundant (back to the normal or close to the normal value) may refer to the ability of such bacteria to digest calcium alginate aerogel. A limitation of this study was the fact that the number of animals was relatively small, and thus the results are expected to be improved with lower standard errors with an increased number of animals. The experiment has to be conducted for a longer time period in order to track the long-term effect of calcium-crosslinked alginate aerogel on liver, kidney and gut microbial community. Nevertheless, the findings of this study enhanced our understanding on the effect of alginate aerogel on liver, kidney and gut microbial community. In combination with the literature finding, these results suggest that Ca-crosslinked alginate aerogel may be considered a safe potential drug carries for oral applications.

Overall, in this work the potential of the alginate aerogels and their hybrids as drug delivery systems was proven to be high, whereas different dosage forms can be successfully realized.

6. References

- [1] J. M. Schultz, K. I. Jensen, and F. H. Kristiansen, "Super insulating aerogel glazing," *Sol. Energy Mater. Sol. Cells*, vol. 89, no. 2, pp. 275–285, 2005.
- [2] N. Hüsing and U. Schubert, "Aerogels—Airy Materials: Chemistry, Structure, and Properties," *Angew. Chem. Int. Ed.*, vol. 37, no. 1-2, pp. 22–45, 1998.
- [3] S. S. Kistler, "Coherent Expanded Aerogels and Jellies," *Nutr.*, vol. 127, no. 3211, pp 741-741, 1931.
- [4] S. S. Kistler and A. G. Caldwell, "Thermal Conductivity of Silica Aerogel," *Ind. Eng. Chem.*, vol. 26, no. 6, pp. 658–662, 1934.
- [5] R. Baetens, B. P. Jelle, and A. Gustavsen, "Aerogel insulation for building applications: A state-of-the-art review," *Energy Build.*, vol. 43, no. 4, pp. 761–769, 2011.
- [6] J. P. Randall, M. A. B. Meador, and S. C. Jana, "Tailoring Mechanical Properties of Aerogels for Aerospace Applications," *ACS Appl. Mater. Interfaces*, vol. 3, no. 3, pp. 613–626, 2011.
- [7] S. S. Kistler, S. Swann, and E. G. Appel, "Aerogel Catalysts - Thoria: Preparation of Catalyst and Conversions of Organic Acids to Ketones," *Ind. Eng. Chem.*, vol. 26, no. 4, pp. 388–391, 1934.
- [8] D. L. Plata, Y. J. Briones, R. L. Wolfe, M. K. Carroll, S. D. Bakrania, S. G. Mandel and A. M. Anderson, "Aerogel-platform optical sensors for oxygen gas," *J. Non-Cryst. Solids*, vol. 350, pp. 326–335, 2004.
- [9] J. Long, A. Fischer, T. McEvoy, M. Bourg, J. Lytle, and D. Rolison, "Self-limiting electropolymerization en route to ultrathin, conformal polymer coatings for energy storage applications," *PMSE Prepr*, vol. 99, pp. 772–773, 2008.

- [10] G. A. Sprehn, L. W. Hrubesh, J. F. Poco, and P. H. Sandler, “Aerogel-clad optical fiber,” U.S. Patent 5,684,907, 1997.
- [11] J. L. Gurav, I. K. Jung, H. H. Park, E. S. Kang, and D. Y. Nadargi, “Silica Aerogel: Synthesis and Applications,” *J. Nanomater.*, vol. 2010, pp. 1–11, 2010.
- [12] C. A. García-González, M. Jin, J. Gerth, C. Alvarez-Lorenzo, and I. Smirnova, “Polysaccharide-based aerogel microspheres for oral drug delivery,” *Carbohydr. Polym.*, vol. 117, pp. 797–806, 2015.
- [13] U. Guenther, I. Smirnova, and R. H. H. Neubert, “Hydrophilic silica aerogels as dermal drug delivery systems – Dithranol as a model drug,” *Eur. J. Pharm. Biopharm.*, vol. 69, no. 3, pp. 935–942, 2008.
- [14] I. Karadagli, B. Schulz, M. Schestakow, B. Milow, T. Gries, and L. Ratke, “Production of porous cellulose aerogel fibers by an extrusion process,” *J. Supercrit. Fluids*, vol. 106, pp. 105–114, 2015.
- [15] C. A. García-González, M. Jin, J. Gerth, C. Alvarez-Lorenzo, and I. Smirnova, “Polysaccharide-based aerogel microspheres for oral drug delivery,” *Carbohydr. Polym.*, vol. 117, pp. 797–806, 2015.
- [16] T. Athamneh; A. Amin, E. Benke, R. Ambrus, C.S. Leopold, P. Gurikov., I. Smirnova, “Alginate and hybrid alginate-hyaluronic acid aerogel microspheres as potential carrier for pulmonary drug delivery,” *J. Supercrit. Fluids*, vol. 150, pp. 49–55, 2019.
- [17] M. A. Marin, R. R. Mallepally, and M. A. McHugh, “Silk fibroin aerogels for drug delivery applications,” *J. Supercrit. Fluids*, vol. 91, pp. 84–89, 2014.

- [18] P. Zanen, L. T. Go, and J. W. Lammers, "Optimal particle size for beta 2 agonist and anticholinergic aerosols in patients with severe airflow obstruction," *Thorax*, vol. 51, no. 10, p. 977, 1996.
- [19] C. López-Iglesias, A. M. Casielles, A. Altay, R. Bettini, C. Alvarez-Lorenzo, and C. A. García-González, "From the printer to the lungs: Inkjet-printed aerogel particles for pulmonary delivery," *Chem. Eng. J.*, vol. 357, pp. 559–566, 2019.
- [20] V. Baudron, P. Gurikov, and I. Smirnova, "A continuous approach to the emulsion gelation method for the production of aerogel micro-particle," *Colloids Surf. Physicochem. Eng. Asp.*, vol. 566, pp. 58–69, 2019.
- [21] C. Jiménez-Saelices, B. Seantier, B. Cathala, and Y. Grohens, "Spray freeze-dried nanofibrillated cellulose aerogels with thermal superinsulating properties," *Carbohydr. Polym.*, vol. 157, pp. 105–113, 2017.
- [22] K. Ganesan T. Budtova, L. Ratke, P. Gurikov, V. Baudron, I. Preibisch, P. Niemeyer, I. Smirnova and B. Milow, "Review on the Production of Polysaccharide Aerogel Particles," *Materials*, vol. 11, no. 11, p. 2144, 2018.
- [23] U. Prüße, U. Jahnz, P. Wittlich, J. Breford, K. D. Vorlop, "Bead production with JetCutting and rotating disk/nozzle technologies," *Landbauforsch. Völkenrode, SH241*, p. 11, 2002.
- [24] S. K. Ghosal, P. Talukdar, and T. K. Pal, "Standardization of a newly designed vibrating capillary apparatus for the preparation of microcapsules," *Chem. Eng. Technol.*, vol. 16, no. 6, pp. 395–398, 1993.
- [25] D. Poncelet, R. Neufeld, B. Bugarski, B. G. Amsden, J. Zhu, and M. F. A. Goosen, "A Parallel plate electrostatic droplet generator: Parameters affecting microbead size," *Appl. Microbiol. Biotechnol.*, vol. 42, no. 2, pp. 251–255, 1994.

- [26] K.D. Vorlop and J. Breford, “Prodn. of solid particles from a liquid medium,” DE4424998A1, 1996.
- [27] U. Prüße, B. Fox, M. Kirchhoff, F. Bruske, J. Breford, and K.-D. Vorlop, “New Process (Jet Cutting Method) for the Production of Spherical Beads from Highly Viscous Polymer Solutions,” *Chem. Eng. Technol.*, vol. 21, no. 1, pp. 29–33, 1998.
- [28] M. Lightfoot, “A Fundamental Classification of Atomization Processes,” *AAS*, vol. 19, no. 11 pp. 104, 2009.
- [29] A. H. Lefebvre, V. G. McDonell, and V. G. McDonell, “Atomization and Sprays,” 2nd ed., *CRC Press*, USA, 2017.
- [30] R. Daly, T. S. Harrington, G. D. Martin, and I. M. Hutchings, “Inkjet printing for pharmaceuticals – A review of research and manufacturing,” *Int. J. Pharm.*, vol. 494, no. 2, pp. 554–567, 2015.
- [31] B.-J. de Gans, P. C. Duineveld, and U. S. Schubert, “Inkjet Printing of Polymers: State of the Art and Future Developments,” *Adv. Mater.*, vol. 16, no. 3, pp. 203–213, 2004.
- [32] C. López-Iglesias, A. M. Casielles, A. Altay, R. Bettini, C. Alvarez-Lorenzo, and C. A. García-González, “From the printer to the lungs: Inkjet-printed aerogel particles for pulmonary delivery,” *Chem. Eng. J.*, vol. 357, pp. 559–566, 2019.
- [33] Y. F. Maa and C. Hsu, “Liquid-liquid emulsification by rotor/stator homogenization,” *J. Controlled Release*, vol. 38, no. 2, pp. 219–228, 1996.
- [34] D. J. McClements, “Food Emulsions: Principles, Practices, and Techniques,” 3rd ed., *CRC Press*, USA, 2016.

- [35] C. A. García-González, M. Alnaief, and I. Smirnova, “Polysaccharide-based aerogels—Promising biodegradable carriers for drug delivery systems,” *Carbohydr. Polym.*, vol. 86, no. 4, pp. 1425–1438, 2011.
- [36] C. J. Chang, C. Y. Day, C. M. Ko, and K. L. Chiu, “Densities and P-x-y diagrams for carbon dioxide dissolution in methanol, ethanol, and acetone mixtures,” *Fluid Phase Equilibria*, vol. 131, no. 1, pp. 243–258, 1997.
- [37] T. Mehling, I. Smirnova, U. Guenther, and R. H. H. Neubert, “Polysaccharide-based aerogels as drug carriers,” *J. Non-Cryst. Solids*, vol. 355, no. 50, pp. 2472–2479, 2009.
- [38] R. Valentin, R. Horga, B. Bonelli, E. Garrone, F. D. Renzo, and F. Quignard, “Acidity of Alginate Aerogels Studied by FTIR Spectroscopy of Probe Molecules,” *Macromol. Symp.*, vol. 230, no. 1, pp. 71–77, 2005.
- [39] M. Robitzer, L. David, C. Rochas, F. Di Renzo, and F. Quignard, “Nanostructure of Calcium Alginate Aerogels Obtained from Multistep Solvent Exchange Route,” *Langmuir*, vol. 24, no. 21, pp. 12547–12552, 2008.
- [40] P. Gurikov, R. SP., J. S. Griffin, S. A. Steiner III, and I. Smirnova, “110th Anniversary: Solvent Exchange in the Processing of Biopolymer Aerogels: Current Status and Open Questions,” *Ind. Eng. Chem. Res.*, vol. 58, no. 40, pp. 18590–18600, 2019.
- [41] A. Ghafar, P. Gurikov, R. Subrahmanyam, K. Parikka, M. Tenkanen, I. Smirnova, K.S. Mikkonen, “Mesoporous guar galactomannan based biocomposite aerogels through enzymatic crosslinking,” *Compos. Part Appl. Sci. Manuf.*, vol. 94, pp. 93–103, 2017.
- [42] A. Veronovski, Z. Novak, and Ž. Knez, “Synthesis and Use of Organic Biodegradable Aerogels as Drug Carriers,” *J. Biomater. Sci. Polym. Ed.*, vol. 23, no. 7, pp. 873–886, 2012.
- [43] G. W. Scherer, “Theory of Drying,” *J. Am. Ceram. Soc.*, vol. 73, no. 1, pp. 3–14, 1990.

- [44] J. Weissmüller, H. L. Duan, and D. Farkas, “Deformation of solids with nanoscale pores by the action of capillary forces,” *Acta Mater.*, vol. 58, no. 1, pp. 1–13, 2010.
- [45] P. H. Tewari, A. J. Hunt, and K. D. Lofftus, “Ambient-temperature supercritical drying of transparent silica aerogels,” *Mater. Lett.*, vol. 3, no. 9, pp. 363–367, 1985.
- [46] J. S. Griffin, D. H. Mills, M. Cleary, R. Nelson, V. P. Manno, and M. Hodes, “Continuous extraction rate measurements during supercritical CO₂ drying of silica alcogel,” *J. Supercrit. Fluids*, vol. 94, pp. 38–47, 2014.
- [47] C. A. García-González, M. C. Camino-Rey, M. Alnaief, C. Zetzl, and I. Smirnova, “Supercritical drying of aerogels using CO₂: Effect of extraction time on the end material textural properties,” *J. Supercrit. Fluids*, vol. 66, pp. 297–306, 2012.
- [48] A. E. Lebedev, A. M. Katalevich, and N. V. Menshutina, “Modeling and scale-up of supercritical fluid processes. Part I: Supercritical drying,” *J. Supercrit. Fluids*, vol. 106, pp. 122–132, 2015.
- [49] M. Mukhopadhyay and B. S. Rao, “Modeling of supercritical drying of ethanol-soaked silica aerogels with carbon dioxide,” *J. Chem. Technol. Biotechnol.*, vol. 83, no. 8, pp. 1101–1109, 2008.
- [50] Y. Özbakır and C. Erkey, “Experimental and theoretical investigation of supercritical drying of silica alcogels,” *J. Supercrit. Fluids*, vol. 98, pp. 153–166, 2015.
- [51] M. J. van Bommel and A. B. de Haan, “Drying of silica aerogel with supercritical carbon dioxide,” *J. Non-Cryst. Solids*, vol. 186, pp. 78–82, 1995.
- [52] I. Selmer, A.-S. Behnecke, J. Quiño, A. S. Braeuer, P. Gurikov, and I. Smirnova, “Model development for sc-drying kinetics of aerogels: Part 1. Monoliths and single particles,” *J. Supercrit. Fluids*, vol. 140, pp. 415–430, 2018.

- [53] L. W. Hrubesh and R. W. Pekala, “Dielectric Properties and Electronic Applications of Aerogels,” in *Sol-Gel Processing and Applications*, pp. 363–367, 1994.
- [54] R. J. Contolini, L. W. Hrubesh, and A. F. Bernhardt, “Aerogels for microelectronic applications: Fast, inexpensive, and light as air,” Lawrence Livermore National Lab., UCRL-JC-113650; CONF-9303198-3, CA (United States), 1993.
- [55] G. Poelz and R. Riethmüller, “Preparation of silica aerogel for Cherenkov counters,” *Nucl. Instrum. Methods Phys. Res.*, vol. 195, no. 3, pp. 491–503, 1982.
- [56] Y. Sallaz-Damaz, L. Derome, M. Mangin-Brinet, M. Loth, K. Protasov, A. Putze, M. Vargas-Trevino, O. Véziant, M. Buénerd, A. Menchaca-Rocha, and E.Y. Belmont, “Characterization study of silica aerogel for Cherenkov imaging,” *Nucl. Instrum. Methods Phys. Res. Sect. Accel. Spectrometers Detect. Assoc. Equip.*, vol. 614, no. 2, pp. 184–195, 2010.
- [57] Yu. N. Kharzheev, “Use of silica aerogels in Cherenkov counters,” *Phys. Part. Nucl.*, vol. 39, no. 1, pp. 107–135, 2008.
- [58] N. Y. Hebalkar, “Improved process for producing silica aerogel thermal insulation product with increased efficiency,” U.S. Patent, 15/744,011, 2019.
- [59] A. A. Günay, H. Kim, N. Nagarajan, M. Lopez, R. Kantharaj, A. Alsaati, A. Marconnet, A. Lenert, and N. Miljkovic, “Optically Transparent Thermally Insulating Silica Aerogels for Solar Thermal Insulation,” *ACS Appl. Mater. Interfaces*, vol. 10, no. 15, pp. 12603–12611, 2018.
- [60] Y. Xie and J. Beamish, “Ultrasonic velocity and attenuation in silica aerogels at low temperatures,” *Czechoslov. J. Phys.*, vol. 46, no. 5, pp. 2723–2724, 1996.

- [61] L. W. H. John G. Reynolds Paul R. Coronado, “Hydrophobic Aerogels for Oil-Spill Cleanup? Intrinsic Absorbing Properties,” *Energy Sources*, vol. 23, no. 9, pp. 831–843, 2001.
- [62] V. P. Krainov and M. B. Smirnov, “Nuclear fusion induced by a super-intense ultrashort laser pulse in a deuterated glass aerogel,” *J. Exp. Theor. Phys.*, vol. 93, no. 3, pp. 485–490, 2001.
- [63] S. Cumana, I. Ardao, A.-P. Zeng, and I. Smirnova, “Glucose-6-phosphate dehydrogenase encapsulated in silica-based hydrogels for operation in a microreactor,” *Eng. Life Sci.*, vol. 14, no. 2, pp. 170–179, 2014.
- [64] I. Smirnova, S. Suttiruengwong, and W. Arlt, “Feasibility study of hydrophilic and hydrophobic silica aerogels as drug delivery systems,” *J. Non-Cryst. Solids*, vol. 350, pp. 54–60, 2004.
- [65] X. Wang, J. Wang, S. Feng, Z. Zhang, C. Wu, X. Zhang, and F. Kang, “Nano-Porous Silica Aerogels as Promising Biomaterials for Oral Drug Delivery of Paclitaxel,” *J. Biomed. Nanotechnol.*, vol. 15, no. 7, pp. 1532-1545, 2019.
- [66] M. Mohammadian, T. S. Jafarzadeh Kashi, M. Erfan, and F. P. Soorbaghi, “Synthesis and characterization of silica aerogel as a promising drug carrier system,” *J. Drug Deliv. Sci. Technol.*, vol. 44, pp. 205–212, 2018.
- [67] *Cabot Corporation*. “Aerogel,” available: <http://www.cabotcorp.com/solutions/products-plus/aerogel> (accessed Nov. 2019).
- [68] C. I. Merzbacher, S. R. Meier, J. R. Pierce, and M. L. Korwin, “Carbon aerogels as broadband non-reflective materials,” *J. Non-Cryst. Solids*, vol. 285, no. 1, pp. 210–215, 2001.

- [69] C. Moreno-Castilla and F. J. Maldonado-Hódar, “Carbon aerogels for catalysis applications: An overview,” *Carbon*, vol. 43, no. 3, pp. 455–465, 2005.
- [70] J. C. Farmer, D. V. Fix, G. V. Mack, R. W. Pekala, and J. F. Poco, “The use of capacitive deionization with carbon aerogel electrodes to remove inorganic contaminants from water,” UCRL-JC--119844, CONF-950718--1, 80970, Lawrence Livermore National Lab, 1995.
- [71] T. Lu, Q. Li, W. Chen, and H. Yu, “Composite aerogels based on dialdehyde nanocellulose and collagen for potential applications as wound dressing and tissue engineering scaffold,” *Compos. Sci. Technol.*, vol. 94, pp. 132–138, 2014.
- [72] V. S. S. Gonçalves, P. Gurikov, J. Poejo, A.A. Matias, S. Heinrich, C.M. Duarte, and I. Smirnova, “Alginate-based hybrid aerogel microparticles for mucosal drug delivery,” *Eur. J. Pharm. Biopharm.*, vol. 107, pp. 160–170, 2016.
- [73] S. T. Nguyen, J. Feng, S. K. Ng, J. P. W. Wong, V. B. C. Tan, and H. M. Duong, “Advanced thermal insulation and absorption properties of recycled cellulose aerogels,” *Colloids Surf. Physicochem. Eng. Asp.*, vol. 445, pp. 128–134, 2014.
- [74] J. Feng, S. T. Nguyen, Z. Fan, and H. M. Duong, “Advanced fabrication and oil absorption properties of super-hydrophobic recycled cellulose aerogels,” *Chem. Eng. J.*, vol. 270, pp. 168–175, 2015.
- [75] P. Gupta, B. Singh, A. K. Agrawal, and P. K. Maji, “Low density and high strength nanofibrillated cellulose aerogel for thermal insulation application,” *Mater. Des.*, vol. 158, pp. 224–236, 2018.
- [76] M. Martins, A. A. Barros, S. Quraishi, P. Gurikov, S. P. Raman, I. Smirnova, A. R. C Duarte and R. L. Reis, “Preparation of macroporous alginate-based aerogels for biomedical applications,” *J. Supercrit. Fluids*, vol. 106, pp. 152–159, 2015.

- [77] K. Chen and H. Zhang, "Alginate/pectin aerogel microspheres for controlled release of proanthocyanidins," *Int. J. Biol. Macromol.*, vol. 136, pp. 936–943, 2019.
- [78] G. Cassin, S. Diridollou, F. Flament, A. S. Adam, P. Pierre, L. Colomb, J. L. Morancais, and H. Qiu, "Concealing a shiny facial skin appearance by an Aerogel-based formula. In vitro and in vivo studies," *Int. J. Cosmet. Sci.*, vol. 40, no. 1, pp. 58–66, Feb. 2018.
- [79] Y. Nagamatsu, M. Willien, and D. Candau, "Composition containing composite particles for screening out UV radiation, with a mean size of greater than 0.1 μM , and hydrophobic silica aerogel particles" U.S. Patent, 9/913,782, 2018.
- [80] G. Cassin and S. P. Fristot, "Cosmetic composition comprising silica aerogel particles and silicone oils," U.S. Patent 9/956,434, 2018.
- [81] J. S. Boateng, K. H. Matthews, H. N. E. Stevens, and G. M. Eccleston, "Wound healing dressings and drug delivery systems: a review," *J. Pharm. Sci.*, vol. 97, no. 8, pp. 2892–2923, Aug. 2008.
- [82] S. Thomas, L. A. Pothan, and R. Mavelil-Sam, "Biobased Aerogels: Polysaccharide and Protein-based Materials," *R. Soc. Chem.*, Vol. 58, 2018.
- [83] F. De Cicco, P. Russo, E. Reverchon, C. A. García-González, R. P. Aquino, and P. Del Gaudio, "Prilling and supercritical drying: A successful duo to produce core-shell polysaccharide aerogel beads for wound healing," *Carbohydr. Polym.*, vol. 147, pp. 482–489, 2016.
- [84] C. López-Iglesias, J. Barros, I. Ardao, F.J. Monteiro, C. Alvarez-Lorenzo, J. L. Gómez-Amoza, and C. A. García-González, "Vancomycin-loaded chitosan aerogel particles for chronic wound applications," *Carbohydr. Polym.*, vol. 204, pp. 223–231, 2019.

- [85] S. P. Raman, C. Keil, P. Dieringer, C. Hübner, A. Bueno, P. Gurikov, J. Nissen, M. Holtkamp, U. Karst, H. Haase, and I. Smirnova, “Alginate aerogels carrying calcium, zinc and silver cations for wound care: Fabrication and metal detection,” *J. Supercrit. Fluids*, vol. 153, p. 104545, 2019.
- [86] M. Biondi, F. Ungaro, F. Quaglia, and P. A. Netti, “Controlled drug delivery in tissue engineering,” *Adv. Drug Deliv. Rev.*, vol. 60, no. 2, pp. 229–242, 2008.
- [87] D. A. Osorio, B. E. Lee, J. M. Kwiecien, X. Wang, I. Shahid, A.L. Hurley, E. D. Cranston, and K. Grandfield, “Cross-linked cellulose nanocrystal aerogels as viable bone tissue scaffolds,” *Acta Biomater.*, vol. 87, pp. 152–165, 2019.
- [88] R. R. Mallepally, M. A. Marin, V. Surampudi, B. Subia, R. R. Rao, S. C. Kundu, and M. A. McHugh, “Silk fibroin aerogels: potential scaffolds for tissue engineering applications,” *Biomed. Mater. Bristol Engl.*, vol. 10, no. 3, p. 035002, 2015.
- [89] S. Quraishi, M. Martins, A. A. Barros, P. Gurikov, S. P. Raman, I. Smirnova, A.R.C. Duarte, and R. L. Reis, “Novel non-cytotoxic alginate–lignin hybrid aerogels as scaffolds for tissue engineering,” *J. Supercrit. Fluids*, vol. 105, pp. 1–8, 2015.
- [90] M. Piątkowski, J. Radwan-Pragłowska, Ł. Janus, D. Bogdał, D. Matysek, and V. Cablik, “Microwave-assisted synthesis and characterization of chitosan aerogels doped with Au-NPs for skin regeneration,” *Polym. Test.*, vol. 73, pp. 366–376, 2019.
- [91] W. Yin, S. M. Venkitachalam, E. Jarrett, S. Staggs, N. Leventis, H. Lu, and D. A. Rubenstein. “Biocompatibility of surfactant-templated polyurea–nanoencapsulated macroporous silica aerogels with plasma platelets and endothelial cells,” *J. Biomed. Mater. Res. Part A*, vol. 92, no. 4, pp 1431-1439, 2010.

- [92] L. Goimil, M. E Braga, A. M. Dias, J. L. Gomez-Amoza, A. Concheiro, C. Alvarez-Lorenzo, H. C. de Sousa, and C.A. García-González, “Supercritical processing of starch aerogels and aerogel-loaded poly(ϵ -caprolactone) scaffolds for sustained release of ketoprofen for bone regeneration,” *J. CO₂ Util.*, vol. 18, pp. 237–249, 2017.
- [93] Z. Ulker and C. Erkey, “An emerging platform for drug delivery: Aerogel based systems,” *J. Controlled Release*, vol. 177, pp. 51–63, 2014.
- [94] C. A. García-González, E. Carenza, M. Zeng, I. Smirnova, and A. Roig, “Design of biocompatible magnetic pectin aerogel monoliths and microspheres,” *RSC Adv.*, vol. 2, no. 26, pp. 9816–9823, 2012.
- [95] A. Veronovski, G. Tkalec, Ž. Knez, and Z. Novak, “Characterisation of biodegradable pectin aerogels and their potential use as drug carriers,” *Carbohydr. Polym.*, vol. 113, pp. 272–278, 2014.
- [96] A. Veronovski, Ž. Knez, and Z. Novak, “Preparation of multi-membrane alginate aerogels used for drug delivery,” *J. Supercrit. Fluids*, vol. 79, pp. 209–215, 2013.
- [97] H. M. Courrier, N. Butz, and T. F. Vandamme, “Pulmonary drug delivery systems: recent developments and prospects,” *Crit. Rev. Ther. Drug Carr. Syst.*, vol. 19, no. 4–5, 2002.
- [98] D. Lu and A. J. Hickey, “Pulmonary vaccine delivery,” *Expert Rev. Vaccines*, vol. 6, no. 2, pp. 213–226, 2007.
- [99] W. Yang, J. I. Peters, and R. O. W. III, “Inhaled nanoparticles—A current review,” *Int. J. Pharm.*, vol. 356, no. 1–2, pp. 239–247, 2008.
- [100] “Your asthma puffer is probably contributing to climate change, but there’s a better alternative,” *The Conversation*. <http://theconversation.com/your-asthma-puffer-is-probably-contributing-to-climate-change-but-theres-a-better-alternative-92874> .

- [101] N. R. Labiris and M. B. Dolovich, "Pulmonary drug delivery. Part II: The role of inhalant delivery devices and drug formulations in therapeutic effectiveness of aerosolized medications," *Br. J. Clin. Pharmacol.*, vol. 56, no. 6, pp. 600–612, 2003.
- [102] P. Zanen, L. T. Go, and J. W. Lammers, "Optimal particle size for beta 2 agonist and anticholinergic aerosols in patients with severe airflow obstruction.," *Thorax*, vol. 51, no. 10, p. 977, 1996.
- [103] A. M. Healy, M. I. Amaro, K. J. Paluch, and L. Tajber, "Dry powders for oral inhalation free of lactose carrier particles," *Adv. Drug Deliv. Rev.*, vol. 75, pp. 32–52, 2014.
- [104] Z. Liang, R. Ni, J. Zhou, and S. Mao, "Recent advances in controlled pulmonary drug delivery," *Drug Discov. Today*, vol. 20, no. 3, pp. 380–389, 2015.
- [105] P. Villax, and C. Cork, "dry powder inhalers: towards effective, affordable, sustainable respiratory healthcare," *ONdrugDelivery*, 08, 2019.
- [106] A. H. de Boer, P. Hagedoorn, M. Hoppentocht, F. Buttini, F. Grasmeijer, and H. W. Frijlink, "Dry powder inhalation: past, present and future," *Expert Opin. Drug Deliv.*, vol. 14, no. 4, pp. 499–512, 2017.
- [107] V. R. Sinha and R. Kumria, "Polysaccharides in colon-specific drug delivery," *Int. J. Pharm.*, vol. 224, no. 1, pp. 19–38, 2001.
- [108] Z. Liu, Y. Jiao, Y. Wang, C. Zhou, and Z. Zhang, "Polysaccharides-based nanoparticles as drug delivery systems," *Adv. Drug Deliv. Rev.*, vol. 60, no. 15, pp. 1650–1662, 2008.
- [109] J. W. Lee, J. H. Park, and J. R. Robinson, "Bioadhesive-Based Dosage Forms: The Next Generation," *J. Pharm. Sci.*, vol. 89, no. 7, pp. 850–866, 2000.
- [110] A. J. Domb, J. Kost, and D. M. Wiseman, "Handbook of biodegradable polymers," 1st ed., *CRC Press*, USA, 2019.

- [111] R. H. Walter and 1933-, *Polysaccharide association structures in food*. M. Dekker, 1998.
- [112] S. Dumitriu, *Polysaccharides : Structural Diversity and Functional Versatility*,” 2nd ed., *CRC Press*, USA, 2004.
- [113] N. W. G. Young, G. Kappel, and T. Bladt, “A polyuronan blend giving novel synergistic effects and bake-stable functionality to high soluble solids fruit fillings,” *Food Hydrocoll.*, vol. 17, no. 4, pp. 407–418, 2003.
- [114] R. M. Gohil, “Synergistic blends of natural polymers, pectin and sodium alginate,” *J. Appl. Polym. Sci.*, vol. 120, no. 4, pp. 2324–2336, 2011.
- [115] P. Laurienzo, “Marine Polysaccharides in Pharmaceutical Applications: An Overview,” *Mar. Drugs*, vol. 8, no. 9, pp. 2435–2465, 2010.
- [116] Y. Li, M. Han, T. Liu, D. Cun, L. Fang, and M. Yang, “Inhaled hyaluronic acid microparticles extended pulmonary retention and suppressed systemic exposure of a short-acting bronchodilator (vol 172, pg 197, 2017),” *Carbohydr. Polym.*, vol. 177, pp. 471–471, 2017.
- [117] D. S. Morais, M. A. Rodrigues, T. I. Silva, M. A. Lopes, M. Santos, J. D. Santos, and C. M. Botelho, “Development and characterization of novel alginate-based hydrogels as vehicles for bone substitutes,” *Carbohydr. Polym.*, vol. 95, no. 1, pp. 134–142, 2013.
- [118] R. Hällgren, T. Samuelsson, T. C. Laurent, and J. Modig, “Accumulation of Hyaluronan (Hyaluronic Acid) in the Lung in Adult Respiratory Distress Syndrome,” *Am. Rev. Respir. Dis.*, vol. 139, no. 3, pp. 682–687, 1989.
- [119] K. Meyer and J. W. Palmer, “The polysaccharide of the vitreous humor,” *J. Biol. Chem.*, vol. 107, no. 3, pp. 629–634, 1934.

- [120] E. A. Balazs, "Physical chemistry of hyaluronic acid," *Fed. Proc.*, vol. 17, no. 4, pp. 1086–1093, 1958.
- [121] O. Camber and P. Edman, "Sodium hyaluronate as an ophthalmic vehicle: Some factors governing its effect on the ocular absorption of pilocarpine," *Curr. Eye Res.*, vol. 8, no. 6, pp. 563–567, 1989.
- [122] M. B. Brown, M. Hanpanitcharoen, and G. P. Martin, "An in vitro investigation into the effect of glycosaminoglycans on the skin partitioning and deposition of NSAIDs," *Int. J. Pharm.*, vol. 225, no. 1, pp. 113–121, 2001.
- [123] F. Castellano, and G. Mautone, "Decongestant activity of a new formulation of xylometazoline nasal spray: a double-blind, randomized versus placebo and reference drugs controlled, dose-effect study. *Drugs Exp Clin Res.*, vol. 28, no. 1, pp. 27-35, 2002
- [124] K. Morimoto, K. Metsugi, H. Katsumata, K. Iwanaga, and M. Kakemi, "Effects of Low-Viscosity Sodium Hyaluronate Preparation on the Pulmonary Absorption of rh-Insulin in Rats," *Drug Dev. Ind. Pharm.*: Vol. 27, No. 4, pp. 365-371, 2001.
- [125] J. S. Patil and S. Sarasija, "Pulmonary drug delivery strategies: A concise, systematic review," *Lung India Off. Organ Indian Chest Soc.*, vol. 29, no. 1, pp. 44–49, 2012.
- [126] A. Nokhodchi and G. P. Martin, "Pulmonary Drug Delivery: Advances and Challenges," 1st ed., *John Wiley & Sons*, UK, 2015.
- [127] E. Johansen Crosby, "spray drying handbook: K. Masters Longman Group Ltd Harlow, Essex 710 pp.," *Dry. Technol.*, vol. 7, no. 2, pp. 419–425, 1989.
- [128] Y. F. Maa and S. J. Prestrelski, "Biopharmaceutical Powders Particle Formation and Formulation Considerations," *Current Pharm. Biotechnol.*, vol. 1, no. 3, pp.283-302, 2000.

- [129] Z. Yu, A. S. Garcia, K. P. Johnston, and R. O. Williams, "Spray freezing into liquid nitrogen for highly stable protein nanostructured microparticles," *Eur. J. Pharm. Biopharm.*, vol. 58, no. 3, pp. 529–537, 2004.
- [130] J. S. Kuo and R. Hwang, "Preparation of DNA dry powder for non-viral gene delivery by spray-freeze drying: effect of protective agents (polyethyleneimine and sugars) on the stability of DNA," *J. Pharm. Pharmacol.*, vol. 56, no. 1, pp. 27–33, 2004.
- [131] A. Chamayou, J. A. Dodds, "Chapter 8 Air Jet Milling," in *Handbook of Powder Technology*, vol. 12, pp. 421–435, 2007.
- [132] G. Pilcer and K. Amighi, "Formulation strategy and use of excipients in pulmonary drug delivery," *Int. J. Pharm.*, vol. 392, no. 1–2, pp. 1–19, 2010.
- [133] C. A. García-González, J. J. Uy, M. Alnaief, and I. Smirnova, "Preparation of tailor-made starch-based aerogel microspheres by the emulsion-gelation method," *Carbohydr. Polym.*, vol. 88, no. 4, pp. 1378–1386, 2012.
- [134] T. Yasuji, H. Takeuchi, and Y. Kawashima, "Particle design of poorly water-soluble drug substances using supercritical fluid technologies," *Adv. Drug Deliv. Rev.*, vol. 60, no. 3, pp. 388–398, 2008.
- [135] F. Leal-Calderon, V. Schmitt, and J. Bibette, "Emulsion Science: Basic Principles," 2nd ed., *Springer Science & Business Media*, USA, 2007.
- [136] T. F. Tadros, "Emulsion Formation and Stability," 1st ed. *John Wiley & Sons*, UK, 2013.
- [137] H. C. Hamaker, "The London—van der Waals attraction between spherical particles," *Physica*, vol. 4, no. 10, pp. 1058–1072, 1937.
- [138] T. F. Tadros, "Applied Surfactants: Principles and Applications," 1st ed., *John Wiley & Sons*, UK, 2005.

- [139] T. F. Tadros, “Steric Stabilization, *Encyclopedia of Colloid and Interface Science*,” 1st ed., Springer, Berlin, Heidelberg: 2013.
- [140] J. W. Gibbs, “On the Equilibrium of Heterogeneous Substances,” *Trans. Conn. Acad. Arts Sci.*, vol. 3, pp. 108-248, 1879.
- [141] E. Piacentini, “Emulsion, in *Encyclopedia of Membranes*,” 1st ed., Springer, Berlin, Heidelberg, 2016.
- [142] T. F. Tadros, “Emulsion Science and Technology: A General Introduction,” 1st ed., Wiley-VCH, Weinheim, Germany, 2009.
- [143] Y. Yamashita, R. Miyahara, and K. Sakamoto, “Emulsion and Emulsification Technology, in *cosmetic science and technology: theoretical principles and applications*,” 1st ed., Elsevier, Netherlands, 2017.
- [144] D. J. Miller, T. Henning, and W. Grünbein, “Phase inversion of W/O emulsions by adding hydrophilic surfactant a technique for making cosmetics products,” *Colloids Surf. Physicochem. Eng. Asp.*, vol. 183–185, pp. 681–688, 2001.
- [145] Y. T. Hu, Y. Ting, J. Y. Hu, and S. C. Hsieh, “Techniques and methods to study functional characteristics of emulsion systems,” *J. Food Drug Anal.*, vol. 25, no. 1, pp. 16–26, 2017.
- [146] Q. Chang, “*Colloid and Interface Chemistry for Water Quality Control*,” 1st ed., Academic Press, USA, 2016.
- [147] R. C. Pasquali, N. Sacco, and C. Bregni, “The Studies on Hydrophilic-Lipophilic Balance (HLB): Sixty Years after William C. Griffin’s Pioneer Work (1949-2009),” *Lat Am J Pharm*, vol. 28, no. 2, pp. 313-317, 2009.
- [148] J. O. Hinze, “Fundamentals of the hydrodynamic mechanism of splitting in dispersion processes,” *AIChE J.*, vol. 1, no. 3, pp. 289–295, 1955.

- [149] G. I. Taylor, "The viscosity of a fluid containing small drops of another fluid," *Proc. R. Soc. Lond. Ser. Contain. Pap. Math. Phys. Character*, vol. 138, no. 834, pp. 41–48, 1932.
- [150] S. Maindarkar, A. Dubbelboer, J. Meuldijk, H. Hoogland, and M. Henson, "Prediction of emulsion drop size distributions in colloid mills," *Chem. Eng. Sci.*, vol. 118, pp. 114–125, 2014.
- [151] R. A. Debruijn, "Deformation and breakup of drops in simple shear flows," Technische Universiteit Eindhoven, Eindhoven, 1989.
- [152] J. T. Davies, "A physical interpretation of drop sizes in homogenizers and agitated tanks, including the dispersion of viscous oils," *Chem. Eng. Sci.*, vol. 42, no. 7, pp. 1671–1676, 1987.
- [153] R. Sescousse, A. Smacchia, and T. Budtova, "Influence of lignin on cellulose-NaOH-water mixtures properties and on Aerocellulose morphology," *Cellulose*, vol. 17, no. 6, pp. 1137–1146, 2010.
- [154] P. Gurikov, S. P. Raman, D. Weinrich, M. Fricke, and I. Smirnova, "A novel approach to alginate aerogels: carbon dioxide induced gelation," *RSC Adv.*, vol. 5, no. 11, pp. 7812–7818, 2015.
- [155] P. Gurikov, S. P. Raman, D. Weinrich, M. Fricke, and I. Smirnova, "A novel approach to alginate aerogels: carbon dioxide induced gelation," *RSC Adv.*, vol. 5, no. 11, pp. 7812–7818, 2015.
- [156] M. Alnaief, M. A. Alzaitoun, C. A. García-González, and I. Smirnova, "Preparation of biodegradable nanoporous microspherical aerogel based on alginate," *Carbohydr. Polym.*, vol. 84, no. 3, pp. 1011–1018, 2011.

- [157] C. Almeida-Rivera and P. Bongers, “Modelling and experimental validation of emulsification processes in continuous rotor–stator units,” *Comput. Chem. Eng.*, vol. 34, no. 5, pp. 592–597, 2010.
- [158] V. Alopaeus, J. Koskinen, and K. I. Keskinen, “Simulation of the population balances for liquid–liquid systems in a nonideal stirred tank. Part 1 Description and qualitative validation of the model,” *Chem. Eng. Sci.*, vol. 54, no. 24, pp. 5887–5899, 1999.
- [159] S. Kumar, R. Kumar, and K. S. Gandhi, “Alternative mechanisms of drop breakage in stirred vessels,” *Chem. Eng. Sci.*, vol. 46, no. 10, pp. 2483–2489, 1991.
- [160] R. L. Bowen, “Unravelling the mysteries of shear-sensitive mixing systems,” *Unravelling Mysteries Shear-Sensitive Mix. Syst.*, vol. 93, no. 11, pp. 55–63, 1986.
- [161] K.G. Renard, G.R. Foster, G.A. Weesies, D.K. McCool, D.C. Yoder, “Predicting soil erosion by water: a guide to conservation planning with the Revised Universal Soil Loss Equation (RUSLE),” Vol. 703. Washington, DC: United States Department of Agriculture, 1997.
- [162] A. J. Hickey, “*Inhalation Aerosols: Physical and Biological Basis for Therapy*,” 1st ed., *Marcel Dekker*, New York, USA, 1996.
- [163] A. Venkateswara Rao and R. R. Kalesh, “Comparative studies of the physical and hydrophobic properties of TEOS based silica aerogels using different co-precursors,” *Sci. Technol. Adv. Mater.*, vol. 4, no. 6, pp. 509–515, 2003.
- [164] J. T. McConville, N. Patel, N. Ditchburn, M. J. Tobyn, J. N. Staniforth, and P. Woodcock, “Use of a novel modified TSI for the evaluation of controlled-release aerosol formulations. I,” *Drug Dev. Ind. Pharm.*, vol. 26, no. 11, pp. 1191–1198, 2000.

- [165] R. Batycky, D. Deaver, S. Dwivedi, J. Hrkach, L. Johnston, T. Olson, J. E. Wright and D. Edwards, "The Development of Large Porous Particles for Inhalation Drug Delivery," in *Modified-Release Drug Delivery Technology*, vol. 183, M. Rathbone, J. Hadgraft, and M. Roberts, Eds. Informa Healthcare, 2002, pp. 891–902.
- [166] M. S. Nagarsenker and V. Y. Londhe, "Preparation and evaluation of a liposomal formulation of sodium cromoglicate," *Int. J. Pharm.*, vol. 251, no. 1, pp. 49–56, 2003.
- [167] M. Glavas-Dodov, E. Fredro-Kumbaradzi, K. Goracinova, M. Simonoska, S. Calis, S. Trajkovic-Jolevska, A.A.Hincal, "The effects of lyophilization on the stability of liposomes containing 5-FU," *Int. J. Pharm.*, vol. 291, no. 1, pp. 79–86, 2005.
- [168] J. S. Patil, V. K. Devi, K. Devi, and S. Sarasija, "A novel approach for lung delivery of rifampicin-loaded liposomes in dry powder form for the treatment of tuberculosis," *Lung India*, vol. 32, no. 4, pp. 331–338, 2015,.
- [169] J. E. Scott and F. Heatley, "Hyaluronan forms specific stable tertiary structures in aqueous solution: a ¹³C NMR study," *Proc. Natl. Acad. Sci. U. S. A.*, vol. 96, no. 9, pp. 4850–4855, 1999.
- [170] J. E. Scott and A. M. Thomlinson, "The structure of interfibrillar proteoglycan bridges (shape modules') in extracellular matrix of fibrous connective tissues and their stability in various chemical environments," *J. Anat.*, vol. 192 (Pt 3), pp. 391–405, 1998.
- [171] R. H. Mikelsaar and J. E. Scott, "Molecular modelling of secondary and tertiary structures of hyaluronan, compared with electron microscopy and NMR data. Possible sheets and tubular structures in aqueous solution," *Glycoconj. J.*, vol. 11, no. 2, pp. 65–71, 1994.

- [172] J. E. Scott, "Supramolecular organization of extracellular matrix glycosaminoglycans, in vitro and in the tissues," *FASEB J. Off. Publ. Fed. Am. Soc. Exp. Biol.*, vol. 6, no. 9, pp. 2639–2645, 1992.
- [173] J. E. Scott, R. Heatley, and W. E. Hull, "Secondary structure of hyaluronate in solution. A ¹H NMR. investigation in dimethyl sulfoxide solution," *Biochem J*, vol. 220, p. 197, 1984.
- [174] R. Pal, "Effect of droplet size on the rheology of emulsions," *AIChE J.*, vol. 42, no. 11, pp. 3181–3190, 1996.
- [175] C. W. Chung, J. Y. Kang, I. S. Yoon, H. D. Hwang, P. Balakrishnan, H. J. Cho, K. D. Chung, D. H. Kang, and D. D. Kim, "Interpenetrating polymer network (IPN) scaffolds of sodium hyaluronate and sodium alginate for chondrocyte culture," *Colloids Surf. B Biointerfaces*, vol. 88, no. 2, pp. 711–716, 2011.
- [176] C. Chaudemanche and T. Budtova, "Mixtures of pregelatinised maize starch and κ -carrageenan: Compatibility, rheology and gelation," *Carbohydr. Polym.*, vol. 72, no. 4, pp. 579–589, 2008.
- [177] F. Heatley and J. E. Scott, "A water molecule participates in the secondary structure of hyaluronan," *Biochem J*, vol. 254, pp. 489, 1980.
- [178] P. Gurikov and I. Smirnova, "Non-Conventional Methods for Gelation of Alginate," *Gels*, vol. 4, no. 1, pp. 14, 2018.
- [179] D. A. Gabriel and M. E. Carr, "Calcium Destabilizes and Causes Conformational Changes in Hyaluronic Acid," *Am. J. Med. Sci.*, vol. 298, no. 1, pp. 8–14, 1989.
- [180] Contipro, "Contipro is respected European Hyaluronic Acid Manufacturer," available: <https://www.contipro.com/> (accessed Oct. 2018).

- [181] V. Baudron, P. Gurikov, and I. Smirnova, “A continuous approach to the emulsion gelation method for the production of aerogel micro-particle,” *Colloids Surf. Physicochem. Eng. Asp.*, vol. 566, pp. 58–69, 2019.
- [182] A. Haug, “Composition and properties of alginates,”. Institute of Seaweed Research, Trondheim, Norvège: Norwegian, 1964.
- [183] E. Chiesa, R. Dorati, B. Conti, T. Modena, E. Cova, F. Meloni, and I. Genta, “Hyaluronic Acid-Decorated Chitosan Nanoparticles for CD44-Targeted Delivery of Everolimus,” *Int. J. Mol. Sci.*, vol. 19, no. 8, p. 2310, 2018.
- [184] R. Gilli, M. Kacuráková, M. Mathlouthi, L. Navarini, and S. Paoletti, “FTIR studies of sodium hyaluronate and its oligomers in the amorphous solid phase and in aqueous solution,” *Carbohydr. Res.*, vol. 263, no. 2, pp. 315–326, 1994.
- [185] F. Mohabatpour, A. Karkhaneh, and A. Mohammad Sharifi, “A hydrogel/fiber composite scaffold for chondrocyte encapsulation in cartilage tissue regeneration,” *RSC Adv.*, vol. 6, no. 86, pp. 83135–83145, 2016.
- [186] R. Shah, “Development and Evaluation of Mucoadhesive Algino-HPMC Microparticulate System of Aceclofenac for Oral Sustained Drug Delivery,” *Indian J. Pharm. Educ. Res.*, vol. 46, no. 2, pp. 120–128, 2012.
- [187] M. Alnaief and I. Smirnova, “In situ production of spherical aerogel microparticles,” *J. Supercrit. Fluids*, vol. 55, no. 3, pp. 1118–1123, 2011.
- [188] Q. Chen, H. Wang, and L. Sun, “Preparation and Characterization of Silica Aerogel Microspheres,” *Materials*, vol. 10, no. 4, p. 435, 2017.

- [189] C. A. García-González, M. Alnaief, and I. Smirnova, “Polysaccharide-based aerogels—Promising biodegradable carriers for drug delivery systems,” *Carbohydr. Polym.*, vol. 86, no. 4, pp. 1425–1438, 2011.
- [190] A. Martinsen, G. Skjåk-Bræk, and O. Smidsrød, “Alginate as immobilization material: I. Correlation between chemical and physical properties of alginate gel beads,” *Biotechnol. Bioeng.*, vol. 33, no. 1, pp. 79–89, 1989.
- [191] M. F. Kemmere and T. Meyer, “Supercritical Carbon Dioxide: In Polymer Reaction Engineering,” 1st ed., *Wiley-VCH Verlag*, Weinheim, Germany, 2005.
- [192] I. Kikic and F. Vecchione, “Supercritical impregnation of polymers,” *Curr. Opin. Solid State Mater. Sci.*, vol. 7, no. 4, pp. 399–405, 2003.
- [193] R. W. Korsmeyer, R. Gurny, E. Doelker, P. Buri, and N. A. Peppas, “Mechanisms of solute release from porous hydrophilic polymers,” *Int. J. Pharm.*, 1983.
- [194] P. L. Ritger and N. A. Peppas, “A simple equation for description of solute release II. Fickian and anomalous release from swellable devices,” *J. Controlled Release*, vol. 5, no. 1, pp. 37–42, 1987.
- [195] D. A. Edwards, A. Ben-Jebria, and R. Langer, “Recent advances in pulmonary drug delivery using large, porous inhaled particles,” *J. Appl. Physiol.*, vol. 85, no. 2, pp. 379–385, 1998.
- [196] T. Pongjanyakul, A. Priprem, and S. Puttipipatkachorn, “Investigation of novel alginate–magnesium aluminum silicate microcomposite films for modified-release tablets,” *J. Controlled Release*, vol. 107, no. 2, pp. 343–356, 2005.
- [197] H. H. Tønnesen and J. Karlsen, “Alginate in Drug Delivery Systems,” *Drug Dev. Ind. Pharm.*, vol. 28, no. 6, pp. 621–630, 2002.

- [198] J. Sun and H. Tan, “Alginate-Based Biomaterials for Regenerative Medicine Applications,” *Materials*, vol. 6, no. 4, pp. 1285–1309, 2013.
- [199] C. Devillé, M. Gharbi, G. Dandrifosse, and O. Peulen, “Study on the effects of laminarin, a polysaccharide from seaweed, on gut characteristics,” *J. Sci. Food Agric.*, vol. 87, no. 9, pp. 1717-1725, 2007
- [200] M. Younes, P. Aggett, F. Aguilar, R. Crebelli, M. Filipič, M. J. Frutos, P. Galtier, D. Gott, U. Gundert-Remy, and G. G. Kuhnle, “Re-evaluation of alginic acid and its sodium, potassium, ammonium and calcium salts (E 400–E 404) as food additives,” *EFSA J.*, vol. 15, no. 11, pp. e05049, 2017.
- [201] C. A. Lozupone, J. I. Stombaugh, J. I. Gordon, J. K. Jansson, and R. Knight, “Diversity, stability and resilience of the human gut microbiota,” *Nutr.*, vol. 489, no. 7415, pp. 220–230, Sep. 2012.
- [202] G. J. Tortora, C. L. Case, and B. R. Funke, “*Microbiology: an introduction*,” 8th ed., Benjamin Cummings, San Francisco, 2004.
- [203] I. A. Brownlee, A. Allen, J. P. Pearson, P. W. Dettmar, M. E. Havler, M. R. Atherton, and E. Onsøyen, “Alginate as a Source of Dietary Fiber,” *Crit. Rev. Food Sci. Nutr.*, vol. 45, no. 6, pp. 497–510, 2005.
- [204] J. M. Round, “Plasma Calcium, Magnesium, Phosphorus, and Alkaline Phosphatase Levels in Normal British Schoolchildren,” *Br Med J*, vol. 3, no. 5872, pp. 137–140, 1973.
- [205] X. Gao, Y. Zeng, S. Liu, and S. Wang, “Acute stress show great influences on liver function and the expression of hepatic genes associated with lipid metabolism in rats,” *Lipids Health Dis.*, vol. 12, p. 118, 2013.

- [206] A. Keppler, N. Gretz, R. Schmidt, H. M. Kloetzer, Hermann-Josef Gröne, B. Lelongt, M. Meyer, M. Sadick, and J. Pill, “Plasma creatinine determination in mice and rats: an enzymatic method compares favorably with a high-performance liquid chromatography assay,” *Kidney Int.*, vol. 71, no. 1, pp. 74–78, 2007.
- [207] E. L. Barry, L. A. Mott, M. L. Melamed, J. R. Rees, A. Ivanova, R. S. Sandler, D. J. Ahnen, R. S. Bresalier, R. W. Summers, R. M. Bostick, and J. A. Baron, “Calcium supplementation increases blood creatinine concentration in a randomized controlled trial,” *PloS One*, vol. 9, no. 10, 2014.
- [208] Y. Dazai, T. Iwata, and K. Hiwada, “Augmentation of the renal tubular dopaminergic activity by oral calcium supplementation in patients with essential hypertension,” *Am. J. Hypertens.*, vol. 6, no. 11, pp. 933–937, 1993.
- [209] T. Nakata, D. Kyoui, H. Takahashi, B. Kimura, and T. Kuda, “Inhibitory effects of laminaran and alginate on production of putrefactive compounds from soy protein by intestinal microbiota in vitro and in rats,” *Carbohydr. Polym.*, vol. 143, pp. 61–69, 2016.
- [210] L. V. Hooper, T. Midtvedt, and J. I. Gordon, “How host-microbial interactions shape the nutrient environment of the mammalian intestine,” *Annu. Rev. Nutr.*, vol. 22, pp. 283–307, 2002.
- [211] M. Li, G. Li, Q. Shang, X. Chen, W. Liu, L. Zhu, Y. Yin, G. Yu, X. Wang, “In vitro fermentation of alginate and its derivatives by human gut microbiota,” *Anaerobe*, vol. 39, pp. 19–25, 2016.
- [212] H. Malnick, K. Williams, J. Phil-Ebosie, and A. S. Levy, “Description of a medium for isolating *Anaerobiospirillum* spp., a possible cause of zoonotic disease, from diarrheal feces

- and blood of humans and use of the medium in a survey of human, canine, and feline feces,” *J. Clin. Microbiol.*, vol. 28, no. 6, pp. 1380–1384, 1990.
- [213] H. Malnick, M. E. Thomas, H. Lotay, and M. Robbins, “Anaerobiospirillum species isolated from humans with diarrhoea,” *J. Clin. Pathol.*, vol. 36, no. 10, pp. 1097–1101, 1983.
- [214] C. P. Davis, D. Cleven, J. Brown, and E. Balish, “Anaerobiospirillum, a New Genus of Spiral-Shaped Bacteria,” *Int. J. Syst. Evol. Microbiol.*, vol. 26, no. 4, pp. 498-504, 1976.
- [215] Z. E. Ilhan, A. K. Marcus, D.-W. Kang, B. E. Rittmann, and R. Krajmalnik-Brown, “pH-Mediated Microbial and Metabolic Interactions in Fecal Enrichment Cultures,” *mSphere*, vol. 2, no. 3, 2017.
- [216] D. I. A. Pereira and G. R. Gibson, “Cholesterol assimilation by lactic acid bacteria and bifidobacteria isolated from the human gut,” *Appl. Environ. Microbiol.*, vol. 68, no. 9, pp. 4689–4693, 2002.
- [217] Y. Wang, F. Han, B. Hu, J. Li, and W. Yu, “In vivo prebiotic properties of alginate oligosaccharides prepared through enzymatic hydrolysis of alginate,” *Nutr. Res.*, vol. 26, no. 11, pp. 597–603, 2006.
- [218] S. Bereswill, I. Ekmekciu, U. Escher, U. Fiebiger, K. Stingl, and M. M. Heimesaat, “*Lactobacillus johnsonii* ameliorates intestinal, extra-intestinal and systemic pro-inflammatory immune responses following murine *Campylobacter jejuni* infection,” *Sci. Rep.*, vol. 7, no. 1, pp. 1–12, 2017.
- [219] G. R. Gibson and X. Wang, “Regulatory effects of bifidobacteria on the growth of other colonic bacteria,” *J. Appl. Bacteriol.*, vol. 77, no. 4, pp. 412–420, 1994.

- [220] S. Hudault, V. Liévin, M. F. Bernet-Camard, and A. L. Servin, “Antagonistic activity exerted in vitro and in vivo by *Lactobacillus casei* (strain GG) against *Salmonella typhimurium* C5 infection.,” *Appl. Environ. Microbiol.*, vol. 63, no. 2, pp. 513–518, 1997.
- [221] V. Liévin, I. Peiffer, S. Hudault, F. Rochat, D. Brassart, J. R. Neeser, and A. L. Servin, “Bifidobacterium strains from resident infant human gastrointestinal microflora exert antimicrobial activity,” *Gut*, vol. 47, no. 5, pp. 646–652, 2000.

7. Appendix

A Curriculum vitae

Name: Tamara Athamneh Date of birth: November 29th, 1985
Marital status: Married Place of birth: Al Sarih

Job History

| | |
|-------------------|---|
| 05/2015 - 01/2016 | Mental health case manager International Medical Corps (IMC) |
| 09/2014 - 06/2015 | Lecturer Jordan University of Science and Technology |
| 09/2009 - 02/2010 | Pharmacist Jordan Health Aid Society |

Education

| | |
|-------------------|--|
| 05/2016 - 06/2020 | PhD in Pharmaceutical Technology University of Hamburg and Hamburg University of Technology (TUHH) |
| 09/2011 - 04/2014 | Master of Science in Pharmaceutical Technology Jordan University of Science and Technology |
| 09/2003 - 02/2008 | Bachelor in Pharmacy Jordan University of Science and Technology |

B Conference contributions and publications

In context with this work, the following contributions have been presented at conferences and journal articles have been published or submitted.

Conference contributions - oral presentations

Preparation and characterization of alginate- hyaluronic acid nanoporous microspheres as potential carrier for pulmonary drug delivery using supercritical fluid technology. (Awarded the Postgraduate Oral Presentation Awards), Applied Science Private University Pharmacy Fourth International Conference. 2019, Amman, Jordan.

Pulmonary drug delivery with aerogels: Engineering of alginate and alginate-hyaluronic acid microspheres. (Awarded the first prize for the best oral presentation in early career investigator forum), the International Conference on Aerogels for Biomedical and Environmental Applications. 2020, Santiago de Compostela, Spain.

Conference contributions - poster presentations

Hyaluronic acid-alginate aerogel as potential drug carrier. The fourth international seminar on aerogels. 2018, Hamburg, Germany.

Preparation and characterization of alginate- hyaluronic acid nanoporous microspheres as potential carrier for pulmonary drug delivery using supercritical fluid technology. Jahrestreffen der ProcessNet-Fachgruppen Adsorption und Hochdruckverfahrenstechnik. 2019, Freiberg, Germany.

Journal articles with authors contributions and reference chapters

| Title | Journal | Authors | Contribution to the work | percentage | Reference chapter |
|--|-------------------------------------|----------------|---|-------------------|--------------------------|
| Alginate and hybrid alginate-hyaluronic acid aerogel microspheres as potential carrier for pulmonary drug delivery (Published) | The Journal of Supercritical Fluids | Athamneh, T. | Project plan, experiments, data analysis, publication | 90 % | 3.2.1.1 3.2.1.2 |
| | | Amin, A. | Experiments | 5 % | 3.2.1.5.2 |
| | | Benke, E. | Experiments | 2.5 % | 3.2.1.6 |
| | | Ambrus, R. | Experiments | 2.5 % | 4.1.2 |
| | | Leopold, C. S. | Supervisor | | 4.2.3 |
| | | Gurikov, P. | Supervisor | | 4.5 |
| | | Smirnova, I. | Supervisor | | 4.5.6 |
| Pulmonary drug delivery with aerogels: Engineering of alginate and alginate-hyaluronic acid microspheres. (submitted, May, 2020) | Journal of Pharmaceutical Sciences | Athamneh, T. | Project plan, experiments, data analysis, publication | 90 % | 3.2.1.1 3.2.1.4 |
| | | Amin, A. | Experiments | 5 % | 3.2.1.5 |
| | | Benke, E. | Experiments | 2.5 % | 3.2.1.6 |
| | | Ambrus, R. | Experiments | 2.5 % | 3.2.1.7 |
| | | Leopold, C. S. | Supervisor | | 4.1.1 |
| | | Gurikov, P. | Supervisor | | 4.4 |
| | | Smirnova, I. | Supervisor | | 4.5 4.6 |
| Evaluation of the orally administered calcium alginate aerogel on the shift of gut microbiota and toxicity of Wistar rats. (Submitted, June, 2020) | Advanced Healthcare Materials | Athamneh, T. | Project plan, experiments, data analysis, publication | 60 % | 3.2.2 4.7 |
| | | Alnajjar, M. | Experiments, publication | 35 % | |
| | | AbuTayeh, R. | Experiments | 2.5 % | |
| | | Bashiti, I. | publication | 2.5 % | |
| | | Leopold, C. S. | Supervisor | | |
| | | Gurikov, P. | Supervisor | | |
| | | Smirnova, I. | Supervisor | | |

C Hazardous materials

| Substance | supplier | Danger sympoly | Hazard statements | Precautionary statements |
|------------------------|-----------------------|---|--------------------------------|---|
| Glacial acetic acid | Carl Roth, Germany |   | H226 - H290 - H314 | P210 - P260 - P280 - P303 + P361 + P353 - P305 + P351 + P338 - P370 + P378 |
| Methanol | Carl Roth, Germany |    | H225, H301+H311+331 H370 | P210, P280, P305+338+351 |
| Naproxen | | | H302-H360 | |

Sigma Aldrich,
Germany



P201-P280-P301
+ P312 + P330-
P308 + P313



D Acknowledgements

First and foremost, I am grateful to God for the good health and wellbeing that were necessary to complete my PhD. After that I would like to express my deep and sincere gratitude to my supervisors Prof. Dr.-Ing. Irina Smirnova and Professor Dr. Claudia S. Leopold for giving me the opportunity to do research in their labs and for their continuous support of my PhD study and research.

Prof. Smirnova, thank you from heart for your patience, motivation, enthusiasm, and immense knowledge. The door of your office was always open whenever I ran into a trouble. Prof. Leopold, I appreciate the time you spent in reviewing my scientific papers. Your guidance helped me in all the time of research and writing of this thesis.

I would also like to thank Prof. Dr. Pavel Gurikov, our team leader in the TUHH for his generous assistance and dedicated involvement in every step throughout my PhD, starting from guiding me in the lab to writing my scientific papers.

Prof. Rana Obeidat, I cannot thank you enough for your uninterrupted support through my educational path. You were always my role model. I would also like to thank Dr. Mohammad Alnaif for paving the way of my PhD in Germany and for his valuable professional and personal advices that helped me a lot during my stay in Hamburg.

I place on record, my sincere thanks to Dr. Mohammad Alnajjar from the applied science private university- Jordan, for his efforts for the joint research project, and the helpful scientific discussions.

Additionally, I am grateful to Prof. Dr. Hans-Ulrich Moritz for evaluating this thesis. Furthermore, I would like to thank Prof. Dr. Ralph Holl, Prof. Dr. Michael Steiger and Prof. Dr. Markus Fischer for being members of the examination committee.

I would like also to acknowledge my colleagues; Raman, fynn, Imke, Victor and Baldur, without whom I would not have been able to complete this research.

Getting through my dissertation required more than academic support, and I have many people to thank for listening to and having to tolerate me over the past four years. Alaa, Razan, Joana, Miao, Sheila, Isabella I cannot begin to express my gratitude and appreciation for your friendship. Mrs. Meyer-Storckmann, thank you so much for your continuous personal and professional support, I still appreciate your help to find an

accommodation when I arrived Hamburg four years ago. Aya, my dearest friend, thanks a million!! You were always there whenever I needed you and even without I asked.

I deeply thank my parents for their unconditional trust, timely encouragement, and endless patience. My sister Doaa and my brother Mahmood you have also been generous with your love and support despite the long distance between us.

And for my beloved husband Moawia, thanks from heart for all your support, without which I would have stopped these studies a long time ago. I simply couldn't have done this without you. Finally, I thank with love Adham, Yara and Omar. My lovely kids, you were always my motivation, not only in my PhD, but also in my whole life. When I have started my PhD four years ago, I was told many times "You cannot do it with three kids !!!" and I was always replying "It might be difficult to do it with my kids, but it would be definitely impossible to do it without them". Darlings, I appreciate every moment you struggled to learn German, you played alone, you lived apart from your father and family. I promise to compensate you and to spent more joyful time together.

Declaration on oath / Eidesstattliche Versicherung

Hiermit versichere ich an Eides statt, die vorliegende Dissertation selbst verfasst und keine anderen als die angegebenen Hilfsmittel benutzt zu haben. Die eingereichte schriftliche Fassung entspricht der auf dem elektronischen Speichermedium. Ich versichere, dass diese Dissertation nicht in einem früheren Promotionsverfahren eingereicht wurde.

Ort, Datum

Unterschrift (Tamara Athamneh)